University of Bath

PHD

High Performance Single Photon Sources and their application to quantum technologies

Hoggarth, Rowan

Award date:
2019

Awarding institution:
University of Bath

Link to publication

Alternative formats
If you require this document in an alternative format, please contact:
openaccess@bath.ac.uk

Copyright of this thesis rests with the author. Access is subject to the above licence, if given. If no licence is specified above, original content in this thesis is licensed under the terms of the Creative Commons Attribution-NonCommercial 4.0 International (CC BY-NC-ND 4.0) Licence (https://creativecommons.org/licenses/by-nc-nd/4.0/). Any third-party copyright material present remains the property of its respective owner(s) and is licensed under its existing terms.

Take down policy
If you consider content within Bath's Research Portal to be in breach of UK law, please contact: openaccess@bath.ac.uk with the details. Your claim will be investigated and, where appropriate, the item will be removed from public view as soon as possible.

Download date: 05. May. 2023

Citation for published version:
Hoggarth, R 2017, 'High Performance Single Photon Sources and their application to quantum technologies', Ph.D., University of Bath.

Publication date:
2017

Link to publication

University of Bath

General rights
Copyright and moral rights for the publications made accessible in the public portal are retained by the authors and/or other copyright owners and it is a condition of accessing publications that users recognise and abide by the legal requirements associated with these rights.

Take down policy
If you believe that this document breaches copyright please contact us providing details, and we will remove access to the work immediately and investigate your claim.

Download date: 14. May. 2019

High Performance Single Photon Sources

and their Practical Application to Quantum Technologies

submitted by

Rowan Hoggarth

for the degree of Doctor of Philosophy

of the

University of Bath

Department of Physics

December 2017

COPYRIGHT

Attention is drawn to the fact that copyright of this thesis rests with the author. A copy of this thesis has been supplied on condition that anyone who consults it is understood to recognise that its copyright rests with the author and that they must not copy it or use material from it except as permitted by law or with the consent of the author.

This thesis may be made available for consultation
within the University Library and may be
photocopied or lent to other libraries for the purposes
of consultation with effect from ..... (date)

Signed on behalf of the Faculty of Science .....

Acknowledgements

The work presented here would not have been possible without the help and support of a great many people. I would like to especially thank my supervisor Dr. Peter Mosley, and our group post-doc Dr. Robert Francis-Jones who have between them taught me a great deal and provided immeasurable patience during the process. Without their support and encouragement none of this would be possible.

Over the last three years I have made a large number of fiends amongst the students and staff within the department and in particular the transitory inhabitants of WH3.42, you know who you are. I would like to thank the wider past and present members of the Center for Photonics and Photonic Materials who have provided a diverse and interesting research environment and innumerable opportunities to learn about wider topics in photonics.

I would like to thank my mother Fiona, brother Calum and sister Iona for their love, understanding and support over the last three years and during the stressful times in my studies. You have kept me sane and helped me to see the positive side of every unexpected problem.

Finally and most sincerely I thank Hiroko and Jim Sherwin who have most directly made my studies possible through their generosity.

Abstract

Optical quantum information processing has advanced over the last decade from a hypothetical goal and motivational reason to study single photon phenomena, to a practical and established branch of physics. Quantum information processing with photon states remains in its infancy, but is evolving rapidly towards implementable technology and real applications in the areas of metrology, communications and computer science. Of primary interest to continuing development are the sources necessary to generate single photon states of light. Contemporary sources provide well controlled states of light using nonlinear processes to generate photon pairs in a probabilistic manner. In order to supply state of the art information processing experiments with multiple concurrently delivered photons, multiple sources must operate together. The spontaneous nature of each source causes the multi-photon delivery probability to scale unfavorably, and at present places limits on the complexity of photonic computation.

The work presented in this thesis comprises two separate parts relating to multiplexed photon sources and development of an optical fibre for performing a quantum walk. Active multiplexing of four temporal emission modes of a photon pair source into a single temporal mode is demonstrated in a fiber integrated and resource efficient implementation. An optical fibre with 37 coupled cores is fabricated for implementing a two dimensional quantum walk. The suitability of the fabricated fibre is verified with bright light and single photon interference.

Contents

1 Introduction **8**

1.1 Motivation 8

1.2 Photons & Their Properties 10

1.2.1 Representing a State 10

1.2.2 Pure and Mixed States 11

1.2.3 The 50:50 Splitter 14

1.2.4 Photon Statistics 18

1.2.5 Correlation 20

1.3 Outline for This Thesis 21

2 Photon Pair Sources **23**

2.1 Material Polarization 23

2.2 Four Wave Mixing in a PCF 25

2.2.1 Photonic Crystal Fibre 25

2.2.2 Four Wave Mixing 25

2.2.3 Phase Matching Degenerate FWM in PCF 27

2.2.4 Low Power FWM 28

2.2.5 Factorable States 32

2.3 Three Wave Mixing in a Crystal 33

2.3.1 Spontaneous Parametric Down Conversion 35

2.3.2 Polarization of Three Wave Mixing 37
2.4 Heralding Operation of a Photon Source 38
2.5 Equipment Considerations 40
2.5.1 Single Photon Detectors 40
2.5.2 Pulsed and Continuous Lasers Used 45
2.5.3 Telecommunication Parts 46
2.6 Two Specific Sources Used 48
2.6.1 Fibre Integrated FWM Source 48
2.6.2 Free-space β-BBO SPDC Source 49

3 Electronics for Photon Counting Experiments 52
3.1 Challenges for Data Acquisition 53
3.1.1 Correlation Counting 53
3.1.2 Timing Alignment 54
3.2 Introduction to the FPGA 55
3.2.1 Physical Logic Implementation 55
3.2.2 Development of FPGA codes 61
3.2.3 Programming 63
3.3 Design of the Counting Electronics 65
3.3.1 Requirements 65
3.3.2 Choice of Programmable Logic 66
3.4 Design Detail 67
3.4.1 Design of a Display and Communications Board 71
3.4.2 Design of a 2nd Prototype 73
3.5 Design of the Time Delay Electronics 76
3.5.1 Problems Encountered with Existing Electronics 77
3.5.2 Design of the Time Delays 77
3.6 Qualification Testing 80

4 Multiplexing **84**

4.1 Motivation . . . 84

4.2 Introduction . . . 85

4.3 Other Temporal Schemes . . . 88

4.3.1 Binary Delay *Ladder* . . . 89

4.3.2 Recycling Loop . . . 91

4.3.3 Parity Offset Loops . . . 92

4.4 Statistical Model . . . 94

4.5 Temporal Loop Construction . . . 97

4.6 Loop Control Scheme . . . 98

4.7 Temporal Loop Construction Measurements . . . 104

4.7.1 Switch Insertion Loss & Speed . . . 104

4.7.2 Construction of the Loop Delay . . . 107

4.7.3 Initial Verification Tests . . . 108

4.8 Pump Laser Preparation . . . 109

4.8.1 Spectral Qualities . . . 109

4.8.2 Pulse Frequency . . . 110

4.8.3 Power & Additional Optics . . . 111

4.9 Noise Gating . . . 112

4.10 Temporal Multiplexing Results . . . 113

4.11 Summary . . . 119

5 Two-dimensional Quantum Random Walk of Single Photons in a Multi-core Optical Fibre **124**

5.1 Introduction . . . 124

5.1.1 Discrete Quantum Walks . . . 127

5.1.2 Continuous Time Quantum Walks . . . 129

5.1.3 Implementing a Quantum Random Walk in Fibre . . . 131

5.2 Prior Published Work 132
5.3 Fibre Fabrication and Design Constraints 134
5.3.1 Core to Core Coupling 136
5.3.2 Muti-Core Design 137
5.3.3 Fabrication Process for Fibre 140
5.3.4 Forming Rods 141
5.3.5 Stacking the Preform 142
5.3.6 Drawing Cane 143
5.3.7 Drawing Fibre 146
5.3.8 Glass Inhomogeneity 146
5.4 Behavioral Simulation of Multi-core Coupling 149
5.5 Bright Light Characterization 150
5.6 Single Photon Interference 153
5.7 Proposed Future Work 162

6 Summary **165**

Publications

[1] Robert J. A. Francis-Jones, Rowan A. Hoggarth, and Peter J. Mosley. All-fiber multiplexed source of high-purity single photons. *Optica*, 3(11):1270–1273, 2016.

[2] R A Hoggarth, R J A Francis-Jones, and P J Mosley. Resource-efficient fibre-integrated temporal multiplexing of heralded single photons. *Journal of Optics*, 19(12):125503, 2017.

[3] Rowan A. Hoggarth, Robert J. Francis-Jones, and Peter Mosley. Temporal multiplexing of heralded single photons with a resource-efficient fiber loop. In *Conference on Lasers and Electro-Optics*, OSA Technical Digest (online), page FTh4E.2, San Jose, California, 2017. Optical Society of America.

Chapter 1

Introduction

1.1 Motivation

The quantum mechanical model of nature is rich in effects not seen in everyday macro-scale life. Increasingly technological innovation and physical sciences research have become concerned with observing, simulating and controlling non-classical phenomena. Major branches include (but are not limited to) Quantum Information Processing (QIP); the study of the implications of representing information with the state of quantum system, Quantum Key Distribution and related cryptographic applications (QKD)[1], and Quantum Enhanced Measurement (QEM)[2]. It is perhaps intuitive that the problem of representing a quantum system for simulation or storage might be addressed with another quantum system, this is particularly attractive given the computational resource scaling of conventional simulations of quantum systems [3].

Besides the practicalities of simulating interesting quantum systems (eg. Biological molecules), when some classical problems are re-cast into the QIP domain, alternative and in some cases highly efficient solutions can be found. Notable examples being the quantum Fourier transform leading to Shors prime factoring algorithm [4], which has

significant implications for classical cryptography. In order to use QIP a particular physical system must be chosen as a host. Broadly speaking the choice of system can be categorized by the representation form of the quantum information (qubits). Before introducing the three most explored schemes it is worth noting the parameters of merit for a system. Coupling strength with respect to the environment determines the de-coherence time (hence useful lifetime) for the qubit, it also impacts the ability to prepare, measure and operate upon a state. The Available physical degrees of freedom of the system provide options for the representation of a qubit, but also dictate the engineering required to prepare a pure state. Finally in any practical scheme we must consider the physical resources required to reach an acceptable starting state of the system. Perhaps the simplest system is a single simple harmonic oscillator, realized by a bound electron of an atom, ion, quantum dot, colour centre etc. and these systems have been explored extensively in the past [5][6] (for a review see [7]) and are typically operated upon by external electromagnetic fields via a cavity coupling[8] [9]. In order to achieve coherence times suitable for experimentation cryogenic temperatures often have to be employed (the diamond nitrogen vacancy can be used at room temperature [10]) and techniques for electromagnetic addressing of the individual qubits are highly non-trivial [11] due to the strong (and indiscriminate among a collection of very similar systems) coupling schemes. The practicalities of cryogenic operation and RF metrology limit foreseeable use of some such schemes outside of a research environment.

An alternative but less common system is the quantised magnetic flux states associated with superconducting quantum interference devices (SQUIDs) [12]. SQUIDs have found extensive use in QEM and their use in QIP is a natural extension. Despite macroscopic size (with respect of quantum dots etc.) SQUIDs suffer from similar extensive engineering requirements for cryogenic temperatures and magnetic fields. A third system, and the scheme of particular interest here, is the use of photons as qubits. Photons have a weak coupling with their environment and with each other, so weak in fact that until recently their use at all was largely hypothetical.

It was assumed that in order to allow a single photon to interact with another on practical time-scales, as would be necessary for implementing two-qubit quantum gates, a medium with an extremely large non-linearity would be needed. A seminal paper [13] introduced a linear interaction scheme referred to as Linear Optical Quantum Computing (LOCQ) requiring no exotic optics. The scheme instead is based around non-classical interference in a beam splitter, an effect which is most visible between pure and indistinguishable quantum states, and so requires pure photon state sources. With the knowledge that a practical, room temperature, non-exotic material based approach to building experiments exists, the field has been catching up with the above schemes. One significant difficulty still to be overcome, and an area of intense research, is the source of the qubits (states that can interfere at the beam splitter) to pass through an experiment; the production of truly indistinguishable deterministic photons remains a problem.

1.2 Photons & Their Properties

1.2.1 Representing a State

A photon is a single quantised excitation of the electromagnetic field, it possesses properties such as spectral distribution, polarization and energy. While we can in principle use any property to encode quantum information, we typically choose (for engineering convenience) either polarization or spatial mode, i.e. which arm of an interferometer or which waveguide mode etc. a photon is found in. A qubit might be represented as shown below, as the superposition of two states for a given spatial mode (occupied and unoccupied).

$$\alpha|0\rangle + \beta|1\rangle = |\psi\rangle \tag{1.1}$$

We can define an operator $\hat{a}^\dagger(\omega)$ to create one photon, and similarly $\hat{a}(\omega)$ to annihilate one photon, where ω labels the frequency (energy) of the created photon. The labels for mode, polarization etc. have been neglected for simplicity.

$$\sqrt{n}|n\rangle = \hat{a}^\dagger(\omega)|n-1\rangle \tag{1.2}$$

$$\sqrt{n+1}|n\rangle = \hat{a}(\omega)|n+1\rangle \tag{1.3}$$

$$|0\rangle = \hat{a}(\omega)|0\rangle \tag{1.4}$$

We can also define the application of both the creation and annihilation operator as the 'number' operator $\hat{n}$ since the state acted upon by both will be left unchanged and the eigenvalues are the square root of the occupation of the state.

$$\hat{n} = \hat{a}^\dagger(\omega)\hat{a}(\omega) \tag{1.5}$$

$$\hat{n}|n\rangle = \hat{a}^\dagger(\omega)\hat{a}(\omega)|n\rangle = n|n\rangle \tag{1.6}$$

1.2.2 Pure and Mixed States

Descriptions of the quantization of the electromagnetic field usually start with a consideration of a cavity, which for a given mode can be solved by the boundary conditions that the cavity imposes. The result is a harmonic oscillator equation, where the number of photons is the principle excitation number. As with all harmonic oscillators the minimum energy state is not zero, each mode contains $\frac{1}{2}\hbar\omega$ *zero-point* energy. This extra half-occupation of a mode allows spontaneous processes to occur such as parametric

down conversion discussed later in 2-4 [14] [15] and spontaneous emission [16].

Clearly this view is incomplete since we wish to consider a free photon (or at least a less constrained one) which necessarily must not be a plane wave, nor have infinite duration. We might determine that the photon has a spectrum as necessitated by its finite duration (but not necessarily transform limited) and that a superposition of single frequency photons normalized and weighted to this spectrum,

$$\int d\omega f(\omega)\hat{a}^{\dagger}(\omega)|0\rangle, \tag{1.7}$$

yields a suitable description of a real photon. The specific frequency measured by a spectrometer etc. when this photon is detected will assume a single value. Equation 1.7 considers only the spectral degree of freedom of a single mode, ignoring spatial distribution (or spatial mode when additional conditions are imposed). In addition to being distributed in time and frequency the photon can occupy a range of momentum and spatial modes and superpositions of modes; photons are inherently non localized.

A pure photon state is any state that can be written as a single state vector (this includes superpositions) whereas a mixed state refers to those states which can only be represented instead as a statistical ensemble of pure states. We write a weighted ensemble of states because we cannot determine the state a system is in. This probabilistic mixture of pure states is quite distinct from the indeterminism of which eigenstate a pure state will be found in when measured. Mixed states can result both from lack of knowledge about the preparation or subsequent evolution of a state, or from the partial measurement of a bipartite state Where the outcome of the measured part is unknown.

The problems of decoherence and the related problems of measurement (wave-function collapse; non time reversibility) continue to be actively debated [17]. A mixed state may be written as a sum of states weighted by their classical probability p_i of being observed.

$$\sum_{i=1}^{\forall i} p_i |\phi_i\rangle\langle\phi_i| = \hat{\rho} \tag{1.8}$$

When considering a system comprising more than one photon the implications of pure and mixed states are made more distinct. If there are as in equation 1.1 two possible states for each photon we note the effect of second photon joining the superposition. When we consider two photons (one in each input mode) we now require four amplitudes to describe the four joint states possible in superposition after the beam splitter:

$$|\Phi\rangle = \alpha_{00}|0\rangle_a|0\rangle_b + \alpha_{01}|0\rangle_a|1\rangle_b + \alpha_{10}|1\rangle_a|0\rangle_b + \alpha_{11}|1\rangle_a|1\rangle_b. \tag{1.9}$$

Where the labels a, b are the two single photon modes and the α_{ij} represent the amplitude with which the relevant terms contribute. For different choices of the amplitudes we find qualitatively different behavior of the system. Take for example the case where $\alpha_{10} = \alpha_{01} = 0$ and $\alpha_{00} = -\alpha_{11}$, such a state is said to be entangled since the measurement of one photon completely implies the state of the other from its result. Conversely it is possible to have a set of amplitudes which allow the state to be factored:

$$|\Phi\rangle = \{\alpha_a|0\rangle_a + \beta_a|1\rangle_a\} \otimes \{\alpha_b|0\rangle_b + \beta_b|1\rangle_b\} \tag{1.10}$$

Such states will turn out later to be of great importance, since the measurement (and destruction) of one photon will not project the remaining photon into a mixed state. In states that are entangled the destructive measurement of one photon has implications for the values for the remaining degrees of freedom on the other photons. However since we cannot in practice measure all the parameters of the detected photon, we

fix, but yet have no knowledge of, the remaining parameters. We can however by repeated measurements discover the average behavior of an ensemble of systems: the density matrix. It has been proven that any entangled state can be written as a superposition of product states, this is called the Schmidt decomposition (Dynamic Mode Decomposition) [18]. The number of modes in this sum is called the Schmidt number, and can be used to quantify the degree of entanglement. A factorisable state necessarily requires only one term in the sum.

1.2.3 The 50:50 Splitter

An instructive experiment (that will also find applications later in determining the indistinguishably of photons) is the the interference of two photons at a beam splitter. Known as Hong Ou Mandel interference[19], the effect is entirely non-classical (we should expect no interference to happen classically). Consider an ideal beam splitter with no loss and having exact splitting ratio of 50%. Such a beam splitter operation might be represented:

$$\hat{U} = \begin{bmatrix} R & T \\ T & -R \end{bmatrix} = \frac{1}{\sqrt{2}} \begin{bmatrix} 1 & 1 \\ 1 & -1 \end{bmatrix} \tag{1.11}$$

where the -1 accounts for the π phase shift picked up on reflection. When a single photon enters the splitter it will exit in superposition of a spatial mode for transmission and a spatial mode for reflection. When the photon is subsequently incident on a detector the superposition collapses into either of the arms with equal probability (equal splitting ratio). When two photons are present, one from each input port, logically both must undergo the same behavior and form superpositions. Where the input ports are labeled i_1, i_2 and the outputs o_1, o_2 we find the following:

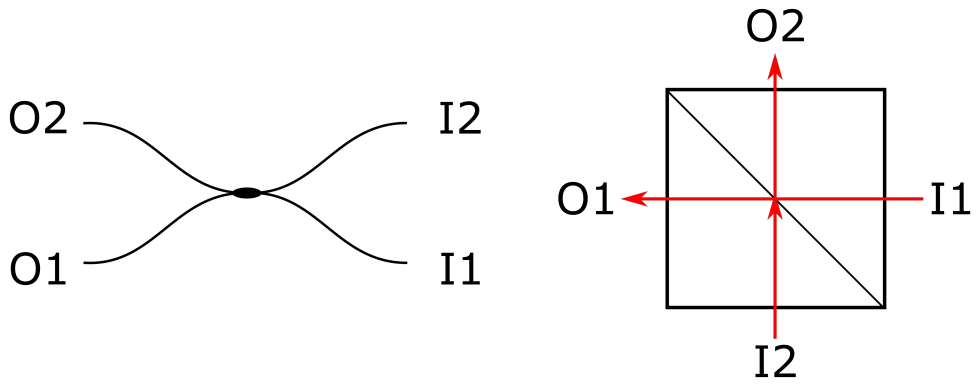

Figure 1-1: Two common forms of beam splitter; both split the beam entering at the input ports into transmission and reflection components. The left splitter is formed by fusing two optical fibres side by side to allow coupling between their modes, these devices always display wavelength dependent splitting ratios due to the wavelength dependent coupling strength in combination with a fixed coupling length. The beam cube on the right is typically able to operate over a wider wavelength range but also displays wavelength dependent properties due to the thickness of the dielectric layer on the hypotenuse, some manufacturers employ thin multi layer stacks to modify wavelength dependence.

$$R\hat{o}_1^\dagger + T\hat{o}_2^\dagger = \hat{i}_1^\dagger \tag{1.12}$$

$$T\hat{o}_1^\dagger - R\hat{o}_2^\dagger = \hat{i}_2^\dagger. \tag{1.13}$$

For a single photon we find simply (putting one photon in port i_1):

$$|\Phi\rangle = (R\hat{o}_1^\dagger + T\hat{o}_2^\dagger)|0\rangle_{o_1}|0\rangle_{o_2}, \tag{1.14}$$

however for two photons we now have (note the cross terms) for the output state:

$$|\Phi\rangle = (R\hat{o}_1^\dagger + T\hat{o}_2^\dagger)(T\hat{o}_1^\dagger - R\hat{o}_2^\dagger)|0\rangle_{o_1}|0\rangle_{o_2}, \tag{1.15}$$

$$|\Phi\rangle = (TR\hat{o}_1^\dagger\hat{o}_1^\dagger + -R^2\hat{o}_1^\dagger\hat{o}_2^\dagger + T^2\hat{o}_1^\dagger\hat{o}_2^\dagger + -RT\hat{o}_2^\dagger\hat{o}_2^\dagger)|0\rangle_{o_1}|0\rangle_{o_2}. \tag{1.16}$$

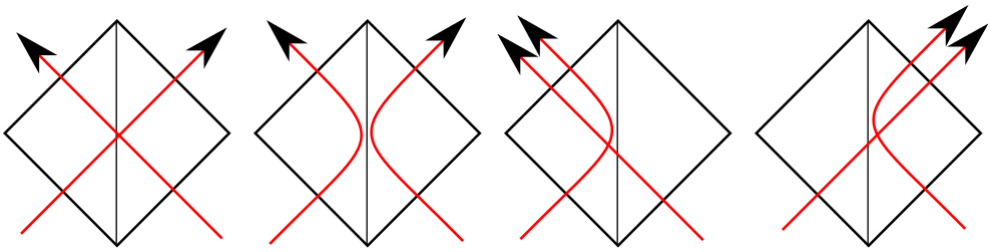

Figure 1-2: Four possible outcomes when two photons are incident on the beam splitter; one photon impinging into each input port. All four possibilities should be detected with equal likelihood if the photons do not interfere. If the input photons are overlapped and indistinguishable the amplitudes corresponding to the first two cases destructively interfere and are not observed.

Since the transmission and reflection probability are identical we see the cross terms will cancel and the output state can be written:

$$|\Phi\rangle = (\hat{o}_1^\dagger \hat{o}_1^\dagger - \hat{o}_2^\dagger \hat{o}_2^\dagger)|0\rangle_{o_1}|0\rangle_{o_2} = \frac{1}{\sqrt{2}}(|2\rangle_{o_1}|0\rangle_{o_2} - |0\rangle_{o_1}|2\rangle_{o_2}). \tag{1.17}$$

This behaviour is often described as 'bunching' and is a characteristic of bosons. In order for the terms to cancel the amplitudes must arrive overlapped at the detector. However for photons not exactly aligned but almost, the bandwidth of said photons may allow the interference to occur for some probability.

When the arrival time of the photons is deliberately delayed or advanced we expect the degree of interference visible to change in accordance with the photon overlap, and the interference to be visible only when considering the two photon events (i.e. other stray photons or loss may decrease the visibility of this effect). The phenomenon is known as the Hong Ou Mandel dip [19] and provides evidence of the existence of non-classical states of light, and the interference of indistinguishable photons.

It is worth noting that the point in time at which the amplitudes must form this superposition is strictly at the point of detection; where the superposition is collapsed.

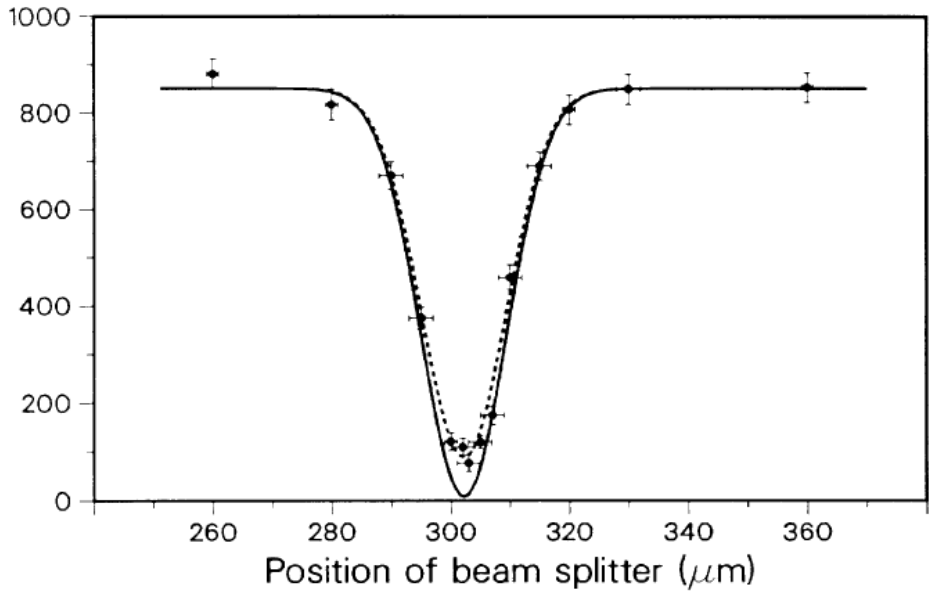

Figure 1-3: Hong Ou Mandel behaviour at the beam splitter. The count rate of events where two photons excited from two different ports of the beam splitter is plotted against beam splitter displacement between two optical paths. When the two paths are of equal length HOM interference causes both photons to be observed to exit from the same port. The ideal curve is shown in black; original data [19] displays imperfect interference likely caused by background counts or imperfect splitting ratio.

The photons do not interact in the local sense while in the beam splitter and need not in general be present within the splitter at the same time [20].

1.2.4 Photon Statistics

When observing bright light experiments little thought is put to the photons within a beam. Consider the structure of timings within the beam, we can have three distinct cases. The simplest starting point is probably monochromatic coherent light like that produced by a laser; the time of arrival distribution when measured by a counter is random. With a constant mean rate, random interval timings, and only two states (present or not) a Poisson distribution is formed [21] (derivation along identical lines to that used to analyze radioactive decay).

A simple extension to 'thermal' (black body) light sources is made by considering the fluctuations of the thermal system and the effect they should have on the mean rate of emission (at a given wavelength). If the rate fluctuates the distribution of photons in the beam will form bunches, the distribution becomes 'super-Poissonian', i.e. wider than it's mean. This bunching is distinct from the previously mentioned bunching in the beam splitter.

Classically light cannot be sub-Poissonian; no distribution of photons is more ordered than perfectly coherent monochromatic single mode light. Logically sub-Poissonian light must have more order than coherent Light, which requires a non random time interval distribution. If with a constant time interval we have a specific number of photons in a given length of the beam, these states are unsurprisingly called number-states [22]. Detecting these states is difficult because of the nature of real photo detectors which exhibit shot noise. Additional complications are found by considering losses from the beam; each of which can be modelled as a beam splitter with appropriate probabilities. Successive losses in this way amount to the same effect as random sampling of

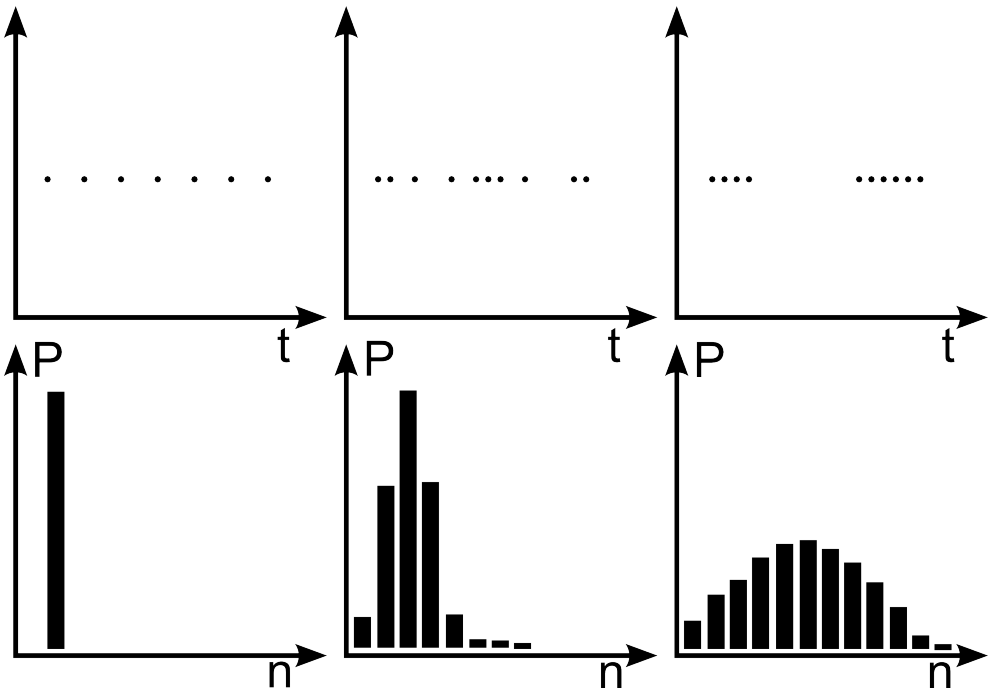

Figure 1-4: Graphs of three classes of statistics: (left to right) showing anti-bunched light with sub-Poissonian distribution, coherent light with Poisson distribution and thermal light with super-Poissonian distribution. The upper three graphs give cartoon representation of the locations of photons within a beam. The lower three graphs show the probability distributions (unnormalized) that n photons arrive within a specific time window (in this case the period of the anti-bunched example).

the ordered beam; the resulting statistics will appear progressively less sub-poissonian. Consider dividing a beam of sub-poissonian light into subsections such that each contains one photon, optical loss is probabilistic and equivalent for each section, by considering the probability of finding in any group of N segments n occupied segments (arranged in any order) a binomial distribution is produced. Careful experimental design is needed to generate and observe sub-poissonian states of light.

1.2.5 Correlation

As previously mentioned, light can be classified by its arrival time statistics. Alternatively a classification as anti-bunched, coherent and bunched can be made via the second order correlation $g^{(2)}(t)$. The $g^{(2)}$ measurement can be applied to identify sub-poissonian photon statistics by first splitting a beam into two modes and looking for correlations between them. sub-poissonian statistics results in an anti-bunched series, identified by $g^{(2)}(t) < 1$. The famous experiments of Hanbury-Brown and Twiss (HBT) [23] with their 'distributed' version of the Michelson intensity interferometer paved the way to a new understanding of correlations in Light. Having received critical review of their astronomical apparatus, a simplified experiment where two photo multipliers receive light from the same source and have their outputs multiplied together and averaged was performed. Neglecting the DC term and allowing for a time (path length) delay between detectors we find this quantity:

$$\langle \Delta I(t) \Delta I(t+\tau) \rangle, \tag{1.18}$$

which is a measure of correlation between inputs. Given that both detectors receive the same input signal (light from the same source), the degree of coherence between beams is being measured. We define a normalized version of this approach as the second order correlation:

$$\frac{\langle I(t) I(t+\tau) \rangle}{\langle I(t) \rangle \langle I(t+\tau) \rangle} = \frac{\langle \epsilon^*(t) \epsilon^*(t+\tau) \epsilon(t) \epsilon(t+\tau) \rangle}{\langle \epsilon^*(t) \epsilon(t) \rangle \langle \epsilon^*(t+\tau) \epsilon(t+\tau) \rangle} = g^{(2)}(\tau). \tag{1.19}$$

Consider the behaviour when the detectors are aligned with a source of single photons, if only one photon is incident at a time we have $g^{(2)}(\tau = 0) = 0$ which contravenes the classical limit of $g^{(2)}(\tau = 0) = 1$ where the input is perfectly coherent. The threefold

$g^{(2)}(\tau = 0)$	Classical term	Quantum term
> 1	Chaotic	Bunched
$= 1$	Coherent	Random
< 1		Anti-bunched

Table 1.1: Classical and Quantum terms used to describe statistics of light.

possibilities are summarized in Table 1.1. The $g^{(2)}$ measurement provides a simple method to discover the statistics of a beam; by observing values below unity (having made corrections for detection efficiency), we can confirm that non classical light has been generated.

1.3 Outline for This Thesis

We shall begin be discussing the methods of photon production in the two types of parametric mixing source that will be used in later chapters. An overview, and then the detailed specifics of the sources are discussed.

We discuss in the next section the apparatus (specifically the electronics) developed for the work for correlation detection and control. Two designs were made use of in both the major sections, the first being a discriminator and correlator unit, the second being programmable delay lines used to re-overlap signals that have passed trough different propagation delays.

Next we introduce the need for photon source multiplexing in order to modify photon pair generation statistics favorably for practical applications. The fibre integrated photon source discussed has been previously used as part of a spatial multiplex scheme which is briefly explained. We present a temporal multiplexing scheme that has been successfully implemented along with the most relevant results and parameters and alongside a model of the losses. This work forms one of the two major themes to be

discussed.

In the final section we introduce the quantum random walk as an established paradigm. A novel variant on the photonic incarnation of the random walk, making use of multi-core fibre optics is proposed. A fabricated fibre for this purpose is presented and demonstrations of the coupling properties with both classical light, and heralded single photons are demonstrated.

Chapter 2

Photon Pair Sources

2.1 Material Polarization

When light is incident on a medium the material's electron distribution is driven by the associated electric field producing a polarization. The polarization evolves in time in step with the external electric field. The positive electric potential of the atomic cores within the material attract the electrons and *bind* them. The potential well in which the electrons are localized is finite and can be overcome with sufficiently high energy. The atomic arrangement creates an effective potential well which reflects the symmetry of the material. Regardless of the shape of the potential at higher energy, low amplitude excitations oscillate in a potential that is locally harmonic. For greater energy excitations the asymmetric shape of the potential begins to have an influence and the polarization state can become anharmonic. We term the relationship between an externally applied field and the resulting polarization *electric susceptibility*.

$$P = \epsilon_0 \chi E \tag{2.1}$$

where P is the material polarization, ϵ_0 is the vacuum permitivity, E is the incident electric field, and χ is the constant of proportionality between the vector fields and is in general a tensor quantity. For small applied fields the polarization response is linear since the potential well approximates a harmonic oscillator; the collection of driven electrons will re-radiate the field without modification (with the exception of a phase shift) in a coherent manner.

For large driving fields we cannot assume the response remains linear. The susceptibility is modified for the cases where electrons are driven to displacements far from equilibrium, in the the regions where the material structure effects on the potential well are noticeable. Discovering the exact form of the susceptibility for a given material requires we have a detailed electronic model, however we can approximate by a power series.

$$\frac{P(\omega)}{\epsilon_0} = \chi^{(1)}(\omega)E(\omega) + \chi^{(2)}(\omega)|E|^2(\omega) + \chi^{(3)}(\omega)|E|^2(\omega)E(\omega) + ... \tag{2.2}$$

Each order of susceptibility is progressively smaller and the high orders can often be neglected. For the cases of the two materials used in the sources discussed later, fused silica glass and beta-barium borate (BBO), the former is amorphous and so lacks the even order contributions since there is no preferential direction or *optical axis*. For BBO all terms in the power series contribute to the susceptibility however the second order term is significantly larger than the third order and so dominates.

2.2 Four Wave Mixing in a PCF

2.2.1 Photonic Crystal Fibre

A contemporary form of optical waveguide in which only a single dielectric material and air are used is the photonic crystal fibre or PCF. A PCF is distinctly different from conventional optical fiber in which the refractive index contrast between the cladding material and the core material is used to guide light. In a PCF an arrangement of air holes throughout the cladding region create a lower effective refractive index than the core region in which there are no air holes. The index contrast between cladding and core is controllable through the size and frequency of air holes, as is the effective core size.

By controlling the amount of air in the cladding region, and the spacing of air holes, the dispersion of the fibre can be tailored as desired by an application. Control over fibre dispersion can be used to select wavelength pairs that can propagate at the same velocity in the fibre, allowing phase matched interactions to occur.

As with conventional optical fiber, light of a given spatial mode is guided up to some cutoff point and for a given wavelength a fibre supports a finite number of modes. Some PCF designs are single mode over a wide spectral range or over their entire guiding range [24]. The ability to tailor fibre dispersion by control of the air hole parameters is a key tool for fibre engineering.

2.2.2 Four Wave Mixing

Mixing four electric fields is possible within a material with third order nonlinearity. There are other third order nonlinear effects however Four Wave Mixing (FWM) proves useful for both quantum and classical optics applications. By considering the aforementioned restrictions of a isotropic medium, co-polarization of each wave, and the

restricted modes of propagation through the fiber we only require a single component from the tensor that relates electromagnetic waves to material polarization [25].

$$P_{4_{NL}} = \frac{3\epsilon_0}{4}\chi^{(3)}_{xxxx}\{|E_4|^2E_4 + 2(|E_1|^2 + |E_2|^2 + |E_3|^2)E_4 + 2E_1E_2E_3^* exp(i\phi) + ...\} \quad (2.3)$$

$$P_{FWM} = \frac{3\epsilon_0}{4}\chi^{(3)}_{xxxx}\{2E_1E_2E_3^* exp(i\phi)\} \quad (2.4)$$

There are other non-linear third order effects in this sum, however the phase dependent term shown in 2.3 is the significant one here. With our previously made assumption of instantaneous response we see that the polarization is in phase with the driving fields if the additional phase ϕ is zero. For any efficient process we desire the contributions from all points in the material to be in phase. The field radiated by the polarization must add constructively to produce a net output of the mixing product.

$$\phi = \{(\beta(\omega_s) + \beta(\omega_i) - \beta(\omega_{pump}) - \beta(\omega_{pump}))z - (\omega_s + \omega_i - \omega_{pump} - \omega_{pump})t\} \quad (2.5)$$

The phase contribution takes the form shown above with dependence on the wavelengths of the four fields, and with the wave-vector associated with each of the fields. Beta represents the phase constant for a given wavelength, which is a function of waveguide mode dispersion.The contributions from wavelength and wave-vector are independent of one another and so must each be zero to match the phase,

$$\delta\omega = \omega_s + \omega_i - \omega_{pump} - \omega_{pump}, \quad (2.6)$$

$$\delta k = \beta(\omega_s) + \beta(\omega_i) - \beta(\omega_{pump}) - \beta(\omega_{pump}) - 2\gamma P, \quad (2.7)$$

where δk and $\delta\omega$ are the wave vector mismatch and energy mismatch respectively. These two quantities must be equal to zero in order to conserve momentum and energy (the $2\gamma P$ term originates from the process of self phase modulation (SPM) in which the medium's refractive index is modified by the pump intensity, producing an intensity dependant shift or *chirp*. The energy matching is parametrically fulfilled and can be thought of as loss from ω_1, ω_2 and gain in ω_3, ω_4. If ω_1, ω_2 are degenerate 'pump' fields then we find a that the remaining components must be equally spaced either side of the pump by some detuning Ω. For historic reasons (analogy with RF parametric frequency conversion) ω_s is known as the 'signal' field and ω_i as the 'idler'.

$$\Omega = (\omega_{pump} - \omega_i) = (\omega_s - \omega_{pump}) \tag{2.8}$$

2.2.3 Phase Matching Degenerate FWM in PCF

The ability to significantly modify the wave guide dispersion of a photonic crystal fiber (PCF) makes them an attractive medium for performing FWM. A fiber can be pumped in either its anomalous dispersion regime or its normal dispersion regime. In the anomalous regime group delay dispersion (β_2, second derivative of β) contributions to the wave-vector from each of the fields are negative and can in principle for sufficiently small values be balanced by the $2\gamma P$ from SPM. For greater powers we might expect a larger Ω to be possible, however this is in practice not the case since at sufficient power the combined third order effects interact and produce a super-continuum (soliton formation, fission and Raman acting together).

Phase matching in the normal regime seems unlikely since β_2 is now positive, however when pumping very close to the zero dispersion wavelength we can neglect β_2 completely and look at higher order dispersion. By writing the phase mismatch in terms of Ω for the degenerate case and then Taylor expanding about ω_{pump} we get the following:

$$\delta k = \beta(\omega_{pump} + \Omega) + \beta(\omega_{pump} - \Omega) - 2\beta(\omega_{pump}) + 2\gamma P \tag{2.9}$$

$$\delta k = \beta_2(\omega_{pump})\Omega^2 + \frac{2\beta_4(\omega_{pump})\Omega^4}{4!} + ... + 2\gamma P. \tag{2.10}$$

With a sufficiently large detuning Ω, the negative β_4 contribution can be balanced against SPM to produce widely spaced signal and idler. If a fibre is engineered to have two zero dispersion wavelengths close in wavelength, the phase matching function forms two closed loops. That is for a given pump wavelength two solutions for signal and idler are possible. The outer solution branch can be used with the advantage of reduced Raman in the final output. A fibre dispersion profile can be devised to produce the desired signal and idler from the desired pump laser (in our case a pulsed fibre laser at 1064nm).

For photonic crystal fibre the dispersion can be calculated numerically from FEM [26] or from plane wave decomposition [27], however there is an empirical dispersion model [28] covering the majority of the common parameter range. Numerical solutions for phase matching can be found, and from them a parameter set to fabricate the desired fibre. The stack and draw technique discussed in Section 5.3.3 is then used to produce the fibre corresponding to these parameters as shown in Figure 5-2.

2.2.4 Low Power FWM

To now consider four wave mixing at single photon level we need to use the interaction picture. In this picture we let the states and also the operators be time dependent. We wish to find the behavior of the creation operator for the signal and idler modes as a function of time. The evolution equation [29] is:

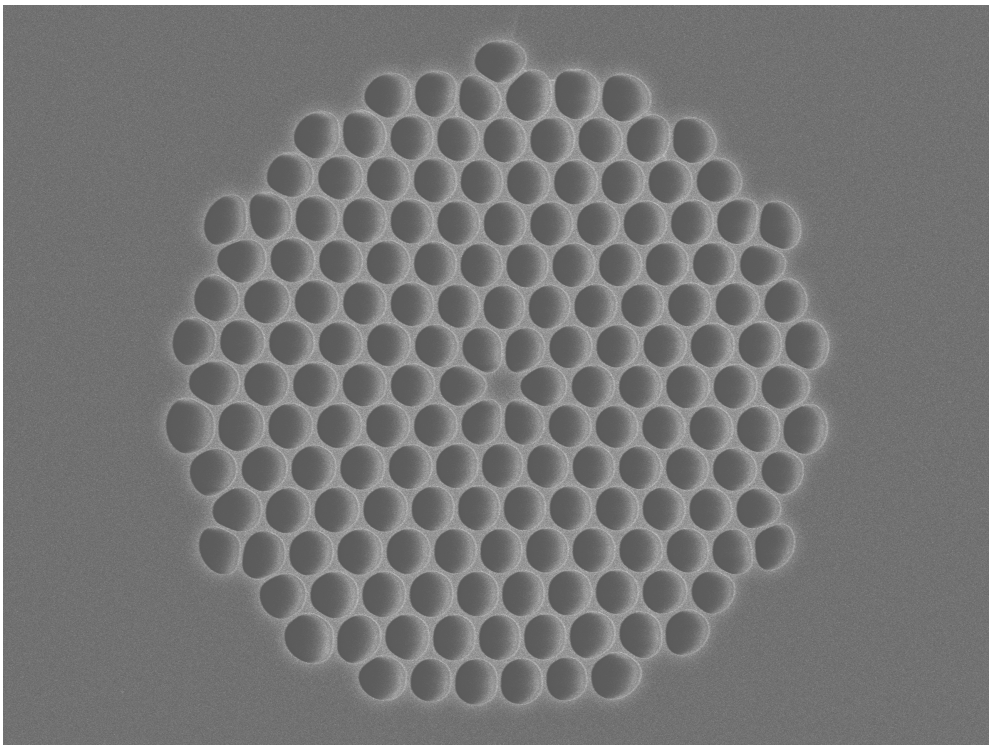

Figure 2-1: SEM micro graph of the final fabricated fibre structure. This design is particularly difficult to draw owing to the small air holes approximately 600nm across (section shown is overinflated to 1μ).

$$\frac{d}{dt}\hat{a}_k^\dagger = \frac{-i}{\hbar}[\hat{a}_k^\dagger, \hat{H}_I], \tag{2.11}$$

where $\hat{H}_I$ is the interaction Hamiltonian for the system. The Hamiltonian must be comprised of the steady state representing a harmonic oscillator and a contribution from the interaction we are studying, which we shall call the interaction Hamiltonian.

$$\hat{H} = \hbar\omega_s(\hat{n}_s + \frac{1}{2}) + \hbar\omega_s(\hat{n}_s + \frac{1}{2}) + \int\int\int dxdydz\epsilon_0\chi^{(3)}_{xxxx}E_pE_pE_sE_i \tag{2.12}$$

$$\hat{H}_I = \int dV\epsilon_0\chi^{(3)}_{xxxx}E_pE_pE_sE_i \tag{2.13}$$

The interaction is similar to the form shown before for bright FWM. The integrals are performed up to some practical limit in which all of the interaction volume is included,

in practice this will be over the length of fibre used and across it's 2D spatial mode field. Since in order for any non-linear interaction to happen the pump field must be strong, a fully quantum description is not needed. The pump will always be a strong classical field, and in our low power limit the photons removed from it to conserve energy will have a negligible effect on its amplitude. This approximation is referred to as the 'un-depleted pump' in most textbooks [30].

$$E_{pump} = E_0 \int_{\infty}^{\infty} \alpha(\omega, \sigma)(e^{-i(\Omega t + \omega t - k_{pump} z - \gamma P_{peak})} + h.c.)d\omega \tag{2.14}$$

Where E_0 is the peak amplitude, α is the spectral shape of the pump which is likely to be a Gaussian or $sech^2$ shape, the exponent represents a plane wave and Ω is the pump central frequency. We have included the non-linear phase term γ (responsible for SPM) but not the spatial distribution of the pump (which is normalized) since we are considering a single spatial mode of a fibre.

The electric fields for signal and idler can be replaced with electric field operators as in [30] which are similar in form to the previously stated pump field:

$$E_s = i \int_{\infty}^{\infty} \sqrt{\frac{\hbar \omega_s}{2\epsilon_s A_{effective} L}} \hat{a}^{\dagger}(\omega_s) e^{-i(\omega_s t - k_s z) + h.c.}. \tag{2.15}$$

We have broken the interaction volume down into the area $A_{effective}$ of the mode and the length L of the fibre. The conjugate can be entirely neglected in our case since we are about to apply the operator to the vacuum state, and the annihilation operator will prevent that term having an effect anyway. An equivalent expression is found for the idler, and both are substituted back into the Hamiltonian.

By solving the time evolution of the creation operator in 2.11 with this Hamiltonian,

$$|\Phi(t)\rangle = exp\{\frac{1}{i\hbar}\int_0^t dt H_I(t)\}|\Phi(0)\rangle \tag{2.16}$$

which expanded to first order is,

$$|\Phi(t)\rangle = \{1 + \frac{1}{i\hbar}\int_0^t dt H_I(t)\}|\Phi(0)\rangle \tag{2.17}$$

we can then substitute in the photonic crystal fibre parameters and field strengths for the classical pump fields, and apply the operator to a vacuum initial state for signal and idler to find:

$$|\Phi\rangle = |0,0\rangle_{s,i} + \int d\omega_i \int d\omega_s f(\omega_i,\omega_s)\hat{a}^\dagger(\omega_i)\hat{a}^\dagger(\omega_s)|0,0\rangle_{s,i}, \tag{2.18}$$

where we have grouped all the frequency dependence into a single function f that we shall call the joint spectral amplitude (JSA). The JSA is composed of two parts, firstly it contains the pump spectral distribution function that we chose before for α, and secondly a 'phase matching function' proportional to $sinc^2$ of the phase mismatch and the interaction length. The joint spectral amplitude cannot be directly measured, since in general it is complex, and we have no way to detect phase. We can measure the joint spectral intensity instead, however We cannot in principle determine from the joint spectral intensity the component Schmidt modes. Techniques do however exist to estimate [31] the Schmidt number numerically, and hence estimate factorability.

2.2.5 Factorable States

From a quantum mechanical perspective the pair of photons generated in FWM is a pure state, however through the phase matching function the pair are entangled in frequency and as such will display strong correlations when measured. If the proposed scheme where one photon is detected as a herald is to be used, we now have a problem that the remaining photon will be left in a statistical mixed state.

There are two possible routes to fix this problem, either the output must undergo selective filtering at cost to the brightness of the source, or the joint spectral amplitude must be created factorable. To be factorable we require the joint state to be the product of two pure states, one for signal and idler. Detecting either will now project the system into the pure state of the remaining photon. The factorability is ultimately traced back to the angle of the phase matching function (the function is approximately bi-gaussian, and its angle of rotation determines for a given signal wavelength, to what degree a particular idler wavelength is implied), which with sufficient dispersion engineering can be minimized. Specifically by pumping where the gradient of the phase matching contour is zero (Group velocity matching) [32] we can minimize spectral correlations. The group velocity matching is considered by taking the central lobe of the phase matching function to be approximately a Gaussian and Taylor expanding (about the zero phase mismatch). We find that to first order the differences in pump and signal/idler group velocity are important. It has been shown [32] that the angle of the phase matching function (and hence factorability) is dependent on the ratio of the group velocity mismatches. Either there must be no difference between the group velocities, or the signal and idler must have opposite mismatch (walking away from the pump in opposite directions at the same rate).

2.3 Three Wave Mixing in a Crystal

The second order nonlinear terms in Equation 2.2 imply that the susceptibility is polarity dependent; the degree to which susceptibility is orientation dependent is often referred to as optical 'rectification'. Any material with inversion symmetry cannot logically produce any such terms as they would identify a direction in the crystal that is not invertible. In some materials however, in particular uniaxial crystals, there is no inversion symmetry ($\chi^{(2)} \neq 0$) and three wave mixing can occur. Besides in bulk crystals, three wave mixing can also occur at a discontinuity in optical properties, for example at the surface boundary of any optical element. The surface second harmonic generation has proved an invaluable aid in microscopy where it provides effective contrast to otherwise invisible boundaries within biological samples[33].

Three wave mixing in bulk material requires energy conservation and momentum conservation in addition to the second order susceptibility terms. All crystals suitable for three wave mixing are birefringent which admits phase matching based around the angle at which the waves propagate within the crystal. Additionally the temperature dependence of the refractive index can be exploited to fine tune the phase matching.

In the case of fibre based four wave mixing, where a long interaction length is desired to counteract the small third order susceptibility, the guided wave behavior simplifies the nonlinear interaction to one dimension. In three wave mixing with its comparatively high susceptibility and crystalline materials a free space optical approach is typically used (short waveguides can also be used). The free space optical interface allows non collinear waves to be used, opening up possibilities to phase match by controlling the angle between the interacting waves.

Although all three wave processes are mathematically equivalent, specific names are given to cases as shall now be discussed.

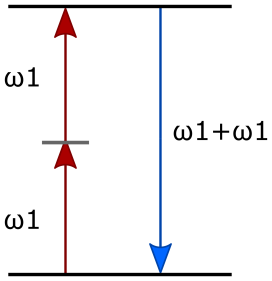

Figure 2-2: Diagrammatic representation of Second Harmonic Generation. Two input photons of identical energy excite the material polarization, and are subsequently re-radiated as a single high energy photon.

Second Harmonic Generation

When two waves of the same frequency are incident in a nonlinear medium with sufficient power, a new wave at twice the frequency can be produced. Since the two input fields are identical they must be either collinear (in which case the second harmonic light is also collinear) or come together at some opening angle symmetrically about the second harmonic light, in order to conserve momentum.

Sum-frequency and Difference-frequency Generation

In much the same way as second harmonic light is produced by degenerate pump light, sum and difference frequencies can be produced by non degenerate input waves. As before, momentum and energy must always be conserved in the interaction. Energy is conserved in exactly the manner for which the process is named; energy being directly proportional to frequency, sums and differences are inherently energy balanced. Momentum conservation however is not as simple since three distinct waves must now propagate together.

The existence of a three wave phase matched solution is not guaranteed at all frequencies and is dependent on the dispersion properties of the material. Combinations of

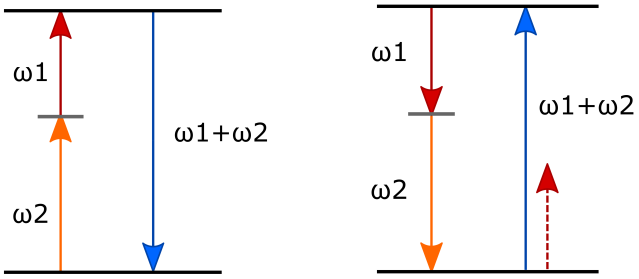

Figure 2-3: Diagrammatic representation of Sum Frequency Generation and Difference Frequency Generation. Two input photons are absorbed by the material, and subsequently re-radiated as a single high energy photon. Alternatively for difference frequency generation a seed photon causes parametric down conversion at the difference frequency, if the resulting process is suitably phase matched (or within some phase matching bandwidth). Here the population of the lower energy input photon is increased in proportion to the difference frequency output.

temperature and angle of propagation within the crystal can phase match many scenarios. Additionally by polling the crystal's characteristic direction periodically to produce a fourth effective momentum component is sometimes employed. Samples produced by electrically polling the crystal at a designed pitch perpendicular to propagation can additionally employ some form of apodization.

2.3.1 Spontaneous Parametric Down Conversion

In the previously mentioned variants of three wave mixing there have always been two waves that are *input* or at least directly controlled; the third being dependent on the state of the others. In the case of spontaneous parametric down conversion we input only a single field and two fields are produced as output. The produced fields may or may not be degenerate, and in general the energy distribution between the two fields is determined by the phase-matching. Conserving momentum implies a relationship between the input and output momenta, or more practically the relative directions of propagation.

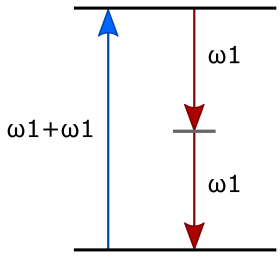

Figure 2-4: Schematic representation of spontaneous parametric down-conversion converts a high energy photon (blue) to two output photons at lower energy. The degenerate case is shown however in general the process is non degenerate.

The specific angles required for a phase matching solution are not necessarily a geometrically unique solution for the crystal; other orientations about some axis of the crystal may also phase match. In the reciprocal process (SFG) the orientation about this rotationally equivalent axis of the crystal plays no important role as the output wave is oriented along this axis. In down conversion the equivalence of the possible orientations causes the output light to be emitted into an annular cone. Each photon is produced diametrically opposite its pair in order to conserve momentum, however the emission is into a superposition of modes oriented around the annulus. For a non-degenerate case two annuli are produced with opening angles appropriate for the angular momentum component of each wave.

The spontaneous part of the process refers to the random down conversion statistics seeded by vacuum fluctuation [14] [15]. The process can be considered a form of stimulated emission where the excited polarization state of the material is stimulated to emit a photon by the presence of a virtual photon from vacuum fluctuation. If an excess of photons are provided externally to *seed* the down conversion by stimulated emission the emission statistics are changed, this can be considered equivalent to the difference frequency generation, noting that the population of the seed light actually increases in the process. In either case the process only proceeds if phase matching is achieved.

2.3.2 Polarization of Three Wave Mixing

In addition to the Three Wave Mixing (TWM) parameters presented, polarization of the input and output waves follows from the birefringent nature of the crystalline materials. When using the birefringence of the nonlinear crystal to phase match TWM there are two distinct solution branches called type I and type II phase matching; referring to either identical or orthogonal polarization respectively of the two fields produced (or the two input fields in sum-generation or SHG). The schemes of phase matching which do not use polarization angle adjustment are termed *non-critical phase matching*, and generally rely on temperature or other external condition.

In type II phase matched SPDC a photon is produced in each polarization. Due to the birefringence of the crystal the output photons are now emitted onto two annuli displaced from one another by some angle, dependent on crystal orientation. There are two important methods that can be employed as a result of this displacement. There is now a collinear solution possible where both photons are emitted onto the axis of the input wave, simplifying the optical alignment significantly. The two collinear photons can be separated by a polarizing beam splitter and easily interfaced to whatever optical system is desired.

An additional but noteworthy method is collecting both photons from an intersection point of the two annuli into a single optical mode; we have no knowledge from which annulus the photon originated. If we can also collect the other crossing point the joint state produced is now entangled in its polarization degree. This can be an effective way to produce entangled pairs, or perform related entanglement operations [34].

In addition to the spatial walk off and angular parameters, some amount of group velocity mismatch occurs. For systems employing very short pulses this can be significant. The thickness of the material is proportional to the induced relative delay. The effect is broadly equivalent to *temporal walk off* within the crystal. Phase matching

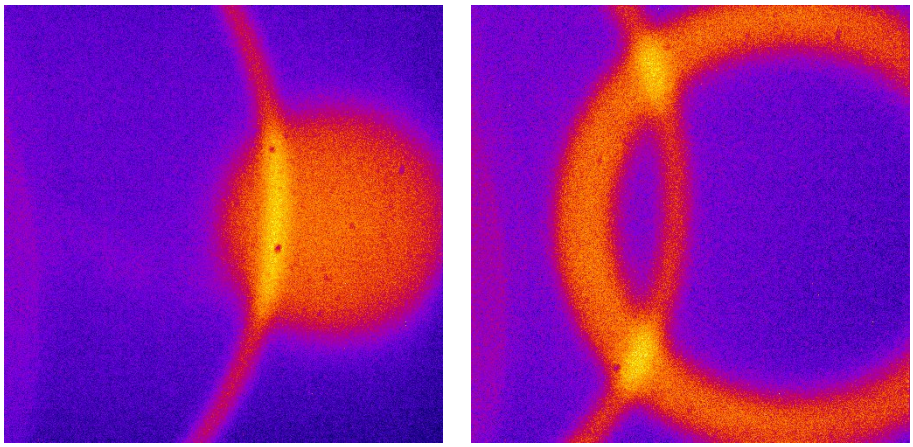

Figure 2-5: Parametric down conversion light from a β-BBO crystal at 810nm, imaged with an EMCCD camera, 10nm bandpass filter, and a Schott wide band pump absorption filter. The left and right panes demonstrate different phase match conditions (rotation of the crystal approximately 2 milliradians) resulting in imbalanced (but conserved) momentum between the two output polarizations.

solutions produce different group velocity mismatch (GVM), and this should be taken into account when selecting a phase matching solution. Ultimately the GVM places limits on the achievable phase matching bandwidth, through the reciprocal relationship with spectral bandwidth.

2.4 Heralding Operation of a Photon Source

Producing suitable photons for use in quantum photonic experiments is critically dependent on the emission statistics of the source, and to some degree the indistinguishably of the produced photons. Photons produced by parametric nonlinear processes such as four and three wave mixing are emitted as pairs allowing the timing of either photon to be inferred from the other.

Photons produced as pairs possess shared quantities such as total energy, and total momentum. Most importantly the simultaneous nature of the emission of two photons

provides a correlation that can be exploited to learn the timing information of one photon by measuring its counterpart. Further the resulting modified statistics with selection can allow experiments that would otherwise only be possible with a deterministic photon source.

The general principle of heralded delivery is to detect one half of a photon pair, and use the gained timing information to *herald* the arrival of the pair's counterpart. The herald signal can post select detection events; effectively deciding which detections to discard and which to keep. By keeping only events that have the desired correlation with the herald photons the resulting data may be treated as if it was derived with a deterministic photon source.

The destructive measurement of the herald photon can be described as a *projective* operation on the remaining photon. The exact properties of each photon is unknown at the point of generation; only the total properties that are implied by phase matching. If for example a specific herald was found to be slightly higher in energy than the mean value, the converse would be implied for the remaining signal photon. As per the prior discussion, for factorable states we do not gain any new implied information; factorability is a highly desirable property for a photon pair source. If additional knowledge is gained by the measurement of the herald (beyond the timing information) we have implicit information about the signal. Similarly if we introduce a statistical bias in the detection, say for example wavelength dependent efficiency, we introduce an undesired bias into the signal.

In order to produce indistinguishable photons, uncoloured by the projective measurement a number of steps may be taken. Simply filtering out cases that might be distinguished by a detector will suffice to remove unwanted information, however the reduced photon number produced is undesirable. To some degree the phase matching conditions chosen will influence the distinguishability, as will the achievable detector parameters. In producing a practical photon source these factors must be traded off

for the configuration most favorable to the experiment at hand.

Timing information from heralding is generally recorded and processed post-experiment however a number of feed forward mechanisms can also make use of the herald signal as shall be discussed in Chapter 4. A convenient alternative to explicit time recording is to correlate the delayed herald detection signal with some subsequent event, and count the occurrences of such correlations. Electronics for performing this operation as discussed later in Chapter 3.

2.5 Equipment Considerations

2.5.1 Single Photon Detectors

Detecting photons requires a macroscopic outcome from the influence of a single photon of incident light. The approaches taken can broadly be classified as either generation of carriers which are then amplified by some process to a detectable current, or to the perturbation of a system *on a knife edge* with the macroscopic effects of the perturbation being evident in some manner.

Superconducting Techniques

A superconducting material can be used as a detector in a number of schemes; the most popular three being transition edge detection, nano-wire detection, and assisted tunnelling.

A superconductor with a bias current flowing can be transitioned to normal conduction by the addition of a very small amount of heat. Since quenching the super conductor is not desirable, a scheme is typically employed where a constant current is fed into a load parallel to the superconductor such that the current is shared. The increase in

resistance of the super conductor causes the current to *steer* so that it decreases in the superconductor and increases in the load resistor, effectively producing a negative feedback which prevents the runaway heating of the superconductor. The current fluctuation is then sensed and can infer the radiation power incident. As the whole system is already at cryogenic temperatures a commonly employed sensitive current measuring technique is to magnetically couple a SQUID device [35].

An intrinsic trade off is formed in devices of this type in the degree of coupling between the superconductor and the temperature bath; without significant coupling the device will be unable to cool back to low impedance, (reset time) however the sensitivity of the device is impacted if too much heat is moved to the bath rather than allowing the temperature rise in the superconductor. Detectors of this type have extremely high performance in sensitivity but are relatively slow (by around two orders of magnitude) compared to avalanche diodes. Significant cryogenic equipment is required to operate the detector which is also a strong detraction from the scheme's appeal.

An alternative strategy is to use a very thin piece of superconductor and allow a quench to occur. Such an approach is easier to read out as a significant change in current occurs and very fast; the dominant timing error being due to the position along the nano-wire at which the quench begins. The material of the wire is sufficiently thin that at the point of incidence a single photon is able create a local hot spot and begin the quench of the whole wire. Bias current is removed by the kinetic inductance of the nano-wire (and possibly an additional series inductor) which creates an effective time constant during which the bias will flow through the input impedance of the amplifier. So long as the cooling rate of the superconductor is faster than the inductive time constant, the device will automatically reset.

The nano-wire detector is both fast (reset time and jitter can be in the order of 100ps) and relatively simple for readout purposes. Unlike the transition edge sensor which behaves as a bolometer, in the quenching behaviour the information about the amount

of incident radiation is lost. Effectively the nano-wire detector can determine with good timing quality the arrival of one or more photons, whereas the transition edge detector can determine the number of incident photons with reduced timing precision, and with a slow reset.

Carrier Generation Techniques

Incident photons above a specific energy threshold may be able to ionize a conductor or liberate a bound electron into the conduction band of a semiconductor. The relevant energies being determined by the surface work function in the case of an ionization or the band gap of a semiconductor. In a photomultiplier tube a photo-cathode coated with low work function material emits an electron into the partial vacuum of the tube. In order to amplify the electron flux produced to a measurable level, an electron multiplying technique is used in which successive electrostatic acceleration and impact ionization of a sequence of electrodes produces an exponentially growing current pulse.

A semiconductor junction through which an electric potential is applied behaves in a similar manner. An impinging photon creates an electron-hole pair which owing to their charges are separated from one another by the electric field. If the electric field is increased carriers are able to reach higher kinetic energy before inevitability colliding with atoms of the material after some mean free length. If the energy is sufficient upon collision one or more additional carrier pairs may be liberated and so the current exponentially increases. The voltage at which this can occur is know as *breakdown* and is characteristic of the material (defects etc.). By operating in the bias range above breakdown (so called Geiger mode) a single carrier pair creation can cause the material to rapidly become conducting.

Once the conduction has begun it will continue as long as sufficient current is supplied. In order to reset the device an active quenching circuit is employed to disable the bias

and re enable it once conduction has stopped. The rate at which this is possible depends among other things on the design of the quenching circuit and on the capacitance of the diode junction, which in turn determines the re-charging time. Additionally the junction may be cooled to reduce a contribution from thermally generated carriers which are not of detection interest.

The performance level available from Avalanche Photo Diodes (those optimized for use as described above) is typically faster to respond and reset than transition edge detection allowing higher throughput but are not as fast as state of the art nano-wire detectors. The great advantage of APD detectors is the simplicity of use without cryogenic support equipment. Avalanche Diodes are mass produced for a number of industrial and telecommunications applications, allowing us to take advantage of the lower cost and high availability and maturity of the technology.

Composite Detectors

The *click* type detectors discussed in the preceding sections which produce a binary outcome for an input of one or more photons, are by far the most common single photon detectors available. Real detectors of this type are not ideal, and are characterized by the probability of firing for a single photon input.

When multiple photons impinge simultaneously on a click type detector the probability of a detection increases. It is effective to consider a set of probabilities for firing given a specific number of photons incident,

$$p(detection|N) = 1 - (p(nodetection|1))^N, \tag{2.19}$$

where N is the number of incident photons and we have assumed that the probability of failure to detect a photon is independent from failure to detect another photon. Not

all detectors behave in this manner; natively number resolving detectors (bolometer type devices) are also not ideal, sometimes failing to detect one or more photons from the input state. The probability for reporting a detection of a number of photons m, having received N photons replaces the expression in equation 2.19. The conditional probability takes a binomial form with m successful contributions from the detection efficiency and, $(N-m)$ contributions of $1-\eta_{detection}$ from the unsuccessful detections

$$p(detect-m|N) = \binom{N}{m} \cdot (\eta_{detection})^m \cdot (1-\eta_{detection})^{N-m}. \tag{2.20}$$

A hybrid option is to share the input photons randomly amongst a number of click type detectors as proposed by [36]. The resulting statistics are an approximation of a true number resolving detector using only binary detectors and power splitters. The advantage posed by such an arrangement is twofold; binary detectors have by and large a faster response and reset time which is advantageous to heralding rates. The ability to determine the number of photons in a heralding event can be exploited in a source operated with a higher probability of generation (higher pump power). The undesirable multi-pair generation events can be detected and ignored, and so not reduce the further usability of delivered photons.

The practical use of a pseudo photon number resolving (PNR) scheme of this type requires a more advanced analysis of the effects of individual detector efficiencies as is presented by [36]. Detector tomography may be employed to determine the relevant parameters and the efficiency determined using the generalized Klyshko scheme presented in [37].

Detectors Used

Throughout the work presented here three single photon sensitive avalanche diode detectors were used: Perkin Elmer / Excelitas SPCM-AQRH-12 (two units) SPCM-

AQ4C (one unit) and the IDQuantique ID210 (two units). The former two models are Si avalanche diode counters with inbuilt electronics and detection efficiency approximately 50% at 800 nm for the AQ4C, and 62% at 800 nm for the AQRH. The ID210 is an InGaAs avalanche photo diode unit with extensive support electronics including an in built computer and logic for trigger and output discrimination. The ID210 is configured for user variable detection efficiency up to 25% @1550 nm however the unit was operated at 10% efficiency in order to reduce dark count contribution. All units contained inbuilt thermoelectric cooling systems to control APD junction temperature.

Dead time (reset time) for the three detectors is significantly different. The SPCM-AQRH-12 units have a 22 ns dead time and the specific units used had dark count rates of 70 and 100 counts per second. The SPCM-AQ4C has a dead time of 50 ns for each of its detector outputs, and a similar 100 counts per second dark count rate for each channel. The ID210 dead time is a minimum of 100 ns but can be artificially extended if desired; the achievable dark rate is highly dependent on the mode of operation as the gated/triggered mode pulses the APD drive. Under the experimental conditions during the multiplexing work presented in Chapter 4, the dark count rate was approximately 20 counts per second with peak gate rate of 5MHz.

2.5.2 Pulsed and Continuous Lasers Used

The laser chosen for the operation of the photonic crystal fibre based photon pair source is a Fianium Femtolase FS-1060. The laser is an optical fibre mode locked oscillator in combination with a Ytterbium doped fibre amplifier. The laser provides pulses approximately 200 fs long at a total output power approaching 0.5W. The spectrum is not transform limited and is filtered by a double pass grating monochromator constructed externally to the main laser. The laser incorporates a free space section at its output comprising collimation, limited pulse picking capability (divide by 10 only), and a transmission grating based pulse compressor. The specific mode locked pulse frequency

is critically dependent on the cavity length as determined by the length of the optical fibre it is fabricated from; nominally a 10MHz oscillation is chosen however the precise oscillation frequency (9.987 MHz) is instead found due to the length error introduced in construction.

Due to the non-standard frequency, and possible thermal drift in frequency, it is necessary to regenerate a clock signal with matching frequency and stable phase relationship to the laser pulse train. In addition to the variations in frequency the laser exhibits significant variation in power, such variations introduce rise time variation when detected and so contribute a timing jitter. Phase stability measured over a large number of pulses between the laser and a derived (from detection) clock signal is unaffected. That is to say the instantaneous frequency variations manifest significantly, but over many pulses the frequency of the laser and derived signal are identical. Techniques for minimizing any impact from the apparent mistiming are discussed in chapter 3 along with any impact from these factors expected when coincidence counting.

2.5.3 Telecommunication Parts

The experiments presented here involving guided waves make significant use of mature telecommunications parts and techniques. The availability of extremely low loss ($<$ 0.2dB per kilometre) single mode optical fibre allows losses arising from routing light from one component to another to be largely ignored; when compared with the losses from other optical parts it has limited significance for overall system losses.

Joining fibre components together is relatively straightforward due to the availability of automated 'fusion splicing' in which fibres are melted together in a precisely aligned way. The losses incurred by fusion splicing depend in part on the quality of the alignment between fibres and the correct parameters for heating and motion during the splice. Since the alignment is performed automatically based on the outer sur-

face of the fibre, any displacement of the mode field from it's ideal central position will introduce significant loss. The practically obtainable results range from almost undetectable loss, to approximately 0.2dB for industry standard fibres for which the ideal parameters and or strategies have been developed. Joining custom optical fibre with itself or with telecommunications fibre has variable results. An approximation used throughout in the discussion and analysis presented here is that a splice joint will represent approximately 0.1dB of loss when using standard fibres.

Telecommunications optical components other than the fibres themselves are generally constructed in one of three ways. A device can be comprised of post processed fibre, as is the case of inscribed Bragg gratings, tapered directional couplers and wavelength division multiplexers. Devices of this type inherently provide a fibre interface for connection to the next stage of the system, where these interface fibres (often referred to as *pigtails*) are of a standard telecommunication fibre type they can easily fusion spliced together. Another technique often employed is to incorporate free space optical components into a sealed package, and to use a collimator or launch optic to interface to a standard optical fibre. Very often parts will also be supplied with a short section of fibre (pigtail) already aligned to the optical mode and fixed in place permanently. Components of this type can also be used in the same manner as post processed fibre components. Thirdly and not dissimilarly to the other kinds, for semiconductor substrate components which incorporate a wave guiding structure, a direct interface without additional free space elements can be produced. It can be seen that the paradigm of standardized fibre pigtail with fusing splicing allows complex systems to be produced with great simplicity.

2.6 Two Specific Sources Used

Two photon sources are used for the experiments discussed in this thesis each with characteristics to suit the application. The source of photons used for multiplexing experiments is a fully fibre integrated source based upon four wave mixing as discussed previously in 2.2.3. The photons generated from the integrated source are ideal for use in conjunction with the aforementioned standard telecommunication parts. Specifically the non-degeneracy has been taken advantage of to simultaneously target the idler photon to telecommunication fibre, and the signal photon to the peak absorption of Si avalanche diodes.

The photon source used in conjunction with fibre to implement quantum random walk or other complex interferences is degenerate and centered on peak detection efficiency for a Si avalanche diode. In order to produce two photons near 800nm the energy conservation requires high energy pump photons. Both the scattering losses and material absorption in fibre (fused silica) for blue wavelengths make an integrated source impractical. Free space parametric down conversion in β Barium borate was instead used; the 800nm outputs being collected into fibre modes for subsequent use.

2.6.1 Fibre Integrated FWM Source

The fibre integrated source [38] was developed as part of efforts to build a spatially multiplexed photon source; the fibre was designed by Dr Francis-Jones [39] and refined and produced jointly over the course of the year preceding the temporal multiplexing experiments. In addition to the short length ($30cm$) of photonic crystal fibre, commercial fibre spliced Bragg gratings, wavelength devision multiplexers, and custom 'bandgap' photonic crystal fibre filters were used to block residual pump light and separate the idler and signal photons into separate fibre modes. The source incorporated a custom produced mode matching taper (adiabatic impedance transformer) allowing

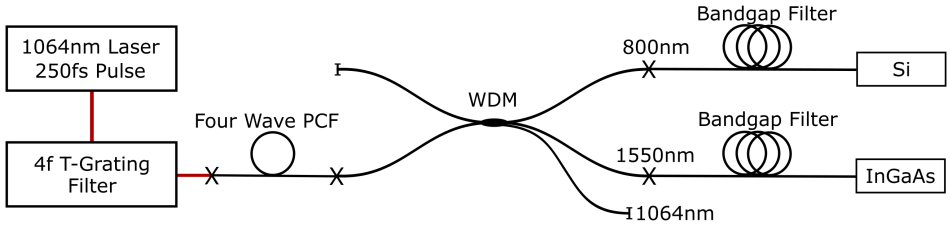

Figure 2-6: Schematic outline of the PCF fibre photon source. For brevity additional pump rejection filtering in the form of fibre inscribed Bragg gratings are not shown. A novel photonic band gap fibre wide band filtering was employed and is discussed in detail in [39]. Photon pairs are created by four wave mixing in the PCF fibre, specifically around 1550nm and 800nm in order to interface well with telecommunications fibre and parts, and Si herald detectors respectively. The third port of the wavelength division multiplexer contains the majority of unconverted pump light, and is a useful means by which to monitor the power coupled into the PCF.

efficient collection of light into the comparatively small telecoms fibre core. Free space polarization and wavelength filtering were implemented in order to optimally pump the four wave mixing from the available laser (2.5.2).

The implementation used in the prior work served as a basis for the further temporal multiplexing experiments. In the later work an additional free space AOM was incorporated, an alternative laser pulse train detector arrangement, alternate electronics for controlling a spiced shutter (*Noise Gate* see. [40]) and an additional InGaAs avalanche photon detector with improved efficiency. The spliced section for separating the output photons remained unmodified. A significant amount of additional detail regarding the phase matching specifics and performance data for this source is available and explained in Dr Francis-Jones' thesis [39].

2.6.2 Free-space β-BBO SPDC Source

Two arrangements of a BBO parametric down conversion source were constructed, one each operating with type I and type II phase matching. The methods discussed in 2.3.1 were employed in the case of type II phase matching in order to produce a collinear (or

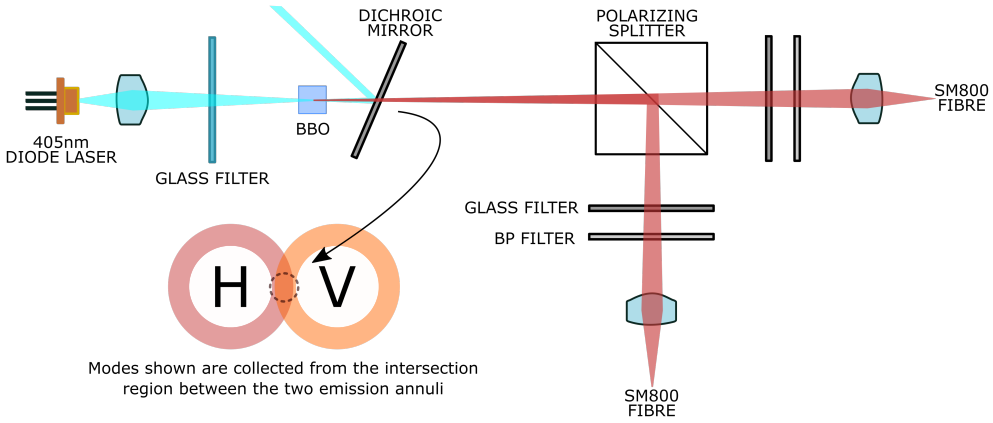

Figure 2-7: Outline schematic of the almost-collinear photon pair source using a β BBO crystal cut for type II phase matching at 810nm with 3 degree opening angle. A surplus Blue-Ray $405nm$ laser diode is focused into the BBO crystal via minimal cleanup filtering. The majority of unconverted pump light is removed after the crystal with a dichroic mirror. At the focus pairs of photons at $810nm$ are produced, and are subsequently separated by polarization and coupled into single mode optical fibre, ensuring only a single mode is selected from the output light. A $10nm$ bandwidth filter at $810nm$ is used to reject any remaining unwanted light, assisted by a wide band glass filter.

nearly collinear) source geometry. In each case a 405nm laser diode (*Blue-Ray* player laser diode replacement) with approximately 20mW output power (thermally stable without forced cooling) was employed as a pump.

Due to the high brightness of the source it was possible to directly image the output light onto an Electron Multiplying CCD camera, as in Figure 2-5. The focusing and phase matching conditions were explored with the aid of the camera, and an initial configuration and mode overlap was readily achieved without photon counting the output modes. After initial alignment, correlation counting was used to select a suitable correlated mode pair from the down converted output.

For each of the constructed sources a large $5mm$ by $5mm$ by $5mm$ crystal was used allowing a wide variety of focusing conditions to be explored. The bandwidth of the

pump laser and of the phase matching was significantly larger than required; for simplicity the majority of the output light was removed by a 10nm narrow bandpass filter centred on 810nm. The 810nm output is able to be guided in standard SM800 optical fibre with a 4μm core. The relatively large $10nm$ bandwidth was chosen as a compromise in order to allow sufficient power for ease of alignment.

Chapter 3

Electronics for Photon Counting Experiments

Experiments with photons can be conducted in broadly speaking one of two ways, by measuring a collection of photons and establishing the integrated behaviour, or by attempting to count each photon as it arrives. The latter technique makes sense only if a detector capable of detecting single photons is available. As discussed previously typical photon counters, including the ones used here, operate on an avalanche process and are unable to resolve the number of photons incident. Detectors of this type produce a pulse output of arbitrary height and duration but for which the leading edge is reliably timed with respect to the incident photons. This chapter describes the suite of electronics that I developed to deal with these signals.

3.1 Challenges for Data Acquisition

3.1.1 Correlation Counting

Analyzing pulse signals can be performed in a number of ways; with preference depending on the application. A simple method is to record a time series of the input state of a signal, the sampling being at least twice the frequency content of the input, i.e. equivalent to the frequency associated with a period of half the coincidence window. For two channels sampled at 1-bit resolution and a coincidence window of 3 ns, an output bit stream of 1.34Gb/s is produced. Although the data is probably highly compressible (a scheme such as Run Length Encoding (RLE) might be used here), the raw data rate exceeds the capacity of a standard 1G Ethernet connection.

An alternative strategy is to transmit events along with a counter representing the time at which the event occurred. This approach uses significantly less data bandwidth for the cases where the number of events is very much less than the number of samples. However with larger event rates approaching half the sample rate the scheme tends to be M times less efficient, where M is the number of bits of information needed to transmit the event time. Clearly such a scheme has merit, but is still capable of producing significant amounts of data with modest count rates. Schemes of a similar character to this type of arrangement are in fact used for importance sampling in equipment like digital storage oscilloscopes (*segmented memory*). On every trigger a burst of information can be captured to memory along with the time base position, building up a recording longer than the available memory in short recording bursts located at the interest points.

If the processing that will be applied to the captured data is known ahead of collection, as it is in the case of photon counting, bandwidth can be saved by performing the processing in real time and recording the results. The quantities of interest here are the raw rate from each counter known as *singles*, and the rate of coincidence between

channels. The need to make adjustments and alignments which influence the counted quantities requires that the otherwise simple integration of counts is split into smaller integration periods and the intermediate results made available. Although eventually all these component sums will be combined, the ability to spot any change of contribution over time is invaluable to practical experimentation. With the integration split so as to provide a 1Hz update rate, the data bandwidth required is a trivial quantity equal to the combined width in bits of the data registers per second.

3.1.2 Timing Alignment

Signals from correlated sources are not always coincident at detection. Depending on coincidence window size there may be problems for coincidence counting if asymmetric delays are not compensated for. Propagation through free space optics, fibre optics, and electrical cables incur a significant delay. A typical 50Ω coax such as Belden 8241 has a velocity of 66%c. The dispersion of optical fibers make delays wavelength dependent, however for illustration Corning SMF28e @ 1550nm has a group index of 1.4682 giving a velocity of 0.681c.

A time skew equivalent to a coax length of just 70cm is able to prevent the overlap of correlated pulses. Non-branded coaxes in our laboratory measured on average 3.1ns for 1m nominal terminated lengths. Furthermore path length differences in the optical fiber before the detection stage are able to skew time of arrival in an equivalent manner. A third unavoidable delay is presented by electronic stages through which a pulse has to pass, for example through a distribution amplifier. In a practical laboratory situation with necessary lengths of coax, spliced fiber optics, and detectors from different manufacturers with different response time, some amount of timing skew is inevitable.

Problems with skew were anticipated and equipment was on hand to provide a variable delay. The need for a greater degree of control both in signal integrity and in ease of

operation while in a darkened laboratory necessitated developing alternative equipment for adjusting the time delay of signals. For a number of experiments the available number of delay channels required was exceeded providing further impetus to develop an in-house solution.

3.2 Introduction to the FPGA

3.2.1 Physical Logic Implementation

Programmable logic devices are integrated circuits designed to provide a logic function determined at some time after manufacture, i.e. programmed depending on the end user task. Devices of this type provide a custom circuit without the significant costs associated with traditional application specific integrated circuit (ASIC) design. Architecturally speaking a diverse range of programmable logic devices exist to suit different use cases, an FPGA is only one specific type.

Before the introduction of programmable logic a custom logic circuit was typically constructed from integrated circuits containing a few logic gates. A designer would use only as many gates as needed and would have complete flexibility to connect any possible path given enough physical PCB area to make connections on. Large designs would take up a large physical area and represent a significant investment in efforts to route. Additionally the power requirements for a large number of individual integrated circuits is in practice high due the buffering of signals and currents up to levels suitable for interconnecting. As the number of gates increases there is a strong incentive to integrate greater numbers of gates into reusable blocks that perform common operations such counters, encoders and flip-flops.

Simple logic functions can be constructed from fundamental combinatorial elements such as AND, OR, and NOT. For a general logic function with a given number of

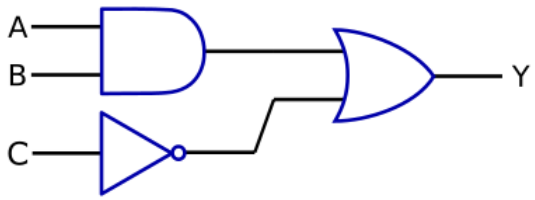

Figure 3-1: An example of a simple three input logic function represented as standard logic gates.

$InputA$	$InputB$	$InputC$	$OutputY$
0	0	0	1
1	0	0	1
0	1	0	1
1	1	0	1
0	0	1	0
1	0	1	0
0	1	1	0
1	1	1	1

Table 3.1: Logical truth table associated with the function shown in Figure 3-1.

inputs and a single output we can completely define the function if every input state is mapped to an output state. We need 2^n bits of information where there are n inputs to completely define the transfer function. Clearly there are many possible arrangements of gates that could produce the same logic function but we can ignore this and (with the exception of transient behavior) treat all these circuits as equivalent. An approach of this sort is known as a *truth table*, an example of which is shown in 3-1 for a simple 3 input logic function.

Logical structures that include a feedback path can be made that have a behavior which depends on a state at a previous time. Bi-stable structures such as flip flops or registers allow a system to have a 'memory' of a previous state. With one or more flip flops and logic functions it is possible to build a state machine.

Real logic gates have an unavoidable propagation delay; the time at which the output of a network of gates reaches a stable state depends on the path length and the technology specifics that the gates are produced in. The propagation delay produces two significant

effects. Firstly the delay before an output can be read must place a limit on how fast an input can change without rendering the corresponding output meaningless. It may also be worth noting that the delay is dependent on the number and type of gates being passed though and not directly on the complexity of the logic. Secondly if, as is often the case, multiple inputs are used to derive an output, and the inputs pass though differing path lengths, the output may make more than one transition on the change of an input. That is to say there are often output states during the *settling* that are neither the state relating to the initial condition or the final condition.

A method universally used to deal with this problem is to sample the output of a system only after an amount of time that exceeds the settling time. This is performed by introducing a *clock* signal which upon a transition causes a flip flop or register circuit to *latch* the value. Naturally latch circuits are also subject to timing requirements and due to their prevalence have nomenclature associated with these timings. *Setup time* is the amount of time a signal has to be present before the arrival of a clock edge in order to be successfully latched. In a similar fashion the time that a signal must remain stable after the clock edge is referred to as *hold time*. There are the analogous notions of reset and release times for an asynchronous signal (typically a reset) which must enter a latch and create behaviour that is not related to the clock.

A design pattern used ubiquitously is to form a chain of alternating logic gates and latches, with all latches being driven by the same clock. In this way a calculation or other logic process executes over a number of steps, and on each clock the previous intermediate result is latched. A pipeline like structure is formed allowing a vary large number of gates to produce a complex and yet reliable output, the only drawback being that n clock cycles were required to propagate the calculation. Logic of this type is said to be *synchronous*

An FPGA consists of a large number of 'logic blocks' (a general manufacturer term) each consisting of a look up table or LUT, an output register, and optionally some

dedicated extra logic for providing *carry* signals for the situations in which the block forms part of an adder. The LUT design typically performs the logic function by way of a binary tree of multiplex gates as shown in 3-2. The input to the multiplex is connected to a memory cell outside of the design which stores a pre-programmed value equivalent to the truth table values. The selection lines to the multiplex act as the inputs to the LUT for the users design. An input state presented on the LUT input lines selects one of the pre-programmed values to be routed to the output. The latch provided with each LUT allows a synchronous design to be produced, however provisions are made to allow the latch to be bypassed since not all designs will always place a latch after every LUT. A simplified diagram of a real logic block for the lattice MachXO2 FPGA is presented in 3-3 for reference. Real world logic blocks found in commercial FPGAs are heavily optimized by the manufacturer for efficiently implementing designs, the choices of LUT specifics are often not a concern for the end user.

In order to build more complex systems, logic blocks can be connected to one another in a network, the routing resources required to maximally connect any block to any other will naturally grow exponentially and would typically be highly underutilized. An alternate *fabric* or *mesh* routing is used instead where a limited number of buses are provided in rows and columns in between logic blocks. Programmable interconnections between buses exist at the cross-points and at the logic blocks allowing great flexibility but significant propagation delays, somewhat dependent on the length of route. There are a number of routing resource types in a modern FPGA to suite typical requirements and design trade-offs. For example routing a clock which must have reliable phase and minimal delay as it fans out to drive many locations. Both the great number of gates (electrical loads) driven by a clock, and the stringent timing requirements mean that greater resources including power have to be used. There are numerous different routing resource types and many trade-offs in their relative abundance and length, in order to produce an integrated circuit which can implement most user functions efficiently.

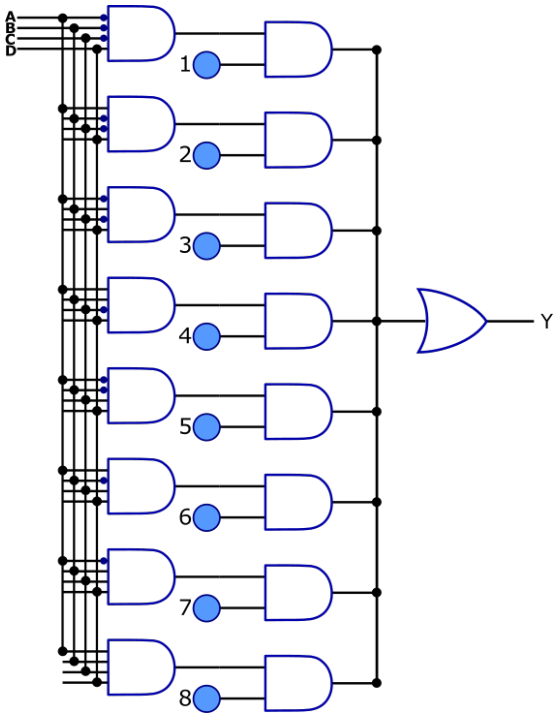

Figure 3-2: A simple four input LUT made from multiplexing logic. The four input lines A,B,C,D feed into AND gates; each gate has negated inputs in one of the possible binary combinations. When a specific input combination is presented only one AND gate is activated. The values on the signals numbered 1 through 8 are derived from an SRAM memory and form the programming of the LUT. The output value Y is selected from the signals 1 through 8 when its corresponding AND gate is active. Stored data is multiplexed onto the output according to the inputs A,B,C (input D behaves as a gate allowing expansion of the scheme to larger widths).

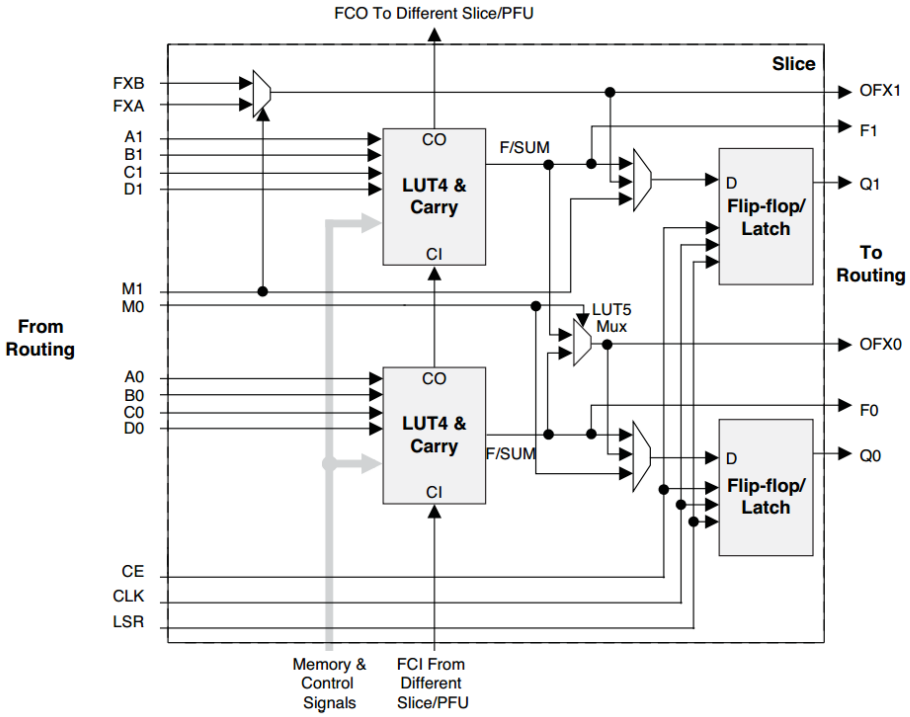

Figure 3-3: A logic block within the Lattice Semiconductor MAchXO2 series FPGA (known as a *slice* by the manufacturer) containing two 4-input LUTs, a pair of output latches and minimal routing options to configure the LUTs as independent or as paired to form an effective 5-input LUT. Note the carry inputs and outputs extend out of the slice to reach other slices, providing a carry chain for adding numbers efficiently.

Finally to be useful an FPGA must sample signals from outside the integrated circuit and make internal signals available to the outside. An external connection to the FPGA fabric can be as simple as a single logic buffer which can be routed the same as any other internal signal, or a comprehensive multi-standards compliant interface with variable voltage thresholds or drive strengths, pre-emphasis and equalization, and in the most modern FPGAs entire state machines that can provide encoding and automatic compensation for electrical conditions. The blocks within an FPGA that handle connection to the outside are referred to as PIO, and are also subject to optimization; a typical FPGA may contain several types of PIO designated for particular uses.

3.2.2 Development of FPGA codes

Although the architecture of an FPGA is important and has significant influence on the final design performance, the logic designer need not manually consider the connections and LUT details. Designs for logic are written in a hardware description language such as Verilog[41] or VHDL[42] that capture the intended design function rather than the gates that implement it. Converting a design from a functional description to a working implementation follows a lengthy process which is fortunately automated by software.

Synthesis

The first step in any compilation process is to synthesize a netlist from the design files. This step includes expanding hierarchical design files into a flat list of all interconnections from primitive to primitive. Not all designs can be synthesized and it is important to bear this in mind when writing in a hardware description language, for example recursion is not synthesizable in real hardware. At this stage design rule checking can be applied and any structure that is incompatible with the target architecture can be found. Additionally any library code can be expanded into the real primitives that

will implement it and be added to the design. At this stage the netlist is a standalone database containing all the logic required for the implementation.

Translate & Mapping

Translation between a generic primitive and a specific primitive supported by a given manufacturer is now performed. This process is unique to each manufacturer and in some cases is little more than a conversion of file type between the synthesis tool and mapping tool.

Mapping is the placing of one or more primitives into a logic block for the final device. Clearly this can be a complex task and is highly dependent on the architecture of the FPGA. Determining which primitives are implemented together in a block is complex and has knock-on effect for the next stages of the process. The manufacturer uses proprietary heuristics to determine optimum mappings for parameters like area or routing resources, but there is no optimum strategy that will work with all designs and all architectures.

The timing characteristics of a design are affected by how the primitives are packed into LUTs. More efficient packing can reduce the propagation time by requiring fewer LUTs between an input or an output, but may also force a sub-optimal routing to take place producing a poor timing performance. The effects of mapping are highly nonlinear and typically not exposed for a user to intervene with. Although most manufacturers provide algorithms to guide mapping based on timing constraints, and typically provide a limited choice of algorithms and effort levels for which the designer can control.

Place & Route

The next step after mapping a design onto logic blocks is to place the blocks inside the FPGA fabric. The resultant timing is once again highly dependent on the placing of

blocks and the delays in routing between them. Algorithms for this step are generally a many parameter optimization problem. Often algorithms mimicking physical processes such as simulated annealing are used to gradually find a design implementation that meets all the user timing requirements. Due to the non-deterministic nature of these algorithms two separate compilings of a design are frequently different in placement and routing despite having the same netlist.

Additional complexity is added at this stage as users may guide the route process by their own intuition, often referred to as *floorplanning*. For large designs it may take a long time to produce an output. To reduce the time required users can often lock certain regions which have previously been verified to work from being altered and this imposes additional constraints on the final implementation.

Export

Finally after an implementation has been generated and has passed verification of timing behavior a programming file can be created. All the LUTs, multiplexers, routing logic, and PIO cells have a known configuration state. A file containing a bit mapping of every control register within the FPGA is generated as final output ready to be programmed into a physical FPGA device.

3.2.3 Programming

The configuration information that controls an aspect of an FPGA such as the cross-point routing connection of two wires is a single bit of memory. For simplicity of design of the FPGA hardware itself, this memory is located near to the point of its use in a manner that is naturally inhomogeneous. Instead of a traditional row and column based access scheme the memory cells may be chained together to form one or more large shift-registers. The memory cells are typically volatile memory meaning that they

do not retain their state during periods of power off; in most commercial designs the memory is simple SRAM which does not require refreshing during run time. At power up the FPGA does not have any function and must first be loaded with a configuration from an external source. Most FPGAs from the major manufacturers are equipped with a state machine that is active on power up, capable of transferring data from an external EEPROM or Flash memory into the configuration memory of the FPGA.

JTAG

JTAG strictly speaking stands for Joint Test Action Group but is used ubiquitously in the FPGA context to refer to IEEE 1149.1 (1990), a test protocol devised by said group. The original concept and purpose for JTAG was to allow the pins of a packaged integrated circuit to be overridden for test purposes. The scheme involved a shift register with a memory associated with every pin of a device which when written to would output a logic level, and when read would indicate the logic state of a pin. The system is designed to be *daisy-chained* through all large integrated circuits on a PCB. In this way with only limited connections to a PCB, every integrated circuit to other-integrated-circuit trace and solder joints can be tested efficiently. This technique was accordingly named boundary-scanning, due to its position at the boundary of the known good integrated circuitry and the unknown external PCB implementation.

To facilitate flexibility of implementation the *JTAG* standards defined not a simple in-out shift register, but instead a rather more elaborate state machine allowing at minimum the testing of pins, the identification of the part from some read-only register, and also a bypass mode in which the simple forwarding of any input to the output is performed. Recognizing the potential to expand upon the standard protocol without loosing backwards compatibility, manufacturers supported additional non-standard modes which could be used to monitor internal status of a part; in the case of an FPGA or CPLD, program the configuration memory. Contemporary FPGAs all support JTAG

programming with slight protocol variations, and the technique has become the de-facto way to program an FPGA. However at least one other interface is typically supported in order to load from an external memory at power up.

3.3 Design of the Counting Electronics

A correlation counter was developed for the purpose of receiving and integrating the pulse signals from the single photon avalanche diodes used in the experiments to be discussed.

3.3.1 Requirements

The two photon counters used during the course of the aforementioned experiments produced approximately 5ns pulses for each arriving photon and provide the leading edge within 300ps (approximate jitter) of the arrival of the photon (or dark event). The ability to reliably receive signals of this type over a 50Ω coax is the primary requirement.

A view was taken that the exact width of the correlation window was largely inconsequential if made sufficiently small that a correlated pair of signals can be reliably distinguished from noise. At a minimum the correlation window must be twice the jitter in the detectors; a more realistic goal of 2-3ns correlation width was decided upon for an initial prototype design. Additionally the counter should cope with the maximum pulse rate deliverable by the detectors. The absolute maximum of 30MHz pulse rate is orders of magnitude greater than any rate seen in the experimental work but is easily achieved with electronics capable of resolving two edges within 3ns. The size of the counter registers should be sized to not roll over their maximum value in the nominal integration time of 1s at the 30MHz rate.

The simplicity and cost effectiveness of electronics is rarely a concern in scientific study. Generally the maximum specification available is selected so as to be able to best capture data. When prototyping electronics for commercial use a great amount of time and high specifications can be aimed for. In the context of a PhD project however the constraints on time and available prototyping equipment require almost certainty in a functioning first prototype. With this in mind a simplistic design was chosen with low specifications as a first iteration; further the initial design was split across two separate PCBs in order to isolate initial problems and continue work on one if the other required a design change.

3.3.2 Choice of Programmable Logic

There are an almost endless variety of FPGAs and alternative programmable logic. The requirements presented before could be achieved with a vast subsection of these parts making the choice of device relatively free. For ease of prototyping and for potentially sharing the designs as a starting point for others to use, a minimum complexity two layer PCB was chosen. Using only the outer layers of PCB allows for inexpensive production and visual inspection for errors.

Integrated circuits with high density packaging such as ball grid array are not easily compatible with low layer count PCBs and there are technical difficulties relating to attaching such packages. In order to facilitate manual soldering and low layer counts, a package with only perimeter pins was required. Additionally the part should be in current production and have freely available software for compiling designs. An FPGA from Lattice Semiconductor (the MachXO2 series) was found with 400MHz synchronous performance that was available inexpensively in the TQFP144 package that is easily soldered with minimal manual dexterity. An additional benefit of this part is that it incorporated a flash memory inside the same package able to provide more than enough memory for configuration of the FPGA. A final convenient aspect

of this part is its built in voltage regulation, for the core voltages this is performed on die allowing a single rail power supply to power to both the core and PIO banks.

3.4 Design Detail

Input interface

External to the FPGA that will provide the majority of the counter functions are three design subsections. In order to receive a pulse signal and interface it to the FPGA a voltage translation is needed. In the laboratory 50Ω coax terminated in either BNC or SMA connectors is used for most signal connections and so the counter must accept a connection from one of these systems; SMA terminations were chosen for their compact size. The output impedance of laboratory equipment varies widely and any device brought into the lab should not be damaged by these signals, if not work with them. In order to protect the FPGA from experiencing voltages above the 3.3V PIO voltage supply maximum, a translation is needed between the variable input conditions and the fixed integrated circuit voltages.

There are a plethora of solutions to voltage level conversion and many dedicated integrated circuits. However the two choices made for the counter prototype were a single Schmidt trigger inverter, and a single OR gate. Single gates in SOT23 type packages were used in order to place the gate directly at the termination resistor. The Schmidt triggers provide a small amount of hysteresis making the input threshold less susceptible to noise. In practice noise was found to be less problematic than initially anticipated and another simple gate with compatible pin configuration was tested without modification to the board. The single OR gates used were able to accept up to 7V input and when combined with the 50Ω termination allowed a signal of 14 volts to be accepted. This additional ability to handle higher accidental voltages was convenient since a direct connection to the 12V power supply of the system would hopefully not

damage an FPGA pin.

An IO buffer of this type is not an ideal or high speed solution but it is robust. Further development of the counter would replace the Schmidt trigger with a fast comparator (with external feedback and compensation) capable of being adjusted to suit the user's voltage needs. High speed comparators of the intended type output a low voltage differential signal (LVDS) capable of higher performance than the previously described single ended IO. LVDS interfaces use two complementary electrical signals to represent the logic state, and drive a constant current allowing a predictable voltage at termination of typically 350mV. The chosen FPGA not only natively supports LVDS signaling but also has limited serialization capability in the form of 7 to 1 *gearbox logic*. Interfaces of this sort are designed for the cases where data is offloaded from an integrated circuit with multiple serial bits per clock, as is common with camera and display interfaces. Utilizing this *gearing* may make a shorter and more controllable correlation window possible and is an additional benefit of swapping to the higher speed interface.

Programming Interface

In order to load programming data into flash memory a standard JTAG interface was used in conjunction with an older development kit from the same manufacturer that incorporated a USB programming interface. The development kit PCB traces that connected the manufacturer-provided programming circuitry to the intended target device were broken into at the point they passed through protection resistors, and a set of flying leads soldered. When connected to the counter board this provided an effective means for the download of configuration data.

FPGA Logic: Pulse Shortening

The first stage on entering the FPGA fabric for any external signal is pulse shortening. Pulses received by the input circuitry are of arbitrary length and need to be reduced in duration before passing through coincidence logic. In order to not introduce additional timing error in the input edge we prefer to not register the input signals against a clock but instead use the gate to gate propagation delay to provide the reference time. An input signal is divided into two copies and fed along two different paths before being combined together by an AND gate. One path logically inverts the signal and passes through a number of LUTs incurring a delay. The remaining path is connected directly to the AND gate and receives only a small amount of routing delay.

In idle state the AND gate has two different logical inputs (the inverted and non-inverted copies of the input) and so outputs a logical low. At the point the input goes high the AND gate initially has two high inputs and outputs a logic high, however after a short delay the logic state propagates through the slower arm and turns the AND gate off. Regardless of how long the input remains applied only a short pulse has been output. Furthermore on the falling edge no output is produced. The length of the output pulse is only determined by the path propagation time difference between the two copies of the input signal.

FPGA Logic: Correlations Counting

A pulse with fixed width can be fed directly into combinatorial logic, its successful overlap with other pulses derived in the same way implies a correlation in the time of arrival of the original pulses. The correlation window between two edges is further reduced by the timing behavior of the function placed between the signals. A signal can be derived for every correlation condition of interest and treated as a clock signal. For every instance of an event this signal can be used to increment a counter. After

a suitable integration time the contents of the counter's accumulator will reflect the counting statistics of interest.

Choosing what quantities to count is important since as the number of inputs increase the possible correlations both pairwise and higher order increase exponentially. The specific correlation counts of interest can be programmed and changed as needed owing to the FPGA's re-configurable nature. For the first prototype with only 4 input channels there are the following counts recorded: *Singles* on each of the four channels; The 6 pairwise correlations; 4 three fold correlations; and finally a four fold correlation. The counters for these 15 quantities are easily accommodated by the modest size of the FPGA chosen. Counter sizes should be picked to prevent overflow, but need not all be same sized. The counters for singles must not overflow in 1s at 30MHz input rate, depending on the expected statistics it may be possible to use smaller counters for the correlations that will occur with less frequency.

FPGA Logic: Buffering and External Readout

The counters in the FPGA are backed by a register of the same width. Upon an external *stop integration* signal the contents of the counter's accumulator value is copied into the register and the counter reset to zero. The frequency of the external stop signals determines the integration time and an assumption is made that it will be applied at least once per second in order to not overflow.

Two alternative strategies were implemented for uploading the register contents from the FPGA. The first and also simplest method was to configure the registers in a manner reminiscent of an SPI interface, however due to the tiny amount of data being accessed (all registers once per integration time) and the sequential access pattern (all registers in order, never a specific register without the others) this was reduced to chaining all registers together and shifting them out in a manner not dissimilar to the

way the FPGA is initially configured.

An alternative method employed in further prototypes was to use *hardened* I^2C logic provided by the manufacturer. Hardened logic is integrated function logic that is sufficiently common and resource expensive that it is implemented as a peripheral rather than by the user logic. In the case of I^2C it is likely the manufacturer was providing the interface as an optional configuration mechanism and provided access to re-use the interface after initialization. The use of a standards compliant interface improves design re-use and allows simple interoperability with micro-controllers supporting the interface.

3.4.1 Design of a Display and Communications Board

To further export the registered data to a computer for recording and analysis an interface is needed. Ordinarily this would be implemented on the same PCB as the FPGA counter however a separate board was produced for the development reasons discussed earlier.

An ATmega32U4 8-bit micro-controller was selected to control the communications interfaces. This chip is part of a series made by Atmel that have exceptional simplicity and free compilers and programming tools. Due to the popularity of development platforms using this processor a great amount of information is available and many libraries have been written for it. This integrated circuit contains an on-board USB controller and dual port memories enabling it to implement USB devices with up to 6 (5 and control) endpoints.

The low speed (max 16MHz) and 8-bit bus widths are significant limitations for performance of this processor, nevertheless it has sufficient capability to perform simple interface and control tasks. The processor is programmed to issue the integration stop signal and read out the contents of the FPGA counter registers once per second. The

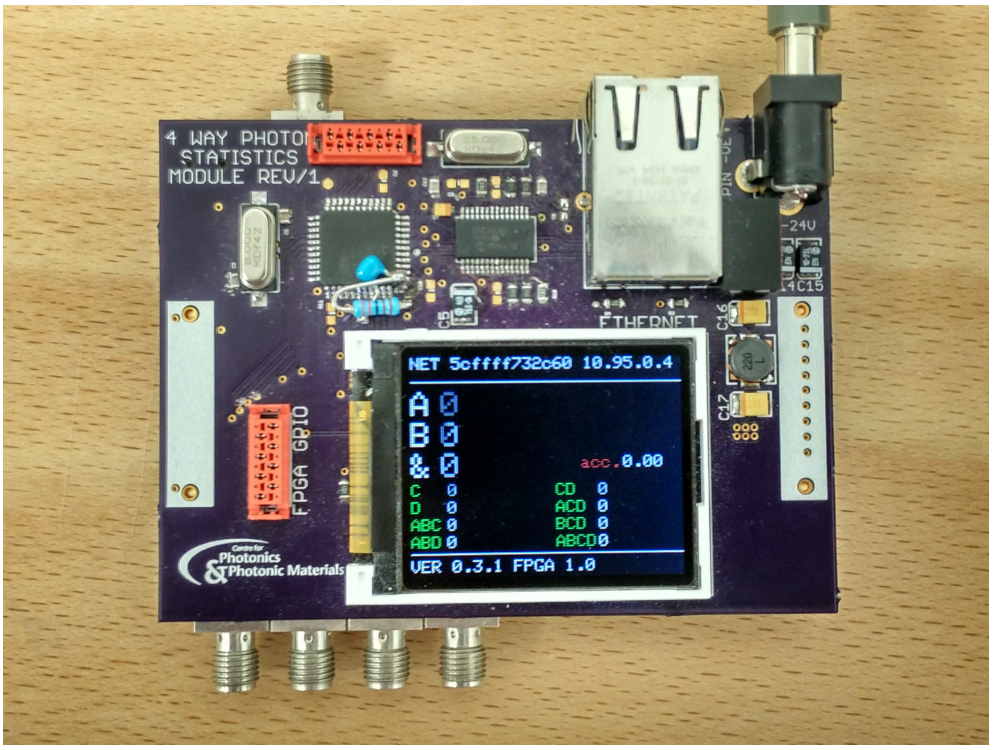

Figure 3-4: Assembled prototype Counter module with Communications and display PCB visible on top. On the TFT screen quick *'heads up'* values of recent count data are provided for use in alignment and setup. Integration data is continually streamed over Ethernet using MQTT protocol and from a virtual communications interface over USB. Although the counter-correlator can be remote controlled, the majority of integration was performed by simply capturing the continuously offloaded stream.

verbatim contents are forwarded for interpretation on a computer.

Two interfaces were selected as candidates for first prototype; Ethernet and USB-CDC. The Ethernet functions are implemented as an external controller chip (Microchip ENC28J60) with the data sheet recommended interface components for coupling to the line. The USB interface used the built in USB control hardware and the Atmel supported open-source library LUFA [43].

Immediate Display

For convenience a small TFT display screen was included in the communications board design. The display lists the count values from the previous second along with some computed values for the expected accidental correlations for the present singles rates. This information allows the counter to be used without connection to the computer for the purposes of alignment and experiment setup. The display chosen is one used in previous-generation mobile phones and has a well known controller with open source libraries. Additionally this display includes the voltage boost circuitry needed to drive a TFT from 3.3V with only a single external capacitor required.

3.4.2 Design of a 2nd Prototype

A second prototype shown in Figure 3-5 was constructed with a view to fixing shortcomings with the initial prototype, and simplifying the two subsystems onto a single PCB. The input discrimination circuitry, and output drive capability was improved in line with the similar improvements made in the second prototype of the delay modules discussed later. The view was taken that the on board delays used in the first prototype were not appropriate due to the small range being insufficient for the experimental work, and the fine detail being generally unnecessary and subject to wild fluctuation as the relatively power hungry unit reaches thermal equilibrium.

The number of available input channels was revised to eight in order to count ancillary pulse information and to apply more complex gating and veto to received pulses. The four output channels were retained as useful outputs for operating external optical switches and muting external detectors where provisions are available. In addition to the 50Ω outputs a number of general purpose outputs with wide voltage tolerance were added for convenience in automating shutters and external delay modules. The additional general purpose outputs are of open collector type and so are capable of

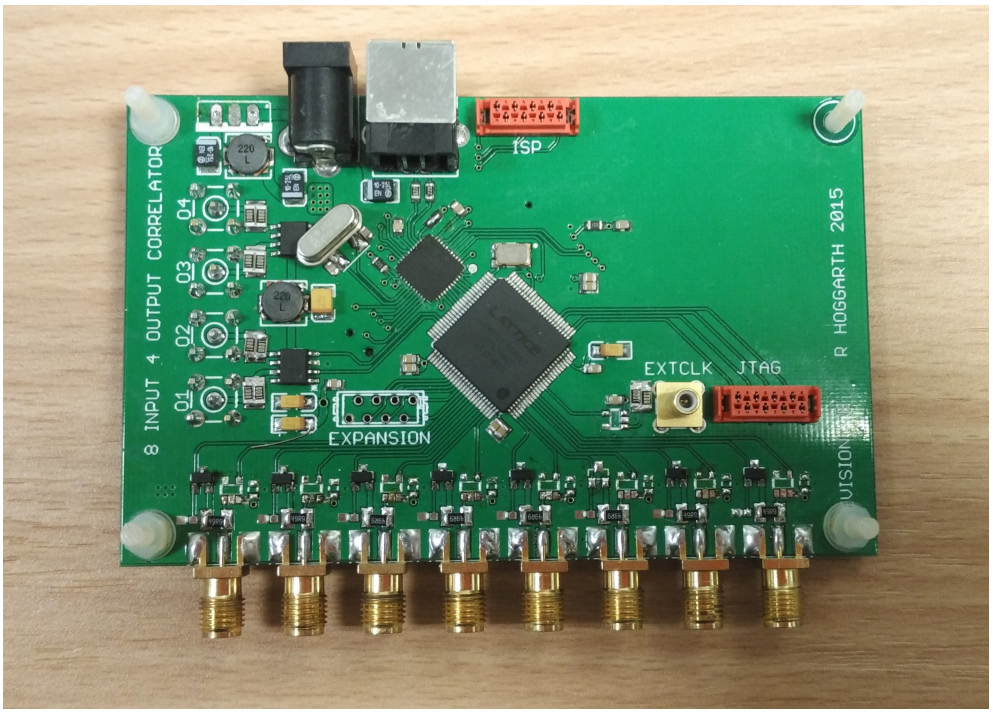

Figure 3-5: Rear view of the second prototype of the counter-correlator with eight input channels in a single board format with an additional four channels of 50Ω output. This version only uses USB for communication and does not have the ethernet hardware interface present.

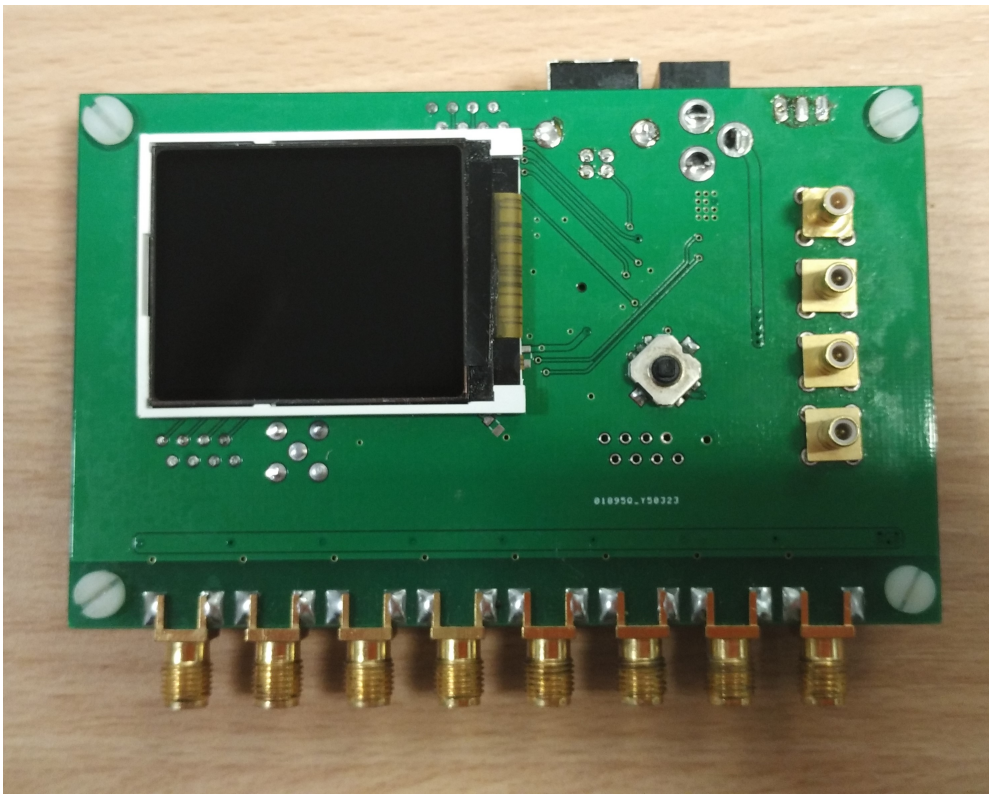

Figure 3-6: Front view of the second prototype of the counter-correlator with eight input channels in a single board format, with the additional four channels of 50Ω output visible to the right hand site of the board. The small TFT display screen is retained from the earlier prototype, along with an additional tactile joystick control input for control without connection to a computer.

handling a wide variety of interface voltages directly.

Additionally a five position jog switch was included for setup purposes, allowing a user to directly configure and use the second prototype without first connecting to it via USB. In a similar manner to the output display screen this minor feature vastly improves convenience for setup or preliminary work.

General Purpose Outputs

The four main output channels provided in the second prototype are able to drive 5V into 50Ω with a fast slew rate. These outputs are logically the same as general purpose outputs but with additional drive power necessary for driving a terminated transmission line.

3.5 Design of the Time Delay Electronics

As previously discussed, signals from correlated sources are not always coincident at detection due to propagation effects and detector characteristics. By delaying signals by appropriate amounts we can make them co-timed at some later time. Static timing offsets (or similar offsets where no decision making is required) are the dominant use case for electronic delays, and shall determine the key specifications required in a delay system as discussed below.

A delay generator or *delay line* as it is often called (in recognition of typical implementations) must have sufficient bandwidth that the signal information is substantially unmodified during transit. In addition the delay caused must be correct for the intended application. The specific delay required for a laboratory scenario is often unknown in advance of the experiment, or unknown to sufficient accuracy for a fixed delay line to be practical. As a result it will usually be required that the delay can be adjusted

easily to suit the situation.

3.5.1 Problems Encountered with Existing Electronics

Prior to designing the delay lines presented here, delays were created with lengths of coaxial cable. Coaxial cables have a distributed impedance which causes a predictable delay over a large bandwidth, allowing in turn a delay to be created proportional to the length of a cable. Specific delays can be created by cutting lengths of coax to suit the application, however the process is cumbersome due to the length measuring and termination techniques required. After a cable has been terminated the delay is easily checked by reflectometry using an oscilloscope; cables created by the author are rarely exactly the delay intended.

As an improvement over bespoke cable delays a switchable cable delay box was available (ORTEC DB463). Units of this type contain a collection of standard lengths of coax in binary multiples of the minimum length; individual sections being coupled together or bypassed by a series of switches. With an appropriate switch combination a delay to the nearest half nanosecond required can be achieved, offering flexibility to adjust the delay while in operation. Unfortunately the physical bulk of the cable magazine is large, and the crosstalk between channels is significant, it is believed that this is due to the manner in which the switching is being performed within the units available.

3.5.2 Design of the Time Delays

In order to have sufficiently many channels for the proposed experiments, more delay lines were necessary. A similar level of resolution around $0.25ns$ was desired, along with the ability to adjust the time delay while an experiment was ongoing. Additionally as seven channels are to be used in the most complex cases envisaged, combining the controls of all delays used into a homogeneous interface of minimum complexity for the

user to operate in the darkened laboratory was desired. Ideally this interface should also be able to operate remotely via the counting electronics communications interface when it is desired that nobody be present in the laboratory.

The availability of clock skew adjustment devices intended for use in large back-plane computer systems provided a cost effective source of integrated semi-analog delay lines. Unlike most digital parts, delays of this type must operate asynchronously, and preserve the original edge shape of the pulse. The devices selected had either an 128 ns or 64 ns delay line comprised of a chain of buffer gates (a circuit that copies it's input to output unchanged except for impedance) incurring delay as the signal propagates, with signal tap points along the line allowing a various delays to be selected. The nanosecond and below timescales are not well suited to tap selection and so the three least significant bits of the requested delay time are instead generated by controlling the current operating point in the (slightly starved) final sections of the chain.

Four delay lines along with buffer amplifiers and termination circuit were incorporated onto a single small PCB. The specific part selected contained an optional shift register to augment the 8-bit parallel register input of the delay setting. With the addition of a dual 4-bit shift register for control bypass modes and to drive indicator LEDs, a 40-bit daisy-chain register was formed with an interface ($\bar{CS}$,DI,DO,RST,CLK) compatible with a standard SPI port.

The use of a standard port allowed the delay modules to be connected to the expansion port of either FPGA correlator, and thus take advantage of automation and remote control. An additional hand held controller was built for convenient manual operation; comprising an up down step control and a next delay selector, the delay under current control being highlighted by the appropriate LED. Internally the hand controller was a simple micro-controller with three momentary switch inputs, SPI output, and power supply regulation for powering the delay modules.

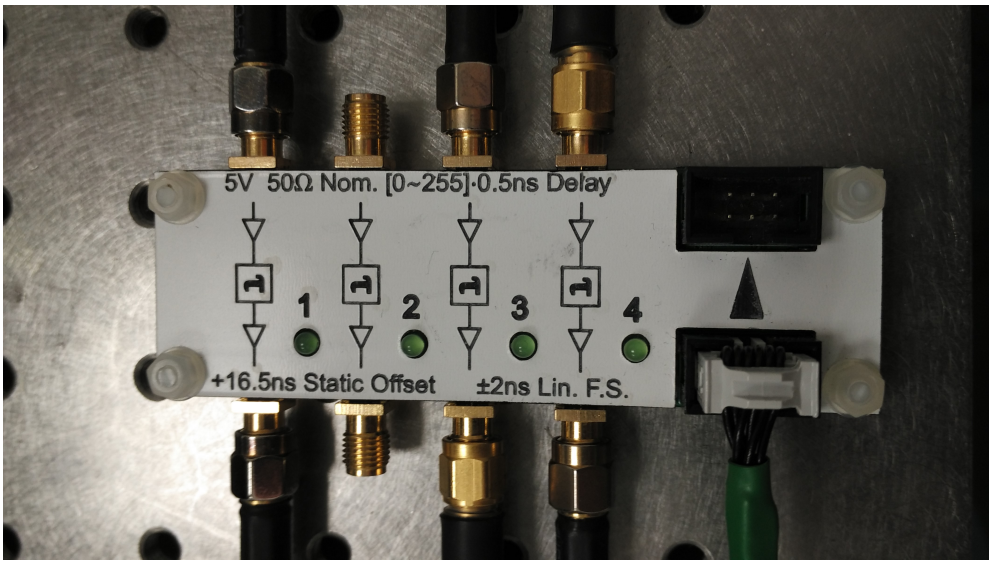

Figure 3-7: One of the delay modules developed for use in correlation experiments. Four input signals are incident on the top row of SMA connectors; delayed copies of input signals are output on the corresponding connector below. all signals are buffered for output and terminated into 50Ω. Control input is fed serially from the cable connected bottom right, and additional modules can be daisy-chained from the unused connector top-right.

Owing to the serial access and daisy-chain style design implemented thus far, an additional output connection was provided on the delay module such that a number of modules can be chained together from a single controller. In order to determine the register size, after reset a number of 1s are clocked out until the whole chain is filled, as the registers initialize to zero the number of clocks required to read back a first 1 is the size of the combined register. Additional check patterns are used to confirm the correct length is set. It is assumed that every multiple of 40 bits is a new module register.

Improvements to the Prototype

After some use in the laboratory, three major shortcomings in the prototype design were identified. The connection to control the modules and daisy chain, while reliable, is inconvenient for laboratory layout and cable management. Additionally the volatility of the delay line register meant that upon power up, the previous settings were lost.

The latter was partly solved in the case of the manual controller which was modified to save the current positions of the delays after every update. The analog characteristics of the first prototypes were not ideal, having appropriate input discrimination and termination, but output drive duty cycle was incorrectly assumed; when resting in the high state continuously and terminated DC to ground a 15% overload of the output buffer occurred.

All three issues were addressed in an updated version of the delay line; the wired link was replaced with low power WiFi (ESP8266) module, the analog outputs improved and each module would independently remember its state. In addition due to the presence of a user programmable processor on the module (inside the WiFi module) manual pushbutton controls were added to allow completely independent manual delay setting. The IBM MQTT protocol was used to control the module over WiFi.

3.6 Qualification Testing

When qualifying parameters of a measurement or setup that are critically dependent on time, higher resolution timing is required than can be afforded by the $0.25ns$ step of the delay modules previously presented. For some measurements an oscilloscope was used to directly measure pulse widths; in cases where a measurement window was to be observed, a more precise variable stimulus was required.

For the purposes of calibration a high resolution delay line was used, with capability of $10ps$ step resolution and analog vernier. The delay module shown in Figure 3-9 was initially constructed to test the efficacy of the chip before subsequent use in the initial prototype correlation counter. However due to the ease of manual use the module can be used to provide a variable known stimulus during verification.

Internally this module operates in a manner similar to the coarse delay lines chosen for the delay modules, however due to the intended high speed application alternative

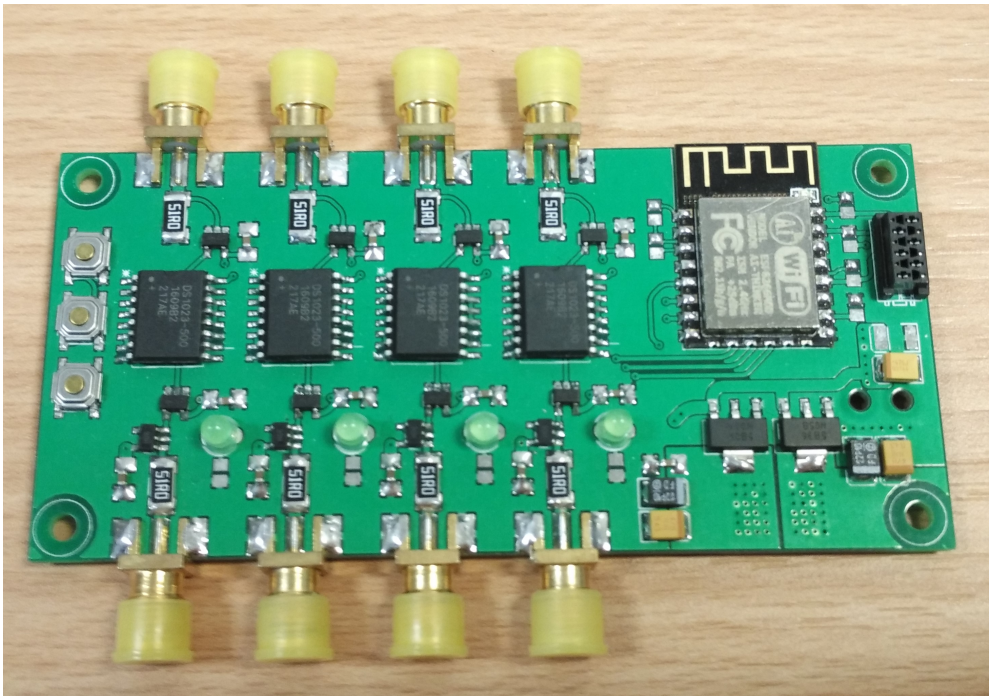

Figure 3-8: Second prototype delay module with on board WiFi and manual controls, shown here without laser-cut plastic covers. The minimal complexity structure of the design is evident by following the signal path from top to bottom on a given channel. The output channels on this revision can truly drive 50Ω outputs continually to 5V without overload. The ESP8266 WiFi System on Module with integral antenna is visible to the top right, this module contains radio circuitry and a Tensilica L106 processor which is available for user programming.

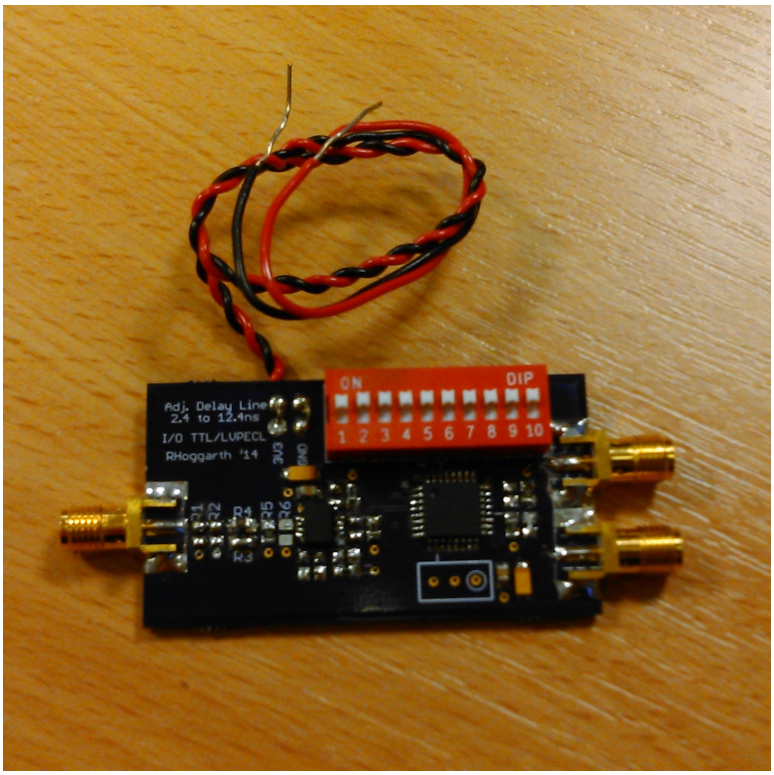

Figure 3-9: Prototype and test delay with 10 bit range and least significant bit delay of $10ps$. The delay is directly controllable via the 10 control lines brought out to switches. Both a true and compliment output signal is generated at 50Ω, and special attention is given to the input signal conversion to positive emitter coupled differential logic. Additionally a voltage input that functions as a vernier within one LSB is provided, however at such small delays the effect of temperature on generated delay is significant.

interfacing was required to translate from emitter coupled logic to single ended 50Ω.

The combined use of correlation counter oscilloscope and precision delay allowed the correct operation of coincident logic, detector dead time and jitter, and coarse delay linearity to be checked prior to use. Some degree of signal degradation is inevitable when passing through additional active delay stages, however only the position of the leading edges must be preserved. The delay action produced is affected by variations in power supply voltage and temperature, and can translate electrical noise into delay variations.

Chapter 4

Multiplexing

The results and experiment detail presented here for temporal multiplexing in a fibre delay line are additionally published as "Resource-efficient fibre-integrated temporal multiplexing of heralded single photons" in the IOP Journal of Optics [44].

4.1 Motivation

In the context of photon sources, multiplexing offers a means to trade off source output characteristics, namely the maximum delivery rate (or *attempt rate*) and probability of photon generation per unit time (or per attempt), against each other. The probabilistic nature of many types of photon source (including the two sources described in Sections 2-6 and 2-7) prevents the use of large collections of sources in quantum optics experiments; the probability of an event simultaneously from n independent sources rapidly becomes small.

The probability of single photon delivery from sources of these types is inextricably linked to the probability of multiple photon delivery. Since we cannot reliably herald the number of photons produced, and require one and only one photon from each source,

we are forced to operate with low brightness. The advent of photon number resolving detectors has not yet alleviated the problem due to their relatively slow throughput (reset and readout time requirements) which itself limits the effective brightness. Additionally the number resolving detector (and the whole heralding channel in general) must be highly efficient; under reporting of photon count may result in multi-pair events being interpreted as single pair events. Pseudo number-resolving detectors offer some improvement, however the increased physical resources required to implement such schemes must be considered [45].

With the assumption that a source is operated in a low probability of pair generation configuration $P_1 \approx 0.01$, we seek to improve the *effective probability* by actively combining the contributions of multiple generation modes. Here the active operations add additional attenuation due to insertion losses, but can also increase output probability. Specifically the cases of multiplexing over spatial mode and temporal mode shall be discussed, the latter with the additional concepts of synchronized, or *relative*, multiplexing.

4.2 Introduction

Multiplexing can be performed in a number of ways, which shall be discussed individually in this chapter in further detail. The general focus will be on temporal multiplexing in an optic-fibre integrated form; an experimental realization of the concept will be presented. A simplified overview is that generation of photons (or photon pairs) from parametric processes is independent in different optical modes. If one could generate photons in two orthogonal modes and subsequently separate them, the statistics of generation in each mode are independent. This is assuming that the generation in one mode does not affect the other through, for example, depleting the pump etc.

As discussed previously in Chapter 2 the generation process in a waveguide is governed

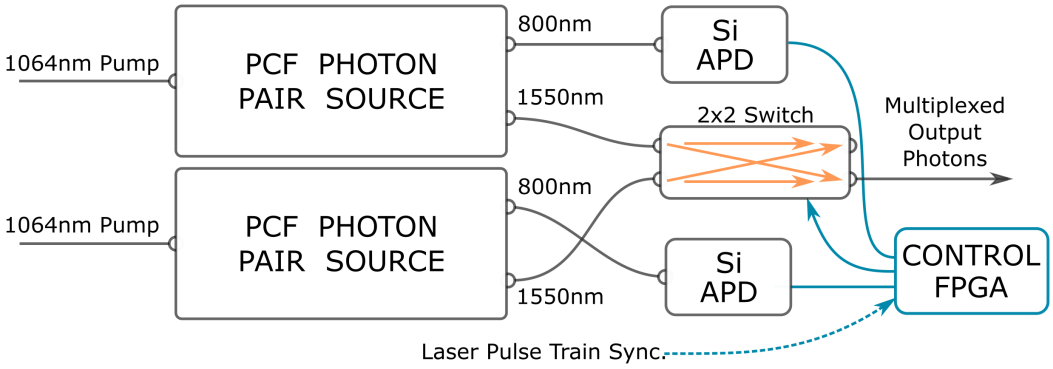

Figure 4-1: An outline of the spatial multiplex scheme, demonstrating the combining of two modes into a single output mode using heralding information. A 2x2 (or 2x1) optical switch is used to route the photons from the selected source to the output fibre. The switching strategy is to remain in one state until a heralding event is observed on the normally disconnected source. The statistical effects are twofold owing to both the increased number of single photon events, and to the halving of integrated noise. In order to switch fully to the correct state before a photon arrives, an optical delay (not shown) is incorporated in each source; the herald signal and feed forward action occur $> 100ns$ before the photon arrives at the switch.

by the phase-matching between the waves which is itself dependent on the dispersion. Phase-matching two parametric processes into two modes of a waveguide simultaneously is relatively difficult, and is compounded by the requirement to produce indistinguishable (except for mode) photons. An alternative strategy is to produce photons in two near identical waveguides by near identical phase-matching with equivalent outcome: two modes with independent photon statistics. Additionally by using very similar phase-matching (and pumping etc.) for each mode we can expect to produce highly indistinguishable photons. Each generation mode is subject to the statistical limitations to its brightness when heralding for single photons, however we are able to combine the modes into a single output mode by an active process such as a switch. In this way we can make an improvement to the output mode statistics.

We refer to the operation as spatial mode multiplexing since we have combined two spatial generation modes together. In principle the spatial modes could be free space

modes, modes of a waveguide or two particular modes in separate waveguides. The obvious advantage as mentioned before being that the similarity of the latter modes is beneficial to efforts for indistinguishably.

Another degree of freedom is the photon's temporal mode, that is to say the photon produced at some particular time is independent of a photon at some subsequent time. We can of course design a method for photons at different points in time to interact by delaying the propagation of one relative to the other.

It may be noted that much like the finite bandwidth of a photon in frequency can be thought of as a superposition of amplitudes at a variety of single frequencies, a temporal mode must have a similar quality in some conjugate fashion. Confusion may arise in nomenclature here as clearly the photon wave-packet is composed of some number of temporal modes; when transform limited that number of temporal modes must be related to the number of spectral modes. In the multiplexing experiments discussed further the pump light is derived from a pulsed laser, the spectrum and envelope of which has a direct impact on the photons produced. On each pulse of the laser a photon may or may not be produced; we shall call the time window in which a photon may be produced a 'temporal mode' or *time bin* since they have the property that photons produced in each window are independent of one another.

With the new definition of temporal mode in mind we could consider numbering each mode continuously from some arbitrary starting point. We could separate all even numbered temporal modes from all odd numbered modes and expect the occupation statistics to be independent. We could arrange for a greater total number of modes in a given time by increasing the pulse repetition rate of the pump laser [46] (assuming that the modes do not overlap each other). Each mode is independently subject to the practical generation probability limitation, as we desire only a single photon occupation or none.

Although by increasing the total temporal modes per unit time we will produce a greater number of single photons, we do not improve the probability of delivering two photons simultaneously from two sources. In order to increase the probability of n-fold simultaneous events the probability of occupation of a time bin must be increased. Consider a train of n time 'bins', if we were able to move any photon from the bins $0 : n-1$ into bin n the probability of occupation of the particular bin n would be the sum of the probability contributions to each bin. The maximum probability of occupation of the destination time bin saturates as 1 (max one photon), so the operation is advantageous only when operating with low photon occupation probabilities. The probability of occupation in each of the remaining time bins has decreased and the probability of occupation of bin n has increased.

A practical realization of this technique is to wait for occupation of a bin signified by a herald signal from the detection of one half of the photon pair. If the herald arrives on the final bin n we do nothing other than pass the herald signal along with the photon to the next stage of the experiment. If however the herald arrives in one of the time bins preceding n we can apply a delay to the photon of the exact duration required such that the photon is moved to bin n. A delay is readily formed by a length of optical fibre, and when time bin n arrives the photon and a new generated herald signal are passed on to the experiment in exactly the same fashion as before.

4.3 Other Temporal Schemes

The specific form of the delay, or more generally its topology has an impact on the implementation of the multiplexing scheme. The same principle of operation can be implemented with different switch and delay technologies, impacting the insertion losses. Free space optical switches with very low insertion loss exist, but it is comparatively

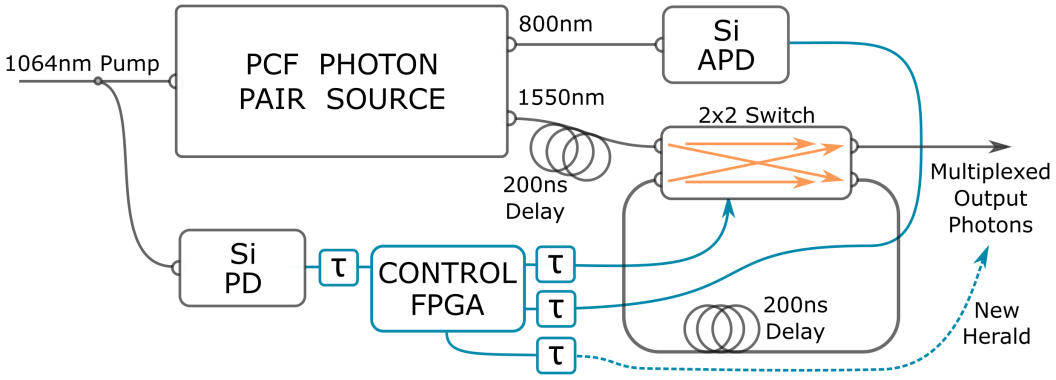

Figure 4-2: Idler photons from a pair source are heralded and delayed in a $200ns$ length of fibre. A timing pulse derived from the laser output pulses is counted modulo m where this is the number of temporal multiplexing time bins. Every herald event is tagged as belonging to the bin during which it arrives. By switching the 2x2 routing switch at appropriate intervals, photons can be made to experience n traversals of a time delay loop, matching the spacing between the time bins. By commanding a delay corresponding to the modulo arrival time of the herald, all photons can be made to exit the loop on the highest time bin. In this manner the contributions generated from a large number of laser pulses are concentrated on a more regular time interval, effectively changing the occupation probability for specific times at the expense of other times.

difficult to make a free space storage loop of a long duration. Conversely for guided wave technologies such as optical fibre it is simple to produce long delays from lengths of waveguide, however the switching element insertion losses are high. Regardless of the particular technology chosen, the topology of the delay network has an effect on the number and type of control elements required.

4.3.1 Binary Delay *Ladder*

Given the availability of switch elements that select between two input modes, the most obvious implementation of a variable delay network is a binary tree. A delay of this type is comprised of a number of stages each with a choice of two paths; a delay or a bypass. The delay path at each subsequent stage is twice that of the preceding stage. The initial stage has some convenient delay value such as the repetition rate of

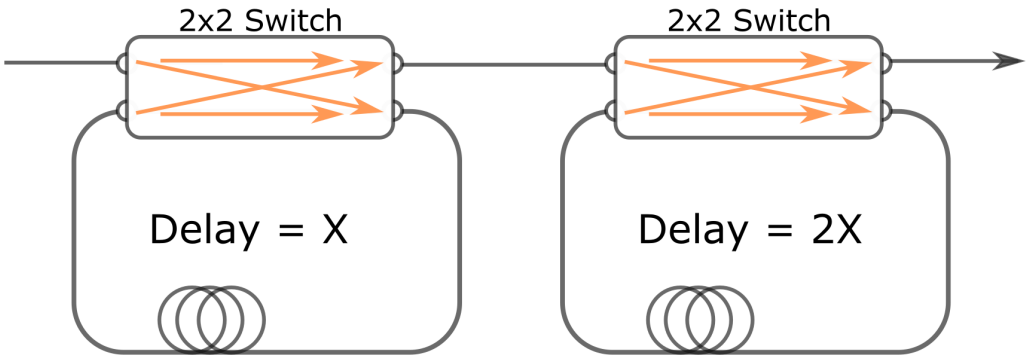

Figure 4-3: Schematic representation of a two stage binary delay network. The specific implementation in 2X2 switches is suited to available optical fibre technology. The number of times a photon must traverse a switch is once per switch in the chain plus one extra traversal per set bit within the commanded delay; $S + SumofBits(Delay)$ where S is the chain length, and assuming the cross and through states have similar loss.

the photon source. By an appropriate choice of either delay or bypass at each stage a total delay can be built up. Multiplexing can take place across 2^s bins, where s is the number of delay stages used.

This configuration as shown in figure 4-3, multiplexes over 2^s bins with only s switches, allowing a relatively large number of bins to be accessed with limited number of switches. Note that the photon must pass each switch twice as shown in figure 4-3, incurring twice the insertion loss. Conversely the photon only passes each switch a single time when the delay is bypassed. The degree of loss suffered by each photon is variable depending on the path taken, wheres with $s + 1$ switches it can clearly be re-arranged to require only a single pass of each switch, and thus incur on average reduced losses, that are significantly more homogeneous as shown in figure 4-4.

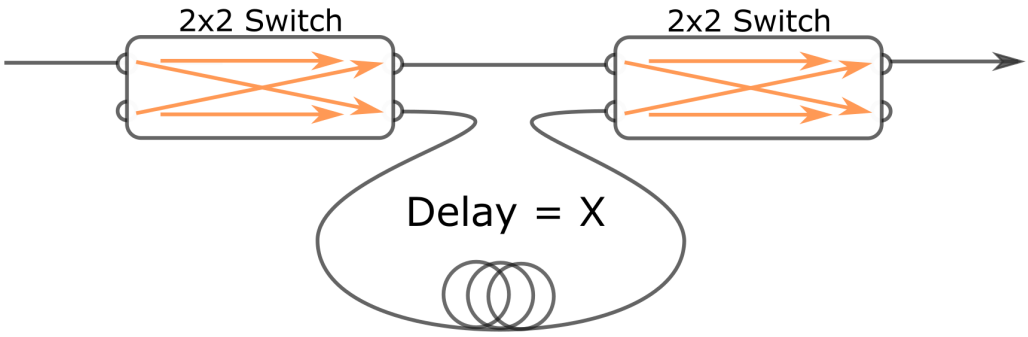

Figure 4-4: Schematic representation of a single stage of an improved delay network. In the form shown $S+1$ optical switches are required, however a more homogeneous and on average lower total loss occurs. It is plainly noted that however long such a binary chain is made, every switch is traversed only once. Assuming the cross and through states of the switch are similar, the loss is constant for whichever delay is selected. If all delay settings are required equally often a lower integral loss is achieved by this configuration, despite having a minimum loss one unit higher than for the scheme shown in 4-3.

4.3.2 Recycling Loop

An alternative topology choice is to create a storage loop with a long delay such that many time bins are contained within the loop and are continually recycled in a manner not dissimilar to delay line memories of 1950's era computers. Schemes of this type can be used in a number of ways; a collection of photons for successive delivery could be accumulated, although this is not a typical requirement. Alternatively when operated as part of a collection of sources the statistics of emission can be improved by always storing a photon if it is not part of a multi-source event, and releasing it from the loop if it would, in combination with the firing state of the other sources, create a multi photon event. The exact behavior of such a scheme is beyond the general overview provided here, however it is clear that an improvement is possible, and the relative loss per photon per storage time is altogether different from the other schemes discussed.

There are yet numerous further and ever more complex manners in which multiple long delay loops could be composed to change photon emission statistics. Combinations of

loops with different length can be employed to re-locate the photon within a delay loop. A loop may be constructed to have more than a single exit point, behaving as if it were two sources.

Combinations of these ideas offer a large number of permutations, and as a result, many forms of source output statistics. As the complexity of these schemes increase, so too does the number of passes of an optical switch, and thus loss. In many of these schemes the number of physical switches required also increases and so the total resources required for a given improvement may not make it worthwhile when compared to simpler and more resource efficient implementations.

4.3.3 Parity Offset Loops

A hybrid idea between the recycling loop and the *which path* schemes is the parity offset loop. The time bins are divided into even and odd times, and are directed onto one of two paths. Note here that the first switching operation need not have knowledge of the herald signal, it is possible to switch on every laser pulse. Switching in this manner can be achieved differently than the *on demand* switching considered else where, and poses less of a technological challenge when operating at higher speed.

Each path contains a delay loop as described previously, however the loops are now two time bins long, and yet can only ever contain a single photon. A static delay is introduced into the odd path of one time bin; this is just additional fibre before the delay loop switch. Finally the two paths are recombined to a single path by a final controlled switch.

A variable delay is produced as per the single delay loop, however the number of times a photon passes a switch, and thus incurs loss is modified. The loss is halved by way of the fewer passes in the double length delay loops, but has the additional loss of the initial odd-even sorting switch and the final switch to select which branch to take a photon

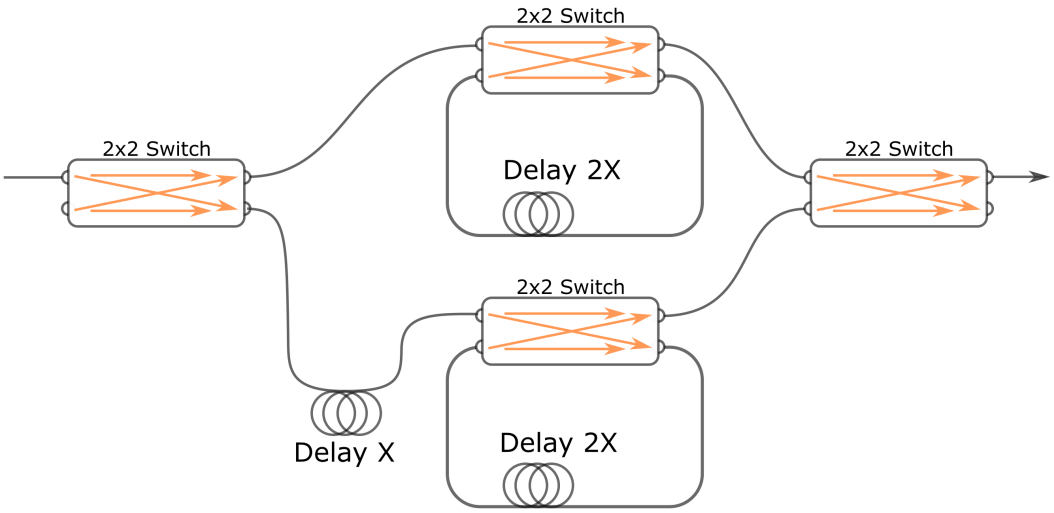

Figure 4-5: Schematic representation of an odd-even parity based hybrid loop scheme. Even delays are enacted on the upper path which comprises a loop twice the delay time. In a similar fashion odd multiples are enacted on the lower identical loop with an additional fibre incorporated prior to the loop switch to offset by one delay time. The offsetting of the two branches by parity reduces the number of switching operations in the loop sections by half at the expense of two extra losses from the initial and final routing switches. For some multiplexing depths, and when each delay value is equally likely, a scheme of this form can offer lower total loss.

from. For some number of bins it may, depending on specific losses, be advantageous to incur these extra fixed losses in order to achieve a greater mean throughput.

The behaviors of the final and initial switches may additionally lend themselves to different technologies with differing optimizations. Specifically the initial switch transitioning on every pulse allows an efficient electrical continuous drive; the final switch and loop switches operate at half the maximum speed of those in a single loop design, all other factors held the same. While limited by switch device specifications, a speed improvement can now be made by increasing the laser repetition rate (assuming the initial high speed odd even sorting is possible).

4.4 Statistical Model

In this section a statistical model of the temporal multiplexing loop arrangement operating over a number of consecutive time bins m with a single switch and delay loop of one time bin is presented. The fibre implementation fabricated and operated over four time bins presented in section 4.5 and onwards is of the type described this model.

The PCF photon source used in combination with the single time bin delay loop operates at a low mean photon number in order that we can neglect multi photon events. The probability of a photon being heralded is therefore the probability of a single pair event (from a thermal distribution) in combination with the system efficiencies of detection and delivery.

$$P_1 = P^{(1)}_{thermal} \cdot \eta_{detect} \cdot \eta_{deliver} \tag{4.1}$$

The action of the loop can be considered to be a simple optical loss combining all factors from the switch, fibre and splices. By lumping these things together and considering a scenario with m time bins each requiring an integer number of passes of the loop. the total delivery probability is unity minus the compound losses from each of the time bins. The relevant losses are the loop lumped loss applied t times as appropriate for the given bin. Bringing this together with the previously defined probability for heralding a single photon we arrive at,

$$P^{(m)}_1 = 1 - \prod_{t=1}^{t=m} (1 - P_1 \cdot (\eta_{loop})^t). \tag{4.2}$$

Comparing P_1 and $P^{(m)}_1$ is not initially useful since the quantities truly represent the probability of delivery per *cycle* rather than per time. For the case of the simplex source this is a single laser pulse; for the multiplex this is m laser pulses. Clearly a fair

comparison must take into account this discrepancy by re-casting the probabilities in terms of either time or per pulse. For a laser repetition rate R and only one output time bin per m bins we find the output rate per second K is simply,

$$K_1^{(m)} = \frac{R \cdot P_1^{(m)}}{m}. \tag{4.3}$$

And for the simplex case is,

$$K_1 = R \cdot P_1. \tag{4.4}$$

We can see without difficulty that an improvement factor f should be defined as in 4.5. Note that the relationship to m is not simple except for in the cases of negligible loss. Consider that the relationship is linear in m with $\eta_{loop} = 1$, and is modified by loss to a logarithmic function.

$$f_{K_1}^m = \frac{K_1^{(m)}}{K_1} = \frac{P_1^{(m)}}{m \cdot P_1} \tag{4.5}$$

Clearly the diminishing returns of multiplexing over greater numbers of bins will form a tipping point beyond which it will not offer an improvement over the simplex case. That is to say, at a point the decrease in the $\frac{1}{m}$ term will outweigh improvement in the $P_1^{(m)}$. The target use case for multiplexed photon sources is, as discussed previously, improving the probability of delivering a number of photons simultaneously from a collection of sources. The rate of simultaneous delivery from such a collection is,

$$K_N^{(m)} = \frac{R \cdot P_N^{(m)}}{m} = \frac{R \cdot (P_1^{(m)})^N}{m}, \tag{4.6}$$

where N is the number of sources that simultaneously fire. Since the firing or not of a

source is independent of each other the product of their respective delivery probabilities results; here we have assumed the sources are identical. The general improvement factor in N sources multiplexed over m time bins is therefore,

$$f_{K_N}^m = \frac{K_N^{(m)}}{K_1^{(m)}} = \frac{1}{m} \cdot \left[\frac{P_1^{(m)}}{P_1} \right]^N . \tag{4.7}$$

Note that the multiplexing improvement is exponential in N, providing an improvement to delivery whenever the probability of multiplexed delivery is greater than the probability of simplex delivery. This result shows the utility of even modest improvements via temporal multiplexing.

Numeric Trials

The model presented in the preceding section was numerically evaluated for a range of lumped losses and multiplexing depths. A detailed study including effects of multiplexing depth and number of sources within a collection, and hypothetical loss values that may become attainable, was carried out by Francis-Jones and Mosley [47]. For the case where loss per delay time is approximately 1dB as per the constructed multiplex, it is expected that an improvement will be possible. The loss experienced by multiplexing over two bins would be (1dB experienced by first bin; 2dB experienced by second bin) on average 1.5dB, since this is less than 3dB (after which half of the light is lost) it is possible to extract useful improvement from two time bins.

For the case of multiplexing over two time bins the single switch temporal multiplexing loop is operating in a manner indistinguishable to that shown in 4-3. For greater multiplexing depths of three or four bins the scheme becomes clearly distinct. The temporal multiplexing loop as constructed will be operated over four time bins.

4.5 Temporal Loop Construction

The construction of the delay loop makes use of standard telecommunications parts and fibre. The photon pair source output wavelength near 1550nm was initially chosen with this in mind. The loop itself is constructed from corning SMF28e and wound onto a plastic fibre spool in order to keep it stable. At 1550nm SMF28e supports only a single spatial mode and two polarization modes. No specific polarization is needed at the system output, however in order to prevent two time bins from being distinguishable the polarization must not have a net change after a trip in the loop. If the polarization is stable then it can easily be compensated by including a fibre polarization controller (a small portion of the fibre is wound onto three small spools in succession in the ratio $1:2:1$, by rotating these about the fibre axis an arbitrary change of polarization can be effected).

The total time delay through the fibre loop and switch element is 200ns to match the repetition rate of the pump laser and thus the photon source. The correct delay was achieved by the methods discussed in Section 4.7 and was achieved to within 1/4 of the effective timing resolution of the detector system in order to prevent the time of arrival from distinguishing which time bin the photon originated from; compound timing error over four bins must be undetectable.

The switching element is a 'Nanona' device from Boston Applied Technologies. It is ostensibly a fibre device and is connected by splicing to the four pigtails provided. Internally the switch is a free space optical device with four sets of collimation optics incorporated. The active element is a electro-optic ceramic material, which in combination with patterned electrodes is able to perform the switching operation. The electric field required in order to have the optical effect is relatively high; the device requires approximately 200V to fully switch.

The high voltage coupled with the not insignificant $50pF$ (measured at $1KHz$) ca-

pacitive load creates a reasonable power requirement to drive the switch, a dedicated drive amplifier able to translate a TTL (H : L) signal into ($0V : V_\pi$) was used. The limitations of the drive electronics and the impact on achievable speed are discussed further in 4.7 along with the test procedures.

In the scheme set out previously in 4.3 we take action on the photon by controlling the loop switch. The switch requires time to change state and to settle, and this only after the time taken by the decision electronics to act. Additionally we should only allow the photon to impinge on the switch in one of its fully determined states and not while its state is transitioning. For these reasons a significant pre-delay is incorporated before entering the delay loop, this is composed of more Corning SMF28e. The pre-delay length is the same as the delay loop period, although it is not required to be accurate.

By delaying the electrical herald signal the relative timing between the loop switch and the photon can be adjusted. Nominally we require the photon to arrive at the loop $100ns$ before the first switching event (if any), in this way the photon will be half way around the loop when the switch changes state, leaving sufficient time for the switch to transition and settle. The pre-delay of $200ns$ allows the the photon to be moved by $\pm 100ns$ relative to the switch timing by way of a simple electronic delay in the herald path. The decision electronics must operate significantly faster than the timings of the experiment, this can be achieved readily with a number of techniques since timings of the order 10ns represent a bandwidth of only 200MHz. It was chosen to use a Field Programmable Gate Array (FPGA) for the purpose due to the ease of reconfiguration and inherent speed capabilities. The topic is discussed in detail in Chapter 3.

4.6 Loop Control Scheme

To control the switchable delay a short term history must be kept. The most recent occurrence of a herald event needs to be known in relation to the current time; a simple

state machine was devised for the purpose.

Laser pulses from the mode-locked fibre laser source necessarily are split off and detected by a fast photo-diode to control the AOM as described in Section 4.8.2. A copy of the pulse signal is first fed into a variable delay line as described in 3.5 and then into an FPGA. This signal consists of short pulses at a repetition frequency close to 10MHz (determined by the laser cavity). Internally a clock was derived from the pulse train either directly by triggering a flip flop, or by feeding a phase locked loop. The latter has the additional benefit that the laser amplitude induced timing jitter is reduced. The option to work with either type of derived clock was included in order to both gain an insight into the trigger jitter and to allow allow for a missing pulse to be spotted (such an event would put the loop out of sync with the AOM).

In either case the resulting clock pulses are converted to a 50% duty signal with significantly better bandwidth properties, and a sufficient duration in each state to satisfy the timing requirements of the FPGA gates. The notions of setup/hold/reset/release timings are discussed in detail in Section 3.2 but a brief explanation is as follows. The registers in synchronous logic are bistable and due to their underlying constriction have a finite speed at which they can transition. Bistable circuits which are being clocked require all signals are stable before the arrival of a clock edge. Additionally they must remain stable after a clock edge in order to transition state deterministically.

Consecutive time bins are labeled by a counter clocked directly by the laser train. Since the experimental construction employs 4 time bins this counter is ideally modulo 4; we do not require a unique labeling scheme beyond which of the four input bins a pulse belongs to. Nevertheless a large counter is used for convenience by providing two additional signals. The 20th bit of the counter very nearly approximates 10Hz when clocked at 10MHz (within 4%) this signal was used to drive an LED to flash rapidly giving an indication of the successful delivery of the clock signal. The higher bits of the counter (32bits in total) were used to measure the total number of pulses, this

can be used in an integrated measurement as an alternative to time, to quantify the probability of pair generation etc.

In addition to the counter a number of *flags* (one bit registers) maintained in order to keep track of the loop status, since the loop was to contain only a single storage bin, a single bit to signify occupation was required. For a storage loop consisting of a greater number of bins a memory of the occupation state of each bin and ideally a counter to represent the number of times the bin has experienced the loop loss, would be necessary.

When a photon is heralded a short pulse is produced by the APD and delivered via a controllable delay to the FPGA. The pulse is registered by a latch, as the exact time of arrival is not in stable phase to the laser pulse train. The latching of the herald occurs at any point in the *previous time bin* form the point of view of the loop, due to the pre-delay fibre. On the subsequent clock if there was a herald event, a further latch is set which actuates the switch, and remains active until the next time bin, on which it is reset. If the herald delay is correctly set then at approximately half the on-period of the switch the heralded photon arrives, making its way approximately half way through the loop fibre before the herald event latch is reset and the switch closes the loop.

For the mode of operation without external information about any other sources, the delivery of a photon should occur on a particular time bin. The logic to control this is simply "if the loop is occupied and it is the delivery time bin: open the switch". This logical condition is met when, in a similar fashion to the input scenario, the photon is approximately half way around the loop. The switch opens, and some time later the photon is once again incident and is diverted out of the loop to be delivered. An additional complexity arises to handle the case where a new photon arrives on the same time bin that a stored photon is delivered, clearly the newly incident photon has experienced less loss having not been stored. An exclusive-or is applied between the loop occupation signal and the latched herald event such that if the loop is occupied

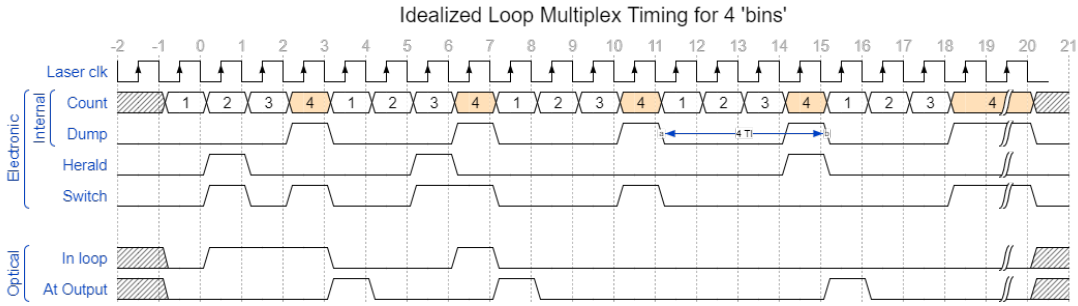

Figure 4-6: Examples of relevant signals to the loop control scheme are shown for four cases of bin occupation. For simplicity detailed timing offsets are removed and the idealized behaviour is shown. Note the switching of the loop from closed to open on the fourth period, in order to release a stored photon from the loop. Additionally for the case where a herald is present at the fourth period note the suppression of the switching signal to allow the photon to bypass the delay.

and there is no herald a switching operation is applied, if however a new herald is incident no switching occurs and the newer photon is allowed to pass through without being stored. If neither the loop is occupied or a new photon is present then the loop switch is not switched. This fourth scenario is also desired behavior and is shown in figure 4-6 as the fourth example cycle.

For the case where multiple sources must fire together, as noted later in Chapter 4, the mutually ready condition is used to trigger output [48]. To summarize the argument for this, consider that if all loops are occupied and output a photon on the designated bin, there are two prior possibilities. One or more of the sources allowed a photon through without passing the loop: this scenario clearly cannot be improved upon. Alternatively the occupation of all the loops occurred at some previous time bin, and all loops subsequently delayed their photon unnecessarily in order to reach the output bin. In this case additional loss was incurred without an improvement; clearly as soon as the collection of sources are all occupied an output should occur. This *relative multiplexing* is readily achieved by a single logic signal shared between the sources which is used to negotiate the output. Each photon source control FPGA outputs a high signal to indicate that it is *not* occupied, but rather than driving the signal

low when occupied instead the output drive is disabled (high-Z state). Externally a weak resistive pull-down is applied, such that when not driven high, the voltage rapidly returns to the low state. An additional pin monitors the state of this external signal and uses it to decide if the loop should switch out; a LOW signal indicates that it should. When this signal is connected in common between the controllers of multiple delay loops it will assume the low condition only when the sources are all in a state of occupied and ready to output, wherein none are driving the signal high and so the signal falls low. The trivial simplicity of this arrangement allows for flexibly combining or separating multiple sources without modification. As only a single delay loop was built, the feature was tested only with dummy signals from pulse generators.

During the alignment and maintenance of the loop, it is advantageous to be able to inspect the state of various signals. Connecting every point of interest in the FPGA to an external pin and driving a 50Ω coax is both mildly impractical and creates problems for timing closure. A practical solution that was implemented was to attach a single auxiliary output connection and cable driver for monitoring, and internally select which of the critical points it is connected to. The status of the external clock (post clean-up), the individual bin clocks (useful for measurements of relative contribution of each bin), the herald input, a second herald input used for working with simultaneous spatial and temporal multiplexing, and the loop switch signal. The choice of which signal to monitor was provided by an 8 position selector switch with binary coded outputs.

The details of FPGA implementations are provided in Section 3 and the following simplified code snippet shown in 4-7 is included for completeness; logic to prevent glitches has been removed for clarity and the functions STRETCH7 and CTR20 represent a pulse stretcher/shortener and a 20bit counter respectively.

Throughout the previous discussion the details of specific timings have been neglected. The choice of a digital synchronous logic for control, forces the user to adopt a simplified point of view. While it is true that the operation of the loop is completely synchronous,

```
module TLD( HeraldIn, EXTCLK2, Clock_50, HeraldOut, LoopSwitch, ActiveLED);
input HeraldIn; output HeraldOut; // herald input and output
input EXTCLK2; input Clock_50; // Clocks
output LoopSwitch;
output ActiveLED;

wire [19:0] Q; wire PLLclk; wire PostDump; wire LoopDump; wire EXTCLK; wire
    HeraldLatched; wire EventOccured; wire LoopSwitchInv;
CTR20 loopCounter(.clk(EXTCLK2), .en(1'b1), .r(1'b0), .q(Q));
assign EXTCLK = Q[0];// ~5MHz internal Clock matches laser train.
assign LoopDump = Q[2] & Q[1];// Periodic (1/4) signal to empty the loop
assign PostDump = (!Q[2]) & (!Q[1]);
assign ActiveLED = Q[19];// LED flashes ~10Hz when correctly triggerd

SR HeraldLatch(.s(HeraldIn), .r(EXTCLK2), .e(1'b1), .q(HeraldLatched));
SR EventLatch(.s(HeraldLatched), .r(PostDump && EXTCLK2), .e(1'b1),
    .q(EventOccured));
PLL Prim_PLL(.inclk0(Clock_50), .c0(PLLclk));
STRETCH7 LoopSwitchPulseStretcher(.delay_clk(PLLclk), .in(LoopDump ^
    HeraldLatched), .out(LoopSwitchInv));

assign HeraldOut = EventOccured & LoopDump;
assign LoopSwitch = !(LoopSwitchInv);//inverted (optical) switch polarity
endmodule
```

Figure 4-7: Simplified code listing for controlling the photon delay loop.

the timing gap between the physical system and the controller logic must be bridged. The time between the laser output and its delivery at the PCF is dependent on the pump preparation optics, the intentional but poorly defined optical delay after the PCF but before the delay loop, and the delay between a herald detection and optical delivery of a photon, all remain undetermined during electronics construction. Special attention was given to the loop delay itself, however designing an electronics control system with specific delays in mind is fraught with difficulty. By allowing for timing variations of $\pm 100ns$ construction proceeded swiftly and with a focus on stability.

4.7 Temporal Loop Construction Measurements

A number of characterizations were performed during the construction of the delay loop and associated apparatus. The following subsections cover in detail how the measurements that had a significant bearing were made.

4.7.1 Switch Insertion Loss & Speed

The most significant source of optical loss in the delay loop is the optical switch. The parameters of interest for a general optical switch (apart from the specific switch states) are its loss and speed of operation. Fibre integrated switches available at present typically operate in one of two ways; optically active materials, or by mechanically redirecting light.

Mechanically redirecting light using a Micro-Eectro-Mechanical System (MEMS) structure can offer a low loss of the order 0.1dB or better. The speed at which the mechanical systems can move position and settle limit the achievable switching rate. In many industrial and telecommunication applications speed of fibre routing is not a critical parameter; the available few KHz speeds are generally acceptable. Additionally it is significantly easier to produce an add-drop type switch arrangement mechanically, but significantly harder to produce the 'swap' style 2 x 2 operation desired for the time delay loop. It is worth noting that other delay structures comprising multiple single pass loops of binary length multiples (and thus log resource scaling, like that shown in 4-3) can make use of add-drop switches.

The maximum rate of photon delivery from a delay loop based source is some integer fraction of the switching speed of the optical delay. In order to deliver high photon rates it is necessary to use a different switch technology capable of a much faster response. Switches of this type are typically comprised of an optically active material that is controlled by an electric field directly. At the time of purchase the *Nanona* (P/N

Input	Output	Voltage	Insertion Loss
1	2	$0V$	0.72dB
1	4	$199V$	0.98dB
3	4	$0V$	0.92dB
3	2	$199V$	1.02dB

Table 4.1: Insertion losses for the delay loop optical switch, measured in the directions indicated for the four paths required. Note that the variation in loss creates a preferred arrangement for splicing the loop.

FOS2200-3300) from Boston Applied Technologies was the fasted available fibre switch with insertion loss of approximately 1dB.

According to manufacturer specifications the switch is capable of achieving a 1MHz switching rate at 50% duty. It was determined that this was unlikely to be a true limit of the switch capabilities, and more likely represented the limitations of the high voltage drive amplifier. Driving the switch with a DG535 function generator, and monitoring a laser passed through the switch with a fast photo-diode, a maximum switch rate of 9.61MHz was achieved (additional cooling for the amplifier was required). The highest achieved speed was significantly less than the the repetition rate of the mode-locked laser selected to drive the photon source, requiring a sub-multiple be used instead.

Before splicing the fibre loop onto the switch, the insertion loss was studied in each state. For the case where V_π was high, a fine adjustment of drive voltage was performed to achieve minimum loss. All losses were checked as cut-back measurements where the power is measured though the device under test, and then again ahead of the device by cutting the optic fibre. The technique eliminates the repeatability problems associated with coupling power into a fibre. Conversely capturing all of the light escaping from a fibre core onto an integrating detector head is straightforward and has minimal impact on the repeatability of results. Shown in Table 4.1 are the four insertion losses for the optical switch. Noting that optical losses are generally direction independent; however these losses were measured in the directions indicated, which are also the directions later used in the loop multiplexing.

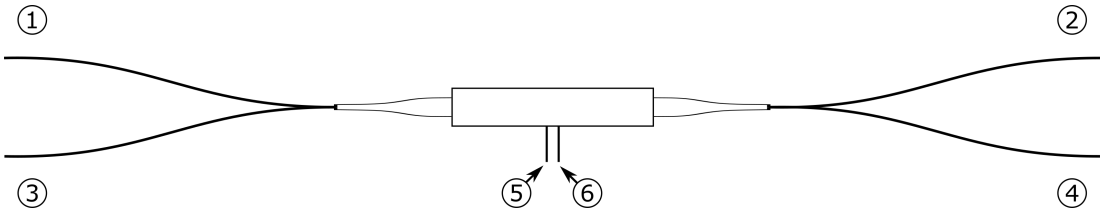

Figure 4-8: Schematic representation of the Boston Applied Technologies *nanona* switch. Ports 1 through 4 are 1m optical fibre pigtails of SMF28; port 5 is electrical ground and is common to the casing of the switch; port 6 is control voltage input. For this switch ports 1 to 2 and 3 to 4 are connected internally in the electrically off state. When approximately 199V is applied to port 6 the optical connections are reconfigured to 1 to 4 and 3 to 2. Table 4.1 surmises the relevant insertion losses incurred.

To obtain an estimate for the maximum achievable switching bandwidth the characteristics of the switch were first measured on an LCR bridge. The load was found to be capacitive (around 50pF) with low ESR and very low leakage. Combining this knowledge with the previously determined optimum operating point $V_\pi = 199$ a step response experiment was configured.

The supply from the high voltage amplifier was fed through a current limiting resistor of $100K\Omega$ to prevent a short circuit from loading the driver excessively. At the base of the switch body, as close as possible to the terminals an SCR was soldered such that in forward conduction the voltage across the switch would be forced to approximately $1V$. The switch was charged to V_π over a few seconds by placing the driver in continuous output, and subsequently shunted by triggering the SCR (manual operation). The triggering produced a single clean and rapid discharge resetting the switch to off position significantly faster than the implied rate provided by the manufacturer data.

By coupling some 1550nm CW laser light into the switch, and monitoring the light in both output ports with photo-diodes onto a single shot oscilloscope capture, it was determined that the commutation happened on a timescale faster than the photo-diode bandwidth (35MHz, Thorlabs DET10C). It was subsequently determined that the high voltage amplifier could be made to operate at up to 9.61MHz before reaching the point

at which it could not sufficiently drive a 50pF dummy load, at this point the additional power dissipated was sufficiently small that with additional cooling from a small fan, the temperature could be maintained within acceptable limits.

4.7.2 Construction of the Loop Delay

The fibre delay loop is comprised of SMF28e; the length of fibre controls the delay to photons stored in it. The exact length of fibre was calculated and re-wound from an automated drum winder onto a reel. The reel provides mechanical strength and constant tension. To finesse the length of the fibre to the desired length tolerance the switch was spliced to one end of the delay and butt coupled to the opposing end such that on the off state a continuous loop of fibre is produced.

A CW light source was attached to the remaining input port on the switch, and a fast photo-diode connected to the output port. The butt coupled section was mounted to a 3 axis micro-positioning stage to allow repeated re-alignment as needed. The same stage is also used to cleave the fibre reliably by delivering axial tension to a single fibre, which is then nicked by a sharp ruby. By taking great care to produce perfect cleaves to the fibre, upon the correct length being found the fibre ends could be directly transfered into the fusion splicer for permanent setting. Using this method takes account implicitly of the unknown delay through the switch (due to pigtail length).

Using an external pulse generator a control pulse of laser light is generated by switching the optical switch into the loop. After 50ns the laser was disabled electrically by the first time delay of the pulse generator and the switch set to the closed position, however the exact time of the pulse is not critical. After a further delay of approximately 700ns the switch was reverted back to its initial state; delivering any remaining light in the loop to the photo-diode. Upon reception the interval between subsequent rising edges of the photo-diode contains 4 times the loop timing error. The process was run continuously

by an advanced pulse generator (DG535) and recorded by an oscilloscope.

The specific APDs (as discussed previously) intended for single photon use have intrinsic jitter of 300psRMS. Light in SMF28 with a velocity of approximately $0.7c_{vac.}$ would take approximately 63mm to develop an equivalent delay. With manipulation in increments of approximately 3mm, the timing error of the delay can be made sufficiently small that for use as a single storage bin, the error should not *label* subsequent delay bins. After four passes of the loop the error in the measured delay is dominated by the time resolving capability of the oscilloscope. Sampling at 4GHz (350MHz analog input bandwidth) the oscilloscope capture can locate the 50% point of the relevant edge within ±250ps, which gives ±63ps per cycle of the delay loop. The resolvable timing difference is equivalent to 13.2mm of SMF28; significantly greater than the minimum manually handleable length of 3mm. Including reading the oscilloscope the overall timing error is estimated to be ±80p per passing of the delay loop.

4.7.3 Initial Verification Tests

After complete splicing of the loop a series of dummy experiments were performed with bright light to verify the expected optical losses, lead-in and lead-out static delays, and relative timing of the existing noise gate (shutter) with respect to the laser pulse train signal. Due to the need for additional pulse picking, synchronization of the noise gate was transfered to a new control signal with adjustable delay.

After all relevant time delays had been determined to within a bracket small enough to be manually searched by remote control of the electronic delays, verification experiments were performed with single photons. Correlation was found between signal and idler for no loop delay, and cross correlation for the case with static delay.

An example of typical loop behavior can be seen in Figure 4-9 in which the switching of an idler photon into the loop is seen, the periodic dump or reset pulse which switches the

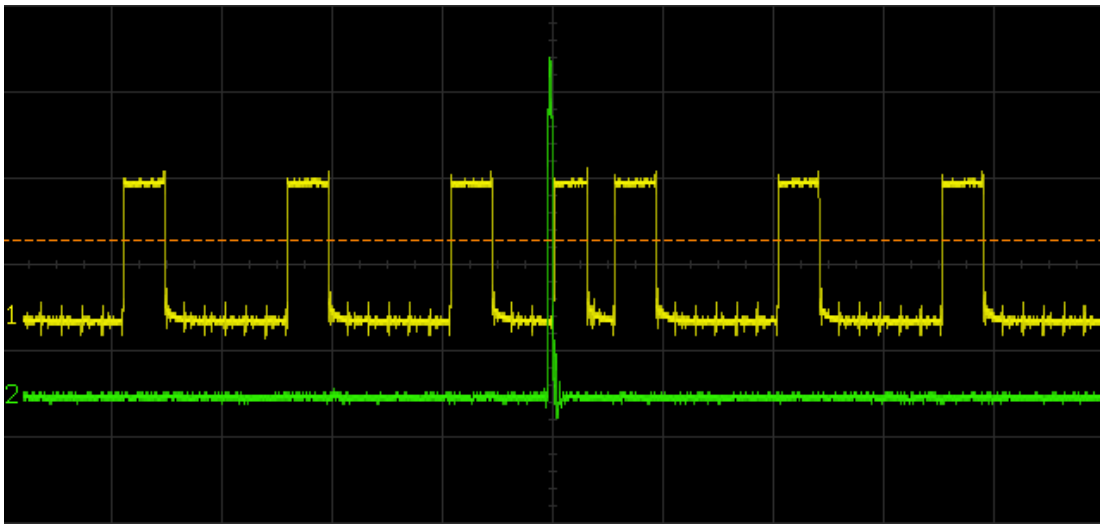

Figure 4-9: A time domain capture of loop behavior during verification. Yellow trace indicates the loop switch control signal: when high, light is coupled into or out of the loop (cross state). Green trace is the herald detector raw signal post input delay. Shortly following the herald detection the loop is set to accept the idler photon; two trips around the loop are then completed before the next periodic 'dump' of the loop contents switching them again into the output fibre on the fourth time bin.

contents of the loop to output is noticeably longer in duration with the herald induced switching. The signal to empty the loop overlaps the final time window slightly to prevent a brief glitch closing of the switch when the photon arrives in the penultimate position. The herald detection has been delayed by $150ns$ in order to align with the operation of the switch approximately $50ns$ before the arrival of the idler photon at the switch.

4.8 Pump Laser Preparation

4.8.1 Spectral Qualities

The PCF photon sources used for multiplexing experiments are pumped by a Fianium Femtolase FS-1060 mode locked fibre laser, Ytterbium doped fibre amplifier (YbDFA) and pulse compressor. The output of the laser is a pulse close to 200fs in duration

and repeating close to 10MHz. The output bandwidth of approximately 14nm is not transform limited and is shaped characteristically by the self phase modulation in the amplifier. In the interests of low noise the portions of the laser bandwidth unnecessary for the desired phase matching are removed. For this a transmission grating monochromator was used in a configuration with a single grating and a fold back mirror. By adjusting the positions of a pair of knife blades on micrometer stages it is possible to block portions of the spectrum from returning to the gating to be re-combined.

Ideally the fibre system would be spliced from the output of the fibre laser directly to the input of the four wave mixing PCF, however the mismatch of laser properties with desired pump properties, and the intention to have some control of output spectrum have necessitated a free space optical portion in the system. The source used to generate photons in this experiment was designed by Dr Francis-Jones; the specifications and performance are described in his doctoral thesis [39] and in [38].

4.8.2 Pulse Frequency

In Section 4.7 the limitations on switching frequency are discussed. Notably since the maximum frequency of optical switch operation is slower than the laser repetition rate it would not be possible to use every pulse of the laser output. A free-space acousto-optic modulator (AOM) was inserted between the monochromator output and the polarization and power control optics. The unit used was a Brimrose FQM-80-20 unit and associated RF generator. In order to select every odd pulse a simple counter divider was built from a 74HC74 dual D-flop to supply a 50% duty and half frequency gate output. Since the laser in question did not provide a suitable synchronization output a fast photo-diode was used to detect a small fraction of the laser output.

The AOM driver has a built in tone generator in addition to the amplifier, and is arranged so that an external input can be mixed with the tone. Although the mixing

products of the gate output and carrier would ordinarily pose a problem, in this case the pulse of laser light is incident only during the times when the AOM is fully 'on' and fully 'off' so that the laser is effectively diverted into two beams composed of odd and even numbered pulses. A copy of the photo-diode signal required for this technique was amplified and delivered to the control electronics as a reference signal to synchronize the delay loop.

Two significant undesirable effects result from the use of the AOM in this manner. The power delivered by the laser used here is subject to variation of several percent, this results in the rising edge of the detected signal at the photo-diode varying in steepness and so introducing variations in the exact time of triggering. This jitter is not present on the optical pulse train, or at any rate to a much lesser degree. Secondly if for whatever reason a pulse is missing, the divider can become out of step, having now switched an odd number of times. The counter in the FPGA however keeps counting and is now out of step with the optical pulse train, making switching operations occur incorrectly at the moment of photon incidence on the switch. Care must be taken to keep the loop controller and the AOM divider supplied with sufficient signal, if at any time the signal level becomes marginal the synchronization is lost.

4.8.3 Power & Additional Optics

Laser output power was monitored for long term drift by a power meter placed on the rejected beam of the polarizing power control optics. Additionally the rejected port of the integrated wavelength multiplexers contains the majority of the input power to the photon sources. In previous work performed with the sources performance was monitored against the rejection power allowing some approximate operating point adjustment, and a convenient input coupling monitor for initial coupling of the PCF.

4.9 Noise Gating

Previous to the discussed experiment, two similar photon sources had been spatially multiplexed together in the manner shown in Figure 4-1 and results published in [38]. During the course of the work it was found that a significant improvement was made to delivery statistics by performing the spatial multiplexing with one source disabled. The effect is due to the *noise gating* of the output mode caused by switching the output to blocked when the source is not firing. A detailed discussion of the idea is presented in [40].

Operation of the temporal multiplex is independent of any additional spatial multiplexing performed. During all previously discussed work an additional optical switch between the photon source output and temporal multiplex input was spliced, inserting a constant 1dB loss. The additional switch allowed two hybrid scenarios to be explored by implementing noise gating (switching the photon source to output on each herald with an appropriate delay) and spatial multiplexing (in which one of the two near identical photon sources is selected as input to the temporal multiplex if it heralds) concurrently with temporal multiplexing. The arrangement prior to the temporal multiplex is exactly that used in [39].

The presented loop data made use of the spatial multiplex in noise gating mode as it was desirable to leave the sources undisturbed and spliced in their time aligned positions. Additionally the reduced noise offered by gating the idler makes time alignment significantly easier due to the improved contrast in observed correlation rate when the correct delay is achieved. Brief experiments were conducted with both spatial and temporal multiplexing by pumping both photon sources, however the temporal loop multiplex performance is dominated by its switching loss and performance did not differ significantly for the effective improved initial photon source. To herald the arrival of a photon at the loop a logical OR between the source heralds was performed

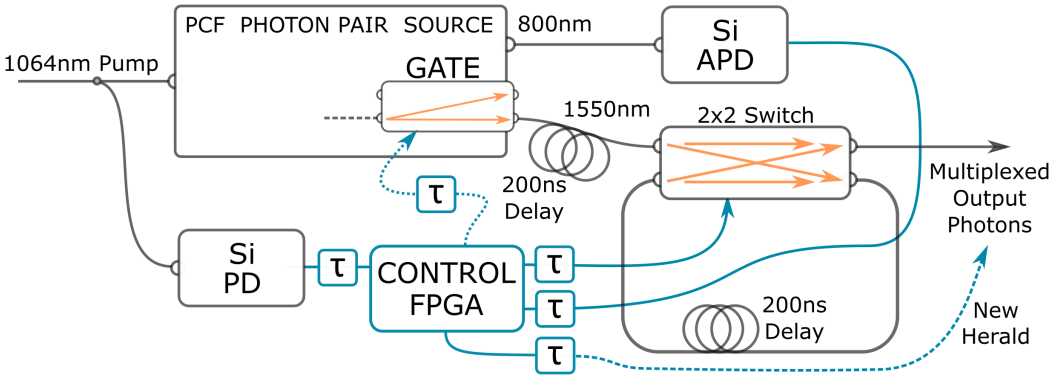

Figure 4-10: In addition to the form of the loop multiplexing scheme presented in Figure 4-2, a second spliced fibre optic switch is included in the idler output path. The switch is used to either gate output photons against the herald to reduce noise delivered in the output port [40]. Alternatively it can be used as the point at which two source output modes could be spatially combined as in [38]. The control scheme for the noise gate is implemented by the FPGA and is to pass the idler mode in a fixed width window around the arrival of a herald photon. As with the other switch control signals, an adjustable electronic delay was used to centre the noise gate window.

along with an additional channel of controllable delay to accommodate any difference in length between the photon sources pre the spatial routing switch.

4.10 Temporal Multiplexing Results

The PCF photon source performance is known but varies significantly depending on the operating point due to the noise power impacting heralding. The noise originates from inner side band (unwanted) four wave mixing and was not completely removed from the output; narrow band filters are not used in this source in order to exploit the spectrally engineered output.

The primary technique for assessing temporal multiplex performance was as follows. At every selected operating power level over a range, an integrated coincidence rate measurement was taken with the multiplexing loop operating, and with the loop disabled but physically still spliced in place. Any variation in source performance during the

process was minimized by performing the measurements in succession several times. By comparing the coincidence rate of delivered photons with and without the loop operational, the effective contribution of the first of the four time bins (the disabled loop effectively selects a fixed delay which corresponds to correct timing for 25% of the heralded events) to the total contribution of all time bins was compared (however the other time bins have been subject to extra losses).

Another secondary technique used to quickly quantify performance was to create a histogram of heralding times versus idler arrivals. A histogram was produced using the time averaged oscilloscope trace of the herald events, triggered on the detection of an idler photon. In each trigger case (for each idler photon observed) the relative position in time of the corresponding herald event (measured as the rising edge position of the respective output pulses) is recorded by the oscilloscope. By averaging multiple traces the relative frequency of a herald at a particular prior time being coincident with output of a photon is approximated.

The histogram method as described is not ideal, as any uncorrelated light (i.e. accidental cross correlation) is not quantified, and so the histogram trace cannot be straightforwardly normalized. While this limitation prevents a meaningful quantitative measurement, during alignment and adjustment of timings the oscilloscope histogram proved an invaluable intuitive tool. Shown in Figures 4-11 and 4-12 are typical examples of what such a histogram looks like; first with the loop disabled, and then with the loop operational. This method does not quantify the contribution from each time bin directly, but rather demonstrates the change in relative timings caused by the loop action.

To explore more quantitatively the contribution to the final output from each time bin a correlation counting experiment was performed. The FPGA was configured to only produce an output herald signal at the appropriate time for detection if the herald event occurred during a specifically selected time bin. By muting the herald for all but

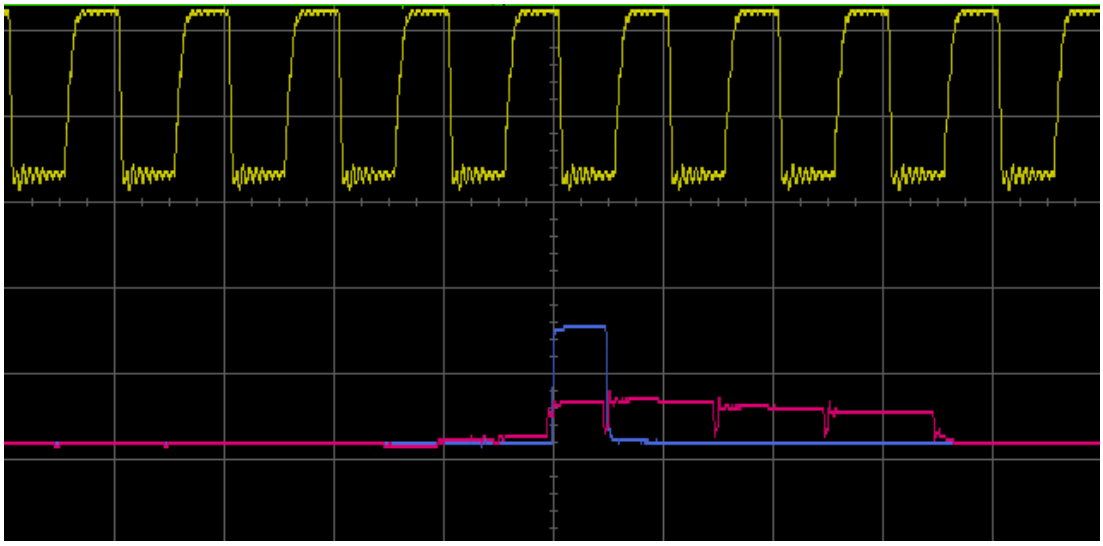

Figure 4-11: Oscilloscope histogram formed from the time averaged trace triggered by the arrival of an idler photon. The pink trace is high when the FPGA indicates a photon should be exiting the delay loop, however in this case the loop is disabled and so the FPGA output is not co-timed with the actual idler photon. It can be seen that output events (where the pink signal is produced) are approximately as frequent from the four distinct time bins. Conversely a histogram could have been performed by triggering on each herald and plotting the arrival times of the idler, however due to the low frequency of idler events it would be problematic to average traces triggered in this manner.

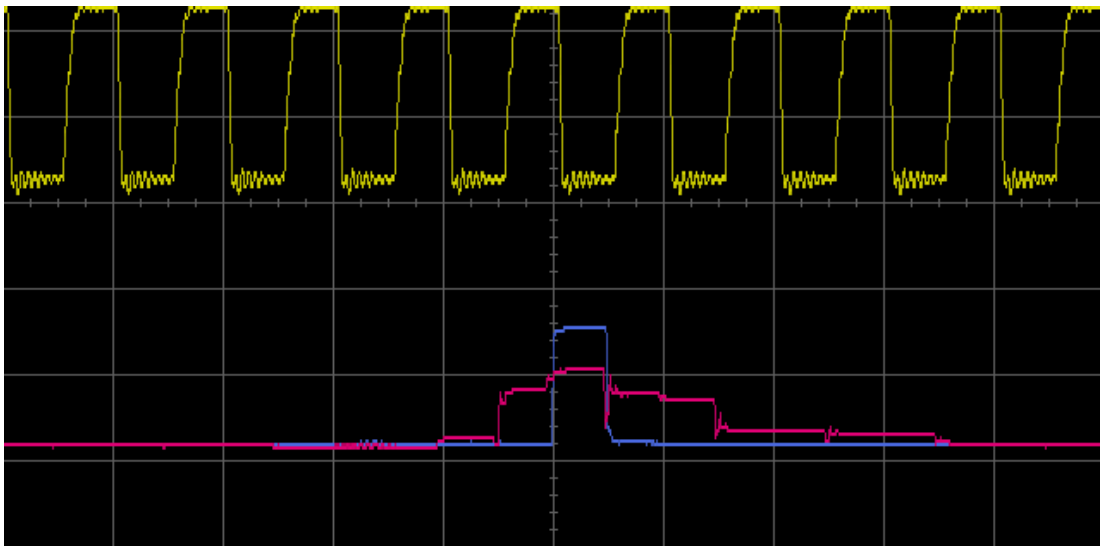

Figure 4-12: Scope histogram produced in the same manner as for example 4-11, however here the loop switch has been enabled. It can be seen that a single time delay relative to the idler is heralded significantly more frequently than before. Ideally only a single bar would be seen here, however some generated heralds from the FPGA and idlers are not aligned. Note that noise in the idler detector should not correlate with the generated herald; the second slightly smaller bar is probably due to marginal or incorrect behavior of the loop.

the selected time bin, and otherwise behaving as before, the contribution to the total count rate from each bin was observed.

It must be considered that selectively disabling the herald signal not only prevents counting of photons from the correlated process of pair generation, but actually also reduces the cross correlation accidental counts. Uncorrelated noise is delayed and attenuated in exactly the same manner as the idler photon; at no time is it possible to present a photon from pair generation with a given attenuation, at the same time as noise which has experienced a different delay or attenuation. It is assumed therefore that the usual estimate of expected cross correlation for the observed raw herald and idler count rates are valid.

Expected cross correlations per second divided by the observed coincidence rate is the probability that a coincidence event was generated by the correlated process and not noise. Cross correlation of noise is usually termed *accidental* counts, giving rise to the *coincidence to accidental ratio* figure of merit.

Where a coincidence to accidental ratio (CAR) is used to qualify performance, the estimated accidental counts are additionally confirmed by intentionally delaying the arrival of herald signals such that no coincidences from the correlated process can be observed. The remaining coincidence count rate is due to the accidental cross correlation alone. Where a pulsed laser is used it is insufficient to offset the time by a small amount as noise power is strongly correlated with the laser pulse. In order to correctly observe the cross correlation the coincidence is measured between herald and idler on produced on consecutive laser pulses.

Contributions to the output mode from each time bin are found by selectively gating the herald output to only fire on a particular bin within each cycle. The proportion of the total output as a fraction of the un-gated heralded output is shown in Figure 4.2. Although $200ns$ are required to propagate around the loop the usable time window

while the switch is not transitioning is significantly shorter. The widths of the usable portion of the time bins were observed by advancing or delaying the switch operation relative to the laser pulse train while observing the loss of counts that occurs when the photon is entering during the switch transition. The slight reduction in the time window for bin 4 is an artifact of the reset logic and is inconsequential to the operation of the source since the photon duration is much shorter than any of the usable bin widths.

The coincidence counts are measured at different input pump power are contrasted against the cross correlation (accidental ratio). Shown in Figure 4-13 the cross correlation rates are plotted against the heralded photon delivery rate (coincidence counts) for the cases where the temporal multiplexing loop switch is enabled or disabled; No other factors being varied between taking the data with and without the loop. The delivery rate for a given cross correlation is seen to be improved by a significant factor when the temporal multiplexing is applied. The data shown in Figures 4-13 and 4-14 (which show the same dataset) is also published in [44] and was collected as a series of integrations at each power level and configuration.

The probability of the output bin being occupied as a function of the correlation counts has variable improvement as shown in Figure 4-14 when the temporal multiplex loop is enabled, with a peak improvement factor of approximately 1.45. For identical delivery probability, when the temporal multiplexing loop is enabled the delivered photons are associated with a lower heralding rate indicating a lower noise. For a given herald rate, a greater proportion of the heralded events are successful photon deliveries with the temporal multiplexing applied.

The improvement factor observed is clearly significantly below the theoretical maximum fourfold improvement attainable by combining four time bins. The result is however significant when considered in the context of multiple photon delivery as per the discussions in Section 4.4, in which an exponential improvement in joint delivery

Herald time bin	Bin width	Contribution
First	121.5ns	0.37
Second	121.5ns	0.35
Third	121.5ns	0.19
Fourth	89.0ns	0.09

Table 4.2: Contributions to output from each time bin. Although $200ns$ are required to propagate the loop, the usable time window while the switch is not transitioning is significantly shorter. The widths of the time bins were observed by advancing or delaying the switch operation relative to the laser pulse train, and observing the loss of counts when the photon is entering during the switch transition. The slight reduction in the time window for bin 4 is an artifact of the reset logic and is inconsequential to the operation of the source.

probability from a collection of sources is shown for any increase in single source delivery probability. The relative multiplexing concepts discussed previously imply that a further increase in improvement factor may be expected when this source is operated as part of a collection; the mean loss applied per delivered photon is lower if any events take place where photons are jointly released from the delay earlier than the final time bin.

4.11 Summary

The temporal multiplexing loop constructed clearly has a modest impact on the emission statistics of the photon source. Other photon sources constructed in different ways and with different spectral parameters can outperform the best photon delivery statistics demonstrated here, however the specific performance is less significant than the demonstrated ability to change emission statistics independently of other source parameters.

The performance of a heralded photon source becomes important when we desire a large collection of sources to mutually fire. In future quantum information processing endeavors based around photon qubits the number of simultaneously deliverable qubits

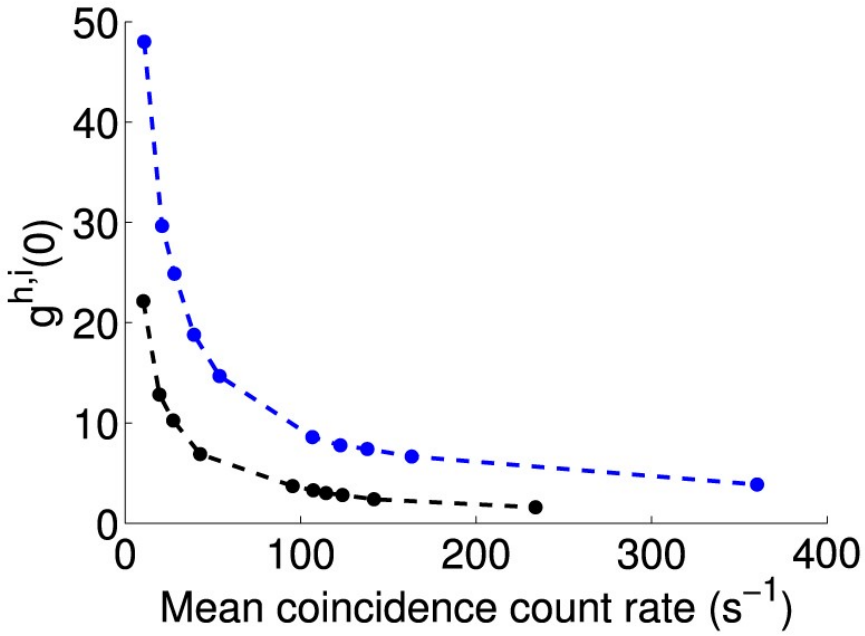

Figure 4-13: The coincidence counts measured at different input pump power are presented against the cross correlation (the ratio of correlations to expected accidental counts) for two configurations. Average accidental correlation counts are predicted as the product of the herald detection rate, idler detection rate and twice the coincidence window; the number of expected simultaneous events if the inputs are uncorrelated. Black represents source performance with the loop optics spliced in but not operational. The blue data are the same operating points with the loop switch enabled. No other factors were varied between taking the data with and without the temporal multiplex. The delivery rate for a given cross correlation (noise) contribution is seen to be improved by a significant factor. The data shown is also published in [44], and was collected as a series of integrations at each power level and configuration over 300s.

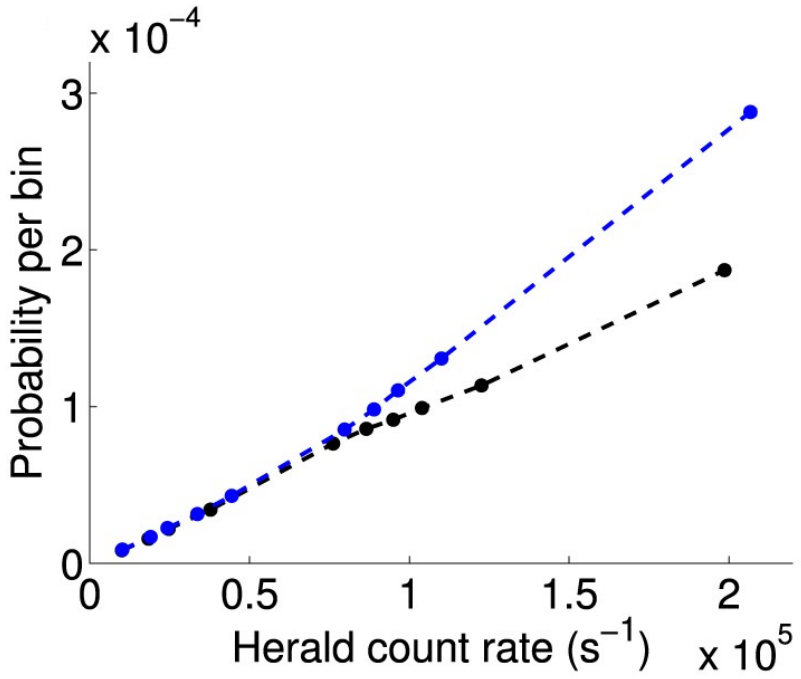

Figure 4-14: For the same data collected and shown in Figure 4-13 and following the analysis presented in [44] we can calculate the probability of the output bin being occupied as the ratio of the correlation counts observed to the fixed number of bins per second, and plot it against the heralding rate. Here we see a variable improvement in occupation probability when the multiplex loop is enabled, and a peak improvement factor of approximately 1.45. For identical delivery probability, with the loop enabled (blue) the delivered photons are associated with a lower heralding rate, indicating a lower noise; conversely for a given herald rate, a greater proportion of the heralded events are successful photon deliveries.

is a critical parameter. A small improvement in delivery rate without an associated increase in either noise or multi photon pulses, has potential to have an exponential improvement on the probability of a group of sources firing together.

Further the use of only a single switching element regardless of the number of temporal bins represents an independent scaling of resources with the number of sources employed. Other contemporary temporal schemes such as [49] and [50] do not scale linearly. Implementing the recycling loop in an integrated fibre optic architecture further reinforces the practical scalability of the demonstrated system, and the inherent compatibility with photonic crystal fibre and associated wide variety of phase matching.

Despite the modest practical success demonstrated, the significant optical loss of the chosen integrated fibre optic switch limits the practical usefulness of such a scheme. In future technological developments a lower loss switch may be available, however the market demand at present is limited by the availability of low loss but slower MEMS devices which are adequate for most telecommunications purposes. Free space temporal multiplexing such as the recent work by Kaneda [51] achieve vastly improved performance owing to the low switching losses attainable, however the practicality of producing a collection of identical sources is unknown. Producing a long precise optical delay in free space, in a compact robust manner is not trivial, as it is in optical fibre.

Construction of near identical temporal loop multiplexing sources is practical and straightforward provided photonic crystal fibre with sufficiently similar four wave mixing joint spectral amplitudes is available; the PCF being the only significant non-standard element used in the source.

The relative temporal multiplexing made possible by sharing storage loop occupation state information between temporally multiplexed sources was not demonstrated. The improvements possible by this technique are clearly of greater importance where high losses are present. If for the desired operating speed, the available switch losses are a

significant component of the total loss, relative multiplexing may be exploitable. The fibre integrated architecture presented would at present be greatly aided in simultaneous delivery probability between sources by employing this technique.

Overall this work has demonstrated a modest improvement in delivered photon statistics via a practical implementation of temporal multiplexing, in a fibre architecture, with favorable resource scaling requirements.

Chapter 5

Two-dimensional Quantum Random Walk of Single Photons in a Multi-core Optical Fibre

5.1 Introduction

Quantum information processing can be accomplished with many physical systems as noted in Section 1.1. The goal of applying quantum information processing is to use an experimentally accessible quantum system to model either another less accessible system, or some other abstract mathematical system. This can be accomplished by preparing a model system that is isomorphic with the system of interest, and subsequently making observations about the behaviour of the model system. With suitable choice of basis to represent the quantum information to be processed, a scheme that maps realizable operations to the abstract operations desired can be found. For example a singe qubit might be represented by photons in a polarization mode basis containing two eigenvectors $|H\rangle$ and $|V\rangle$, where preparation and measurement operations can be

realized using a polarizing filter.

In the KLM [13] scheme known also as Linear Optical Quantum Computing (LOQC) a universal set of operations are mapped onto linear optical elements; the only additional resources being the single photon sources and detectors. Although it is a non deterministic scheme, that is the sucess of an opperation or *gate* is probabilistic and independent, it offers a practical way to implement photonic computing, and can be improved to near deterministic operation with the use of a sufficiently many entangled ancilla states. Since all operations are linear we can simplify the discussion of apparatus to the implementation of an arbitrary unitary matrix describing the operation, applied in terms of the optical modes used as a basis. Photonic qubits are passed through this unitary and then sampled by detectors; results are then post selected when the *gates* function as desired. In practice such unitary operations may be implemented by beam splitters, mirrors, and phase delays, however the specific form of the unitary operations need only be able to realize all opperations (rotations) in the Bloch sphere.

System efficiency is intricately related to the practical implementation. Consider for example that although there are a very large number of ways to implement an interferometer, often a particular arrangement is preferred. Implementations of unitaries may be constructed as an arrangement of optical elements that is somewhat isomorphic to the operation being carried out; consisting of the minimum number of carefully chosen parts. An approach like this will result in the best performance trade offs for the specific unitary and is likely also to be the most compact.

A *statically programmed* optical system is undoubtedly a required first step towards general quantum processing, however it is desirable to be able to modify the unitary arbitrarily during runtime. A philosophical point of note here is that a large number of computational problems which we may want to solve using quantum processing algorithms can be grouped by the type of operations they require. For example a great many algorithms are built upon the Fourier transform, and so by efficiently implement-

ing the transform, we can reproduce a whole class of derivative algorithms. Likewise for the popular classical statistical mechanics technique of Monte Carlo simulation, the core principle enables many further algorithms. If we can structure the optical implementation of the unitary transform in a manner isomorphic to a core algorithmic structure found in a class of problems, we can make use of the wealth of existing algorithms upon a common quantum processing structure.

One particular computational paradigm that has successfully been re-cast into the quantum domain is the 'random walk'. A random walk is as the name suggests a chain of states, in which the next position in phase space is dependent on the previous state and some random element. Structures of this type are used to model stochastic processes like financial markets and chemical reactions, to model connectivity in networks, and in Markov chain Monte Carlo (MCMC) simulation, to name only a few key examples. A quantum random walk is one in which the random walk state is not measured at every step, this allows a superposition state to be formed at any point where the outcome is probabilistic. By superposing the outcomes of each step of the random walk, the available Hilbert space is rapidly explored; all walk pathways up to the number of steps (or the point in a continuous time scheme where the walk is terminated) are simultaneously part of the output state. Upon measurement naturally the state will be found projected into one particular eigenstate.

As an example of a computational problem that can be solved by a quantum random walk in sub exponential time, and where no classical sub exponential solution exists, we can consider the problem presented by Childs et. al. in 2002 [52] as follows. We wish to traverse some graph algorithmically from the ENTRANCE to the EXIT node with the aid of an oracle which can inform us the unique names of connected nodes to the current one, and also the name of the EXIT node so that we can identify the goal when reached. The graphs to be considered are dual binary trees of depth n. The entrance and exit nodes are the root nodes of the two trees; each tree having 2^n leaf nodes after

n generations. The two trees are joined to one another by randomly chosen leaf node pairs, one chosen from each tree. It is important that edges are added until every leaf node has three edges attached. This homogeneity in the coordination number of every node thwarts a classical polynomial algorithm from finding a node with only two edges and working from it towards the exit (the point at which a wrong turn occurred can be inferred by the number of steps before return to another node with only two edges).

A quantum walk explores the graph in sub exponential time, faster than any classical search. This is proved rigorously to be always faster than any classical algorithm by Childs [52] and is a relatively involved problem. The graph edges are coloured such than no node has two edges the same colour, and the oracle operates by providing the name of a connected node, given an edge colour and the name of the current node. The problem is solved efficiently by a breaking the general unitary into separate unitaries for each colour, which the authors go on to demonstrate can be used to simulate the evolution with only polynomial calls to the oracle.

5.1.1 Discrete Quantum Walks

A quantum walk in discrete time (or discrete steps) can easily be partitioned by the two key ideas that define the walk, namely the *walk space* and the *coin space*. The state space in which a walk progresses is the Hilbert space spanned by the displacement or shift operators for the walk. Starting from some initial state, the next state in the walk is reached by applying one of the shift operators. The walk Hilbert space is the state space reachable using combinations of the shift operators. The space may or may not be infinite; a trivial case to consider is the infinite discrete one dimensional space accessed by increment and decrement shift operators.

At each step of the discrete time quantum walk, shift operators are applied to the present state. The choice of which shift operator to employ is controlled by the so

called coin operator (in reference to a coin flip used to pick a direction in a classical random walk) which applies a weighted superposition of displacement operators. The input state is propagated by weighted amplitudes of each shift operator; this can be a simple symmetric and invariant weighting, or more complex time dependent and biased.

Consider the one dimensional state space $\{|n \in \mathbb{Z}\rangle\}$ which we shall call H_{walk} and assume that we start the walk at $|0\rangle$. Two shift operators are required to span all of the available space, specifically increment and decrement. Alternatively we can define a single operator which changes the applied operation depending on the state of the *coin state* ancilla that can be acted on by the aforementioned coin operator.

$$\hat{D}|n, H\rangle \rightarrow |n-1, H\rangle \tag{5.1}$$

$$\hat{D}|n, T\rangle \rightarrow |n+1, T\rangle \tag{5.2}$$

Where $\hat{D}$ is the displacement or shift operator on the extended space formed from the previously defined walk space and the coin space H_{coin} with only two possible states $\{|H\rangle, |T\rangle\}$ labeled heads and tails here to avoid confusion.

$$H_{total} = H_{walk} \otimes H_{coin} \tag{5.3}$$

States of the total space will now include both labels and can be acted upon by equations 5.1.1 and 5.1.1. An operator must be chosen to randomly flip the coin as per a classical random walk, or to place the coin in a superposition of the H and T states. We apply an unbiased coin known as the Hadamard operator which takes the same form as per

the directional coupler and beam splitter discussed previously in the context of Hong Ou Mandel interference.

$$\hat{U} = \frac{1}{\sqrt{2}} \begin{bmatrix} +1 & +1 \\ +1 & -1 \end{bmatrix} \tag{5.4}$$

$$\hat{U}|H\rangle = \left(\frac{1}{\sqrt{2}}|H\rangle + \frac{1}{\sqrt{2}}|T\rangle \right) \tag{5.5}$$

$$\hat{U}|T\rangle = \left(\frac{1}{\sqrt{2}}|H\rangle - \frac{1}{\sqrt{2}}|T\rangle \right) \tag{5.6}$$

By successive application of $\hat{U}$ followed by $\hat{D}$ we can propagate one step of the quantum random walk. For convenience we can compose the two operators together to form a walk operator $\hat{W} = \hat{D}\hat{U}$ and define the walk state after n steps as,

$$|\varphi_n\rangle = \hat{W}^n|\varphi_0\rangle. \tag{5.7}$$

5.1.2 Continuous Time Quantum Walks

Continuous time quantum walks can be considered as continuous evolution of a Schrodinger-picture Hamiltonian on a discrete graph. It is noteworthy that the philosophical concept of a *walk* applies to the discrete space that is traversed, rather than the actual quantum system which can be either discrete or continuous evolution.

The paradigm for continuous quantum walks can be easily understood as follows; problems of interest are represented (or the problem space is) by a mathematical group. The group is composed of a set of elements which represent some quantity of interest such as valid points in state space, or the allowed operators acting on some other space, etc. along with a group operator (typically composition) by which elements can interact to produce further elements of the group. Since a group must be closed to be considered valid, all elements must be reachable by some combination of other elements of the group. A subset of the elements called the generator set is the minimum set of elements from which, by successive group operator applications, all remaining group elements can be reached. For example all integer valued three dimensional Cartesian vectors can be produced by the Cartesian unit vectors (the three generator elements) under addition.

A group has a corresponding Cayley graph which represents it. A group is a precisely defined mathematical object, but does not explicitly demonstrate its underlying structure; it is a set of rules in which a structure can be discovered. A graph on the other hand is an explicit structure; specifically the canonical Cayley graph is n-regular where there are n elements in the generating set. It is readily seen that the Cayley graph must contain all possible *routes* through the group, that is, at every vertex the edges represent application of the group operation with each of the generators. Note that the other well known structures such as Markov chains would be contained within the Cayley graph.

A physical system that is able to implement the graph is constructed, and the graph traversed by either a quantum or a stochastic *walker*. What exactly is considered a solution depends on how the original group was part of the algorithm of interest. For example a group might represent a some abstract problem space, and the shortest route between two points might be a typical solution. The unusual statistics of quantum mechanics allow the graph to be traversed rapidly, but in exchange for a complicated

final readout in which only an eigenstate can be measured. If in some number of runs the quantum walker can sufficiently identify the solution, before a brute force search or classical random walk, then there is said to be *quantum advantage*.

Implementing a quantum walk optically could be viewed as any other LOQC program, that is a quantum walk can be resolved into a series of optical gates. However we could also consider the walk Hamiltonian (as is argued to be the case in the example given) to be of the form of the adjacency matrix for the graph walked. Such an isomorphic treatment leads us to consider optical systems that display the same dynamics, i.e those in which the probability of a move being made to an adjacent graph site is modeled with the coupling of photons between modes using beam splitters.

Physical implementation of a series of optical couplings in a laboratory condition has been explored extensively with free space and guided mode optics. In the schemes where one optical mode represents one node in the graph, the couplings, wave plates, and phase delays must be arranged to match the graph adjacency which is trivial for some graphs and difficult for others.

5.1.3 Implementing a Quantum Random Walk in Fibre

An optical fibre core capable of supporting only a single mode of excitation can represent a node in a graph. The position within the walk being represented by occupation of the relevant optical mode by a photon. A photon present in the mode can transfer to other modes by couplings to adjacent cores. If the cores are weakly guiding the evanescent field extends a significant distance outside the core. If the evanescent field impinges upon another core some amplitude can be transferred, and where the cores are similar, transferred amplitude will coherently combine, effectively causing the photon to couple from one mode to the other. In the typical materials used for commercial optic fibre (glasses) there are no distinguishing directions, thus the coupling rate between

two adjacent cores is dominated (exponentially so) by the separation alone.

If similar cores are arranged together in a pattern, and allow a photon to move amplitude amongst them, a quantum walk should be possible. The mechanical and geometric limitations of fibre fabrication provide three obvious choices for core arrangements as shown in Figure 5-1. The simple line (and by extension a ring) should be perfectly possible, and represents an underlying graph with a single generator. A two dimensional grid of points is possible (with finite extent) and represents a graph with two generators, unfortunately as the graph is not infinite in extent care must be taken; if propagation is stopped before amplitude reaches the outermost cores the implementation approximates the ideal graph. Other behavior beyond the point where the graph has effectively non-uniform coordination is interesting, but not a Cayley graph. A third kind of arrangement is a tree or star formation where branching occurs, again this can exhibit quasi-ideal behavior if stopped before the boundary comes into play, however the fractal like graph becomes rapidly unmanageable to physically implement beyond a few branchings.

5.2 Prior Published Work

Implementing a quantum walk in an photonic system is a well established concept; a review of the topic is provided by Grafe et al. [53]; no attempt is made here to discuss all relevant previous work. The work presented in this thesis represents the first steps towards implementing a photonic quantum walk in a multi-core optical fibre, through verification of the interference of single photons.

Notable implementations of quantum walks include the discrete time walks that have been produced by Silberhorn's group [54],[55],[56] in which a photon walks on a discreet line graph of time displacements by circulating around a loop in which a coin (polarization) and displacement operation (a polarization dependent delay path) are controlled

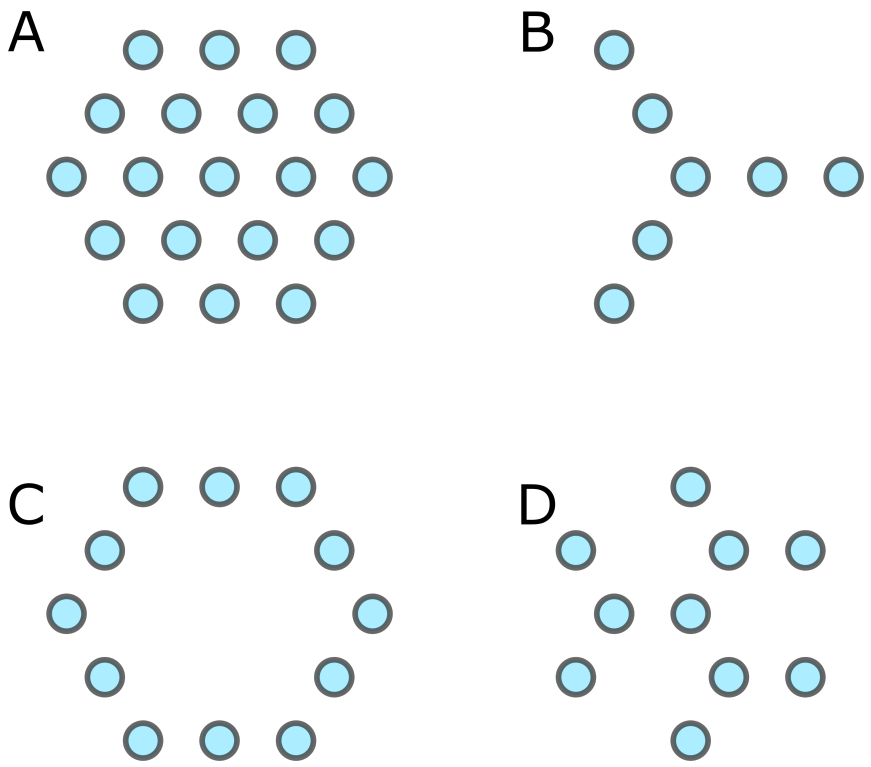

Figure 5-1: Four possible core arrangements on a triangular lattice for a multi-core quantum walk fibre. Arrangement **A** is as implemented in this work; **B** shows an implementation of a walk on a branched line (note that with a larger fibre the arms could be folded to compactly implement a longer walk); In **C** we have a ring representing a walk in one dimension with cyclic boundary conditions; Finally in **D** we implement a uniformly coordinated walk with three adjacent cores, as noted previously the fractal like nature of such walks is difficult to implement in fibre beyond a few repeat units.

electro-optically. Quantum walks in quasi two dimensions have been implemented as small displacements in time equivalent to one axis, and larger increments or decrements in time as another effective axis. The system being constructed by allowing the walker to take one of four different paths on each iteration of the loop [57].

Schemes more similar to the proposed multi-core optic fibre implementation, based around waveguide coupling have been demonstrated by several groups. Networks of two port waveguide couplers implemented by Fabio Sciarrino's group created by laser inscription have successfully implemented quantum walks [58],[59] and boson sampling [60].

Inscribed waveguides arrays like those produced by Nolte [61], in a ring by Owens [62], or Poulios [63] in a 'swiss cross shaped' arrangement, and similar such works demonstrate the flexibility to produce a bespoke physical implementation to match the walk to be investigated. Other processes such as lithography can be used in a similar manner to achieve bespoke arrays of waveguides from to as done in [64] [65].

Interference between modes within a single core, but multi mode optical fibre has been explored by Defienne et al [66] in which photons pairs were were addressed with spatial light modulators into multiple modes of a multi-mode fibre. Correlations were subsequently counted between points in the resulting multi-mode output pattern, and the two photon transfer function inferred.

5.3 Fibre Fabrication and Design Constraints

The proposed multi-core fibre scheme offers some advantages and disadvantages when contrasted with the implementations published. The relative ease of creating a large number of similar optical cores with low loss in a fibre architecture allows large numbers of modes to be harnessed. The single mode nature of each core greatly simplifies readout after the walk, as each specific mode can be coupled repeatably and with low loss, to the

detection system. Due to the stack and draw fabrication process some arrangements are preferred over others; only arrangements that can be created on a triangular lattice are reliably achievable, limiting the practical structures to a 2D array on the triangular lattice, and linear arrays.

Longer structures are readily produced in optical fibre which would be impractical for wafer processes or inscription. The ability to make walks long and core to core coupling rates low may potentially facilitate the use of a control interaction such as counter propagating cross phase modulation pulses to control or modify the progress of the walk.

The multi core fibre must not only fulfill the basic requirements for its purpose as a quantum walk implementation in the form of homogeneous couping strength and core sizes. But in order to be practically integrated with laboratory equipment the fibre must also remain compatible with standard optical parts used in conjunction with it. The photon source selected for qualifying the fibre based approach to quantum walks is the previously discussed collinear β-BBO source operating at 810nm shown in Figure 2-7.

Light collected from the source is coupled into industry standard SM800 fibre with a core diameter of $4\mu m$ core and $125\mu m$ outer diameter. In order to simplify the various coupling methods between SM800 and the walk multi-core fibre, both were desired to have as similar a core as possible. The similarity is particularly useful for butt-coupling fibres together, but is also convenient for coupling with 1-to-1 relay lens configurations.

Overall fibre outer diameter for the multi core fibre is not important since there is no intention to splice pieces of walk fibre together. In order to use existing cleaving tools, coupling and micro-positioning stages, and to remain within the typical operation region of the fibre pulling tower parameters (for which a wealth of prior experience exists) a fibre outer diameter close to standard, and not more than $300\mu m$ is targeted.

5.3.1 Core to Core Coupling

Coupling between cores can be considered from the classical view of Maxwell's equations with weak (dielectric) guiding. Within the core an oscillatory spatial mode profile in the form of a Bessel function is found. At the boundary only the real part of the solution remains and takes the form of a decaying exponential. The decaying field is asymptotic to zero. If another fibre core (or any guiding region) is brought into the evanescent field, some amplitude can couple to the core where it will once again take on an oscillatory form.

We note that the coupling is reversible and light can couple in either direction at the same rate. The coupling strength between two cores depends on the overlap of the evanescent field with the accepting core, clearly this is exponentially dependent on separation. The sensitivity to separation poses a problem for practical fibre fabrication in which small variations in fibre parameters are to be expected. Care is needed in fabrication to produce as symmetric a stack as possible with minimum distortion during fibre pulling. The mean coupling strength is dependent on the overall fibre scale, allowing a parametric sweep over outer diameter, producing couplings that vary in strength. Since we require a short piece of multi-core fibre (in order to repeatably use the fibre segment on the optical bench) we can vary mean coupling strength to generate a coupling length (the length of fibre propagated through for one complete coupling) that is compatible with the mechanics of experimental work.

For the case considered here with only single fibre modes in symmetric circular cores of clad parabolic graded refractive index, the approximate coupling strength was known implicitly from previous experiments with multi-core fibres [67]. In addition the overlap integral in one dimension was calculated using the analytic solutions provided by Snyder and Love [68]. The coupling rate is proportional to the mode field overlap between modes guided in adjacent cores; full closed form solutions for the clad graded power

law index profile are not available, but are known to exponentially reduce overlap with separation as is the case with step index profiles. A detailed analysis and numeric simulation of coupling was not performed beyond an approximation to the nearest half micron; the raw stock materials for producing graded fibre cores (MCVD fused silica with Ge doping) were highly elliptical as-provided from supplier. The circularity was restored in the first drawing operation, however an exact measurement of the core properties was not available prior to starting drawing. In any case the overall fibre scale can be adjusted to compensate for undesirable coupling rates.

5.3.2 Muti-Core Design

The design chosen to fabricate first was a simple grid of cores, as detailed in Figure 5-2. The basic design concept is a close packed arrangement of rods, each containing a single central doped core region. The voids between the close packed rods will be removed by a vacuum while the glass is in its viscous regime. Some distortion is therefore expected which may be compensated for if deemed necessary. The distortion is symmetric on all core rods except those at the stack boundary, for this reason a sacrificial layer of solid rods containing no core are placed around the complete stack in order to provide a distortion symmetric about the outermost core rods.

Additional space between the inner wall of the stack jacketing tube which surrounds and supports the stacked rods during drawing is taken up by packing rods; with the correct tolerance of fit a combination of jamming friction and static charge hold the inner stack in position firmly. The stress induced by distortion is discussed later in 5.3.8, however from prior glass drawing experience the distortion is expected to be sufficiently small that no additional mitigation will be required. Additionally for the design in question we require similarity between cores, but do not require a specific dispersion, nor to a significant tolerance, mode size.

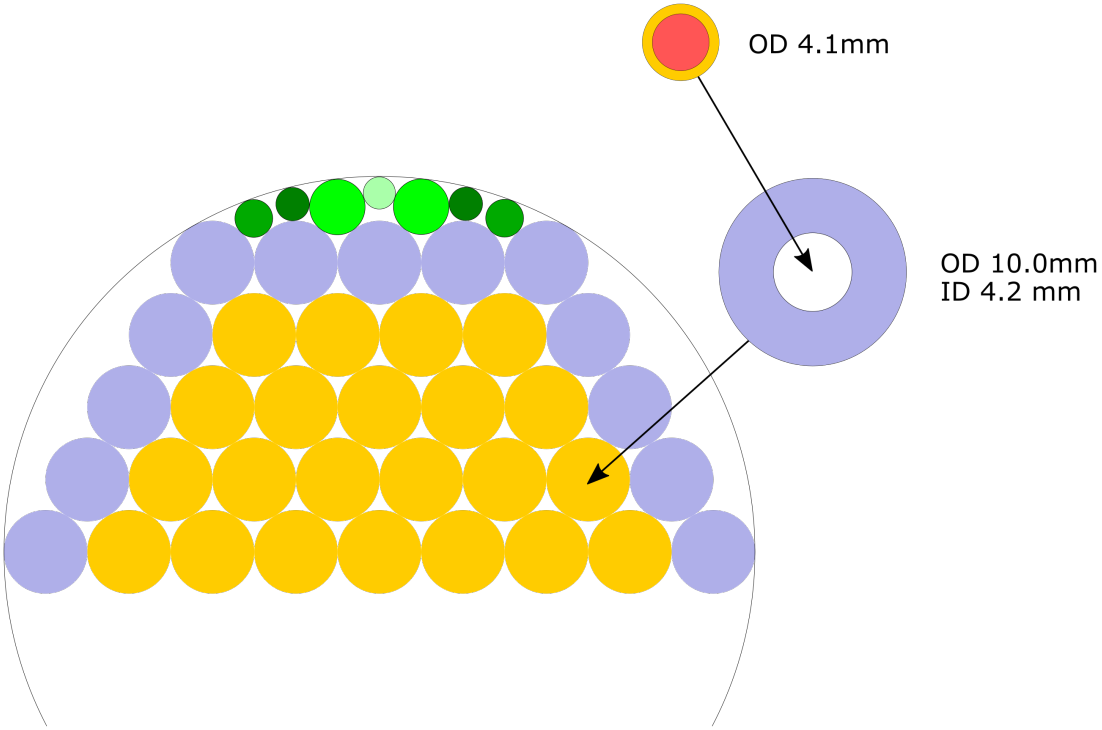

Figure 5-2: The arrangement of glass elements in the form of a stack to be subsequently drawn to a reduced diameter solid cane. Yellow circles represent the core containing rods that have been pre-jacketed to produce the desired coupling when close packed. Lilac circles of identical size represent rods of solid fused silica which act as a mechanical layer to reduce distortion during drawing; note that all core rods have equivalent air space remaining between them, ensure the outer ring of cores does not distort differently than the innermost cores. Four further packing rods denoted in shades of green a added to further reduce the expected distortion by reducing air space and improving homogeneity of air space radially.

Due to the specifications of the available stock of germanium doped glass a pre-draw was necessary. The germania is produced by Molecular Chemical Vapor Deposition (MCVD) on the inside of a heated fused silica tube. By altering the constituent gases flowing through the tube a gradual modification of refractive index is produced. The doping profile in quasi-parabolic form is convenient both optically for inter modal dispersion as shown in [69] [70] and mechanically, since the germanium doping produces large stresses between the layers subsequently built up. Eventually the tube wall is maximally thick and the remaining space is removed by vacuum; collapsing the tube into a solid rod.

The rod available for this work was doped such that the peak refractive index is 0.031 above that of fused silica, and is shaped as an inverted truncated parabola with exponent 2.22. The collapse of the tube into a rod in this case left the final cross section slightly oval, and with only a small layer of un-doped fused silica before the parabola starts. At $31mm$ diameter the rod contains a large amount of doped material which must be first drawn down to a thin rod and jacketed with un-doped silica to form an optic fibre.

In a conventional fibre the cladding is made as thick as necessary such that when the rod is drawn down to fibre the external diameter is $125\mu m$ and the core is appropriately sized for the intended purpose. The exact *jacketing ratio* of core material to fused silica cladding determines the core separation to size ratio when two rods are stacked next to one another.

A summary of the specific glass elements draw are given in Table 5.1 for the preparatory stage in which a fibre cane is produced. After a cane is produced the draw down to fibre is only significant if an overall outer diameter is targeted. In this case once cane was produced, a fixed further draw down was required to bring the cores to appropriate size. Additional glass tubes were selected to jacket the cane to produce a convenient outer diameter for handling, however this step was not design critical and was repeated

Glass Element	Inner Diameter	Outer Diameter
Germania MCVD Rod	$23.9mm$ doped	$31.1mm$
Circularized Germania	-	$4.1mm$
Core Jacket Tube	$4.2mm$	$10.0mm$
Preform Jacket Tube	$12.05mm$	$14mm$
Core Rod	solid	Preform Jacket ID $/9 - 1.5\mu m$
Dummy Core	solid	Preform Jacket ID $/9 - 1.5\mu m$
Packing Rod 1	solid glass	0.670∗Core Rod
Packing Rod 2	solid glass	0.495∗Core Rod
Packing Rod 3	solid glass	0.458∗Core Rod
Packing Rod 4	solid glass	0.390∗Core Rod

Table 5.1: Glass elements used in fibre cane production. The upper table section lists the raw glass stock which was subsequently drawn from; the lower section details the relative sizes of the elements required to produce the planned design. The specific stack element sizes were drawn to match the individual jacketing tube in appropriate ratios in order to control the fit to the desired tolerance. Only the initial stage in which the raw MCVD Germania rod was drawn circular and jacketed have a significance for final core coupling rates; the core size to separation ratio of 0.304 is fixed by the initial jacketing ratio.

on several drawing sessions, each time with similar but not strictly specified tubes.

5.3.3 Fabrication Process for Fibre

Glass fibre is produced industrially and for research by hot drawing a glass preform. The fused silica used for most industrial fibre and the research fibre presented here is melted in a cylindrical and open electric furnace under a protective atmosphere. While the glass is viscous in the furnace hot zone it is pulled downward by a continuous drawing force provided by a motorized capstan, In order to balance mass flow in and out of the hot zone the preform material is lowered inwards continually by a linear actuator or precision crane.

The thin fibre cools rapidly after leaving the furnace along a few meters of length, such that at the point where it is being wound it is cool enough for handling. Microscopic defects, cracks, and soluble organics would rapidly degrade the strength of the fibre if they were allowed in contact. The procedure is performed in a clean-room environment,

and a ultraviolet cured liquid plastic coating is applied while the fibre is in transit to the capstan. In this way the glass surface makes contact with nothing except the protective coating material.

The draw down process is ostensibly simple to model by conserving glass volume in and out of the furnace. The shape of the draw down region due to viscous forces, the conductivity of the material and heating power, shielding gas flow cooling effects, and structure within the preform make drawing from a numeric model impractical. As a first approximation the draw-down ratios are applied, however the subsequent recipe is rapidly improved by trial drawing. Research fibre drawing towers are not standardized in their behavior or features, making experimental drawing necessary.

A conventional telecommunication fibre is produced from a preform which contains an identical refractive index profile to the final design, typically this is an MCVD grown glass with varying constituents throughout the radial coordinate. The solid preform of this type best approximates the ideal drawing of one solid rod into another thinner rod. For multi core fibres and fibres containing air holes there are additional preparation stages required to produce the complex preform, typically a stack of individual simple rods is fused together to produce a *cane* of partially pre-drawn preform, which can subsequently be handled as a single rod of preform material. Some commercial telecoms fibres incorporate stress rods which are inserted into holes withing the preform, however the disparate melting temperatures of the glasses make a cane stage redundant, as the final structure will be dominated by the draw down of the more viscous glass.

5.3.4 Forming Rods

High purity F300 glass rod and tube were drawn to the sizes required on a tower similar to the fibre drawing tower, in which the capstan is replaced with a set of belt drives that centre about the drawing axis and are pneumatically loaded to grip and draw the

rod. Due to the relatively high volume of glass throughput and limited furnace power, the process is slow by comparison to fibre drawing. Rates as low as 50mm/min were required to draw the largest elements to size.

Where a rod is re-jacketed in this step, it is fitted within an appropriate jacketing tube such that the final core and cladding radii are in the desired ratio. At one end of the concentric rods heat is applied by a brief furnace operation or by a hand held Oxy-Hydrogen torch sealing the tube to the inner rod. A brass vacuum collar with rubber o-rings is fitted tightly over the jacket tube, which has a small hole ground into it beneath the seating point for the collar. A vacuum can be drawn in the annular airspace between rod and tube during drawing, collapsing the jacket glass onto the rod as it enters the furnace hot zone.

Rods are flexible but not coil-able and so are trimmed to standard lengths similar to the raw tube stock sizes selected for later stages of the operation. Rods are then packed in an inert atmosphere bag ready for future use in a stacked design.

5.3.5 Stacking the Preform

A wide variety of designs can be formed from triangular or square stacked rods. The final shape of air holes may be inflated artificially or removed by vacuum, allowing a very wide range of possible final fibre cross-sections from similar simple stacking.

As an aid a jig is used to maintain alignment of the elements, consisting of eight guide blocks cut at 60 deg angles and aligned on a linear rail system. A completed stack is bound with copper wire which is easy to work with due to its softness, but sufficiently strong to hold together the stack. The entire stack is slid into a jacket tube removing the copper ties progressively as it is inserted. If this step is completed correctly the stack will be sufficiently constrained such that no elements re-arrange, and also no excessive twist is introduced.

Further thinner rods are now inserted to take up space where the discontinuity between hexagonal stack and circular inner bore meet. The tolerance of fit is typically around $100\mu m$ which will rigidly lock the stack by friction to the extent it cannot be tipped out of the jacketing tube. An example of the completed stack is shown in figure 5-3.

5.3.6 Drawing Cane

Drawing the stack to cane is performed in a manner similar to the drawing of simple rods, with the addition of a vacuum collapse of the interstitial space. As discussed in Section 5-5, planning for the interstitial collapse effects is part of the overall stack design, and the primary motivation for packing the completed stack with additional rods.

Prior to inserting the stack into its jacketing tube a slit is ground into the tube with a diamond cutter wheel, some 10cm along from the end of the tube; this will be used to access the interstitial volume through the side wall later. The end of the stack in which the slit has been made will then be closed and fused to the rods of the stack, this seals out air from entering along the stack interstitial volume from the top, and additionally supports the rods from the fused end. This is important as the rods would otherwise descend independently of the jacket at a rate related to the viscosity gradient across the hot zone. If the internal parts of the stack descend without the jacket an incorrect draw down ratio is achieved.

A vacuum collar is applied over the slit allowing a vacuum to be drawn as in the case for jacketing rods. The interstitial space collapses to produce a single solid rod with the desired refractive index profile. Shown in figure 5-4 is the resultant cane produced from the stack shown in figure 5-3.

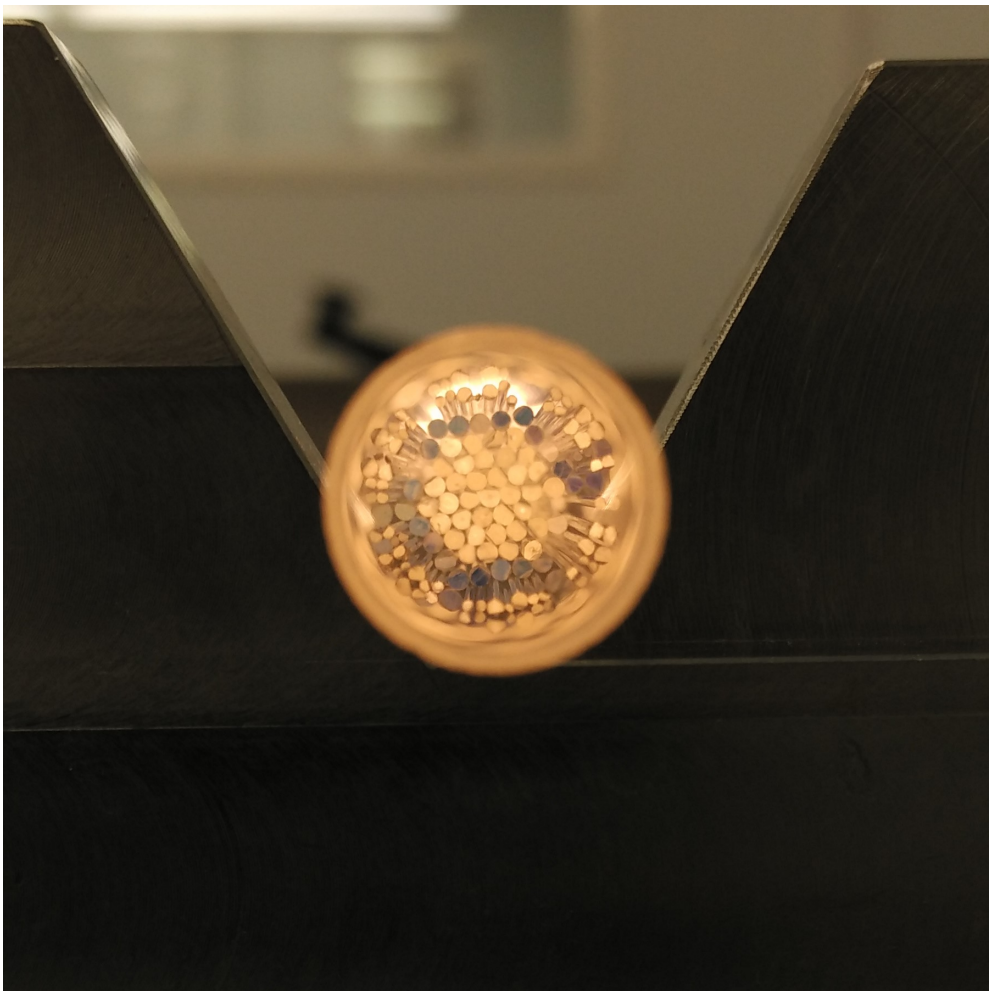

Figure 5-3: A completed fibre stack within a jacketing tube, resting on a stacking jig. Light blue dummy cores are solid F300 silica forming a ring around the 37 close packed working cores. The blue colouration is due to marking ink on the far end of each rod for identification purposes. Slim packing rods are visible to the perimeter of the stack design and extend further along the jacket tube.

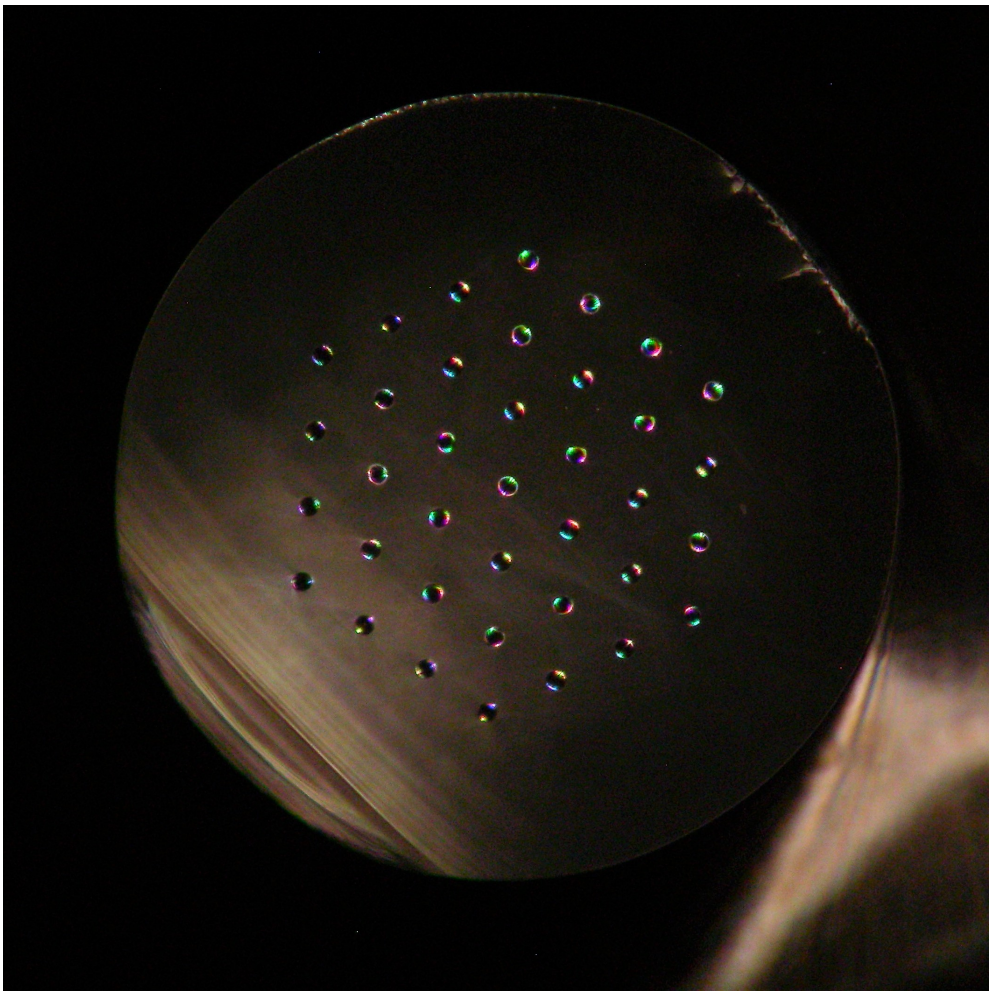

Figure 5-4: A segment of the fully fused form of the same stack shown previously in Figure 5-3, taken under oblique rear illumination to highlight graded index core regions. This sample is approximately 4mm in diameter and is readily examined for circularity, dimension, and defects.

5.3.7 Drawing Fibre

A fibre can be drawn from cane directly as described previously in Section 5.3.3, however it is greatly advantageous for subsequent manipulation, splicing and general handling, that the outer diameter of any fibre is increased by jacketing to the industry standard diameter of $125\mu m$. A final jacketing step is performed concurrently with drawing the fibre to final size. Whilst a fibre is being drawn small samples can be removed from the winding drum and analyzed under a microscope, or in cases where the optical microscope cannot resolve the variation, an optical rig can be used to test the fibre while the draw process continues. The fast feedback cycle allows design parameter approximations to be found in a matter of hours, typically with correctly sized sub-standard (homogeneity, bubbles etc.) material from earlier stage of the process.

Once an operating point has been finalized a quantity of final design fibre, or indeed a variety of parameter swept fibres are drawn off to storage bands on a collection drum. Bands of fibre are marked against the parameters used for further full characterization after the fact, and are rewound onto storage spools as necessary.

5.3.8 Glass Inhomogeneity

The stack and draw technique introduced previously removes air gaps between the stacked glass rods by applying a vacuum. In the hot zone of the drawing furnace the surface tension around the liquid glass, and the bulk tension throughout the glass determine the shape distortion of the rod, and are frozen in place by the solidification of the fibre. The distortion from a circular cross section to a hexagonal cross section (for close packed rods) does not eliminate inhomogeneity at the border between glass that was formerly part of two distinct rods, but is now fused. The origins are not precisely known, but are probably caused by process variation, which in turn causes the softening rods to adhere to one another just prior to the hot zone. The erratic

pattern of adhesion between the rods caused by variations in rod diameter, scratches, and imperfect packing is transfered to erratic shear stress at the boundary between glass originating from each rod.

The primary concern for the fibre design is that the coupling between any core pair is sufficiently similar. The existence of stress at the midpoint boundary between cores is not in principle a problem, however variations in the stress could potentially modify the coupling between cores. Further to the problems of introduced stress variations at the boundary, the doped core of the fibre is slightly elliptical due to the collapse process after vapour deposition of doped glass on the internal surfaces of a substrate tube (the cladding glass is also elliptical). Under high drawing tension the symmetry of a fibre preform can be improved; the doped core rods required for the fabricated fibres were produced with a very high tension (unfortunately not measured by the cane pulling apparatus) resulting in an acceptably round rod.

It was assumed that stresses would develop in the process, and that a slow and hot fibre draw might be advantageous by annealing some of the stress. For these reasons the first parts of the draw were conducted with maximized tension in order to produce geometrically symmetric cores and cane; the second process of drawing the cane to fibre was conducted as slowly and at as high a temperature as possible while maintaining the specification parameters.

As can be seen in figure 5-5, in which we see a section of the final cane prior to drawing to size, the stresses between glass regions are readily visible. The homogeneity is hard to judge quantifiably, and cannot easily be observed once the fibre is drawn to final size.

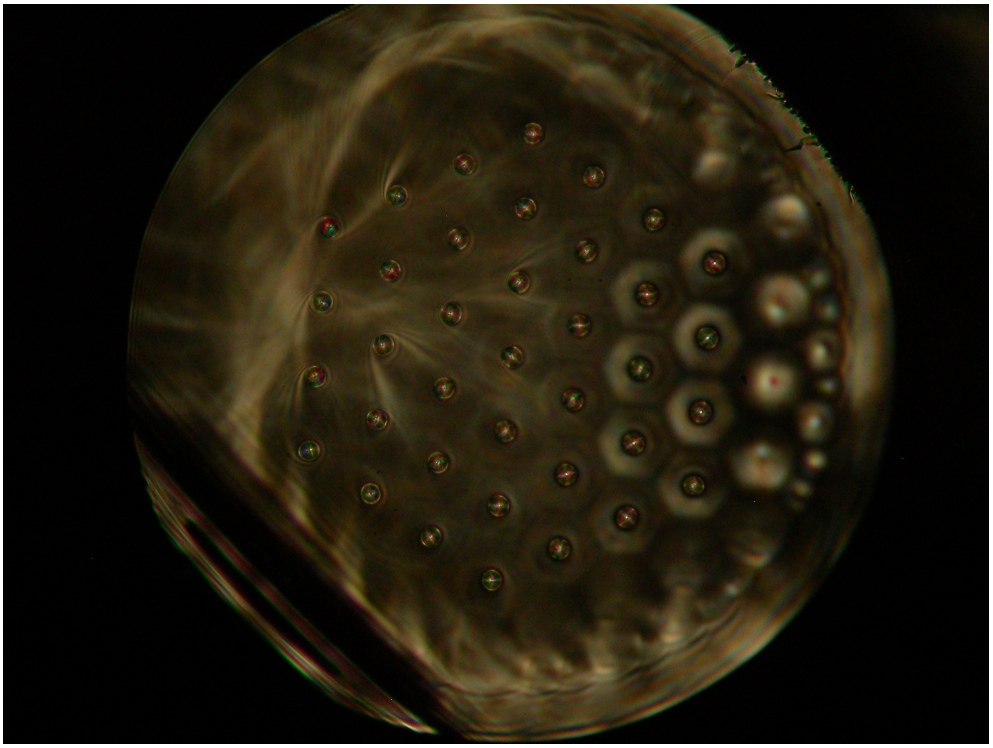

Figure 5-5: Cleaved cross section of 37 core cane. The illumination conditions are transmission through the cane and from an oblique angle. Here the illumination light does not readily guide through the doped cores but instead couples to the waveguide core enclosed and defined by the stressed glass boundaries. Note on the right hand side of the image, the clear hexagonal boundaries between rods, the now visible dummy rod ring used to reduce distortion of the outermost core containing ring, and the visibility of the packing and jacketing glass by their respective stress boundaries.

5.4 Behavioral Simulation of Multi-core Coupling

Coupling rate between a pair of waveguide cores is dependent on a large number of factors as previously discussed. In order to gain insight into the expected evolution of intensity as it couples from core to core, all factors can be reduced to a single parameter representing pairwise coupling rate. This model ignores many aspects of the propagation, including polarization effects and nonlinear effects such as cross phase modulation (XPM). Under the assumption of polarization degeneracy, low power and, identical cores, we expect to see intensity patterns influenced by the arrangement of cores alone.

Some pairs of cores will have vanishingly small coupling rate and are additionally assumed to be zero. Evolution of the state is performed by progressing time (phase rotation of all cores) and coupling amplitude from core to core in a pairwise fashion depending on the amplitude present and a pre-calculated rate. The first order differential equations are neatly surmised as a single matrix equation:

$$\frac{d}{dt}\overline{P} = \hat{M}\overline{P}, \tag{5.8}$$

where $\hat{M}$ is the coupling rate between the amplitude in each core arranged as the vector $\overline{P}$. Coupling phase shift is introduced separately, and phase evolution with time rotated in split step with the coupling operation.

The method described was implemented as a simple C code model in order to visualize the expected power distribution in the multi core fibre. The model considers coupling rate as the proportion of the power transfered in unit time evolution; neither parameter is quantified into real units. The model was used with coupling rates approximated

by one dimensional overlap of Gaussian shaped modes, to gain insight into how the arrangement of cores impacts the interference pattern observed. Shown in Figures 5-6 and 5-7 are two example runs of the code with 37 cores coupled to the nearest neighbors only.

In Figure 5-6 an amplitude of unity was initially placed in the central core, after 720 time steps the simulation shows amplitude in all cores in a radially symmetric distribution. In real experiments the coupling will not be perfect however it is expected that a similar distribution will be found in which after a short propagation a photon can be found in any core, and with a radially diminishing probability. Placing the initial amplitude in an off-centre position should in principle evolve in an identical manner until some amplitude reaches the outermost cores; radial symmetry is lost after the coupling back of amplitude that has reached the discontinuity in the arrangement. An output like that shown in Figure 5-7 in which the propagation has been allowed to continue for 7000 time steps is formed, with only a single mirror symmetry. In order to propagate for the maximum length before reaching the discontinuity of the pattern, a real experiment will couple photons exclusively to the centre-most core.

5.5 Bright Light Characterization

In order to perform an approximate alignment and to confirm that a sufficiently short length of fibre was selected, a $800nm$ fibre coupled diode laser was coupled into the central core of a short section of multi-core fibre. The light exiting the multi core fibre was imaged onto an Andor Luca Electron Multiplying CCD camera. In the interference pattern shown in Figure 5-8 the input coupling was not to the central core, in the orientation shown it is one core directly to the right hand side of the central core.

In the interference pattern shown in Figure 5-8 there is light in the outermost cores. Although valid evolution, the coordination of the outermost ring is different to the cores

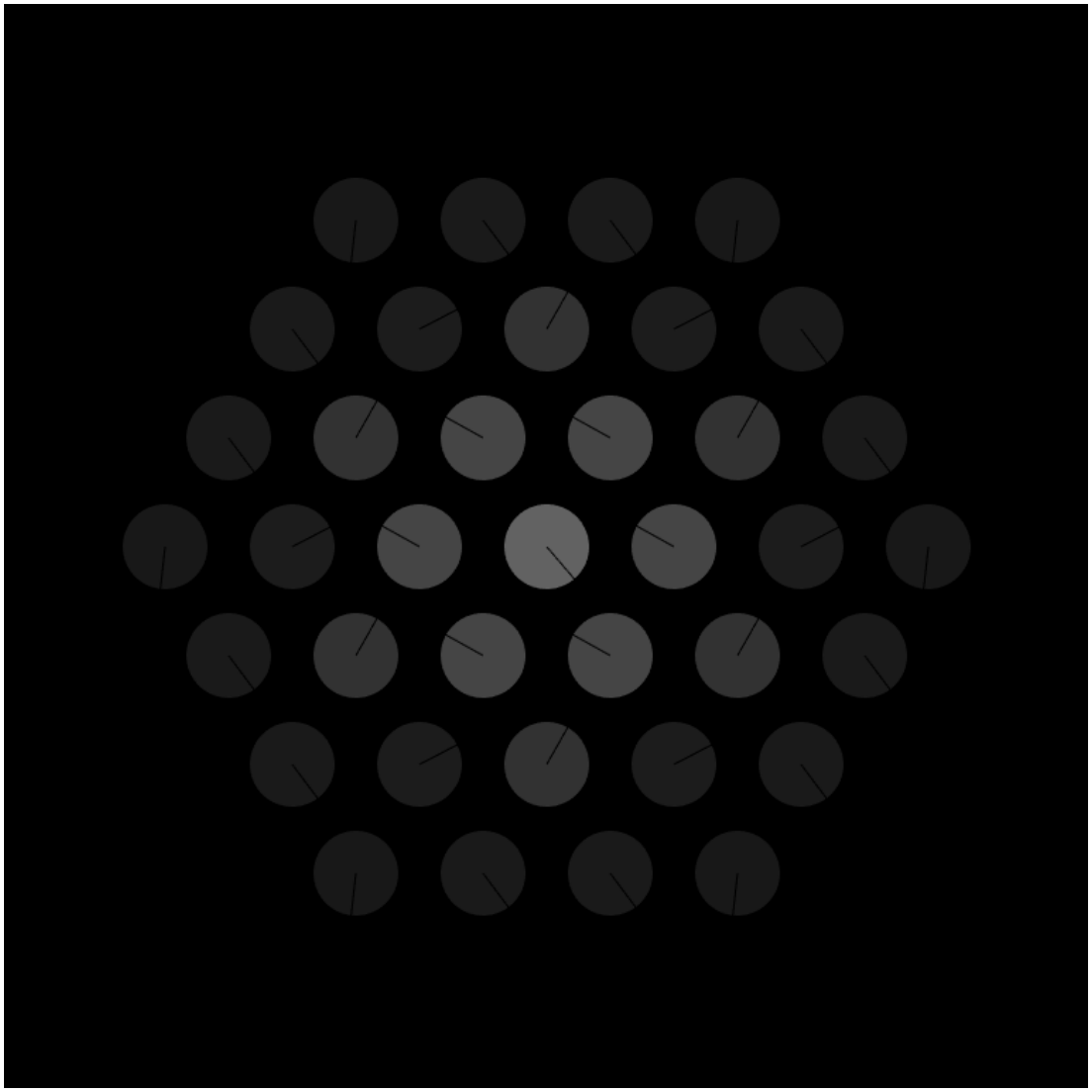

Figure 5-6: Schematic representation of the calculated output light from a 37 site triangular lattice of cores. Each core is represented by a circle with brightness proportional to the amplitude present in the core and phase indicated by the angular position of a radial line from the centre of each circle. For the case shown amplitude has been injected into the centre most position and propagated over 720 arbitrary time steps. Less than 1% of the amplitude has reached the outermost cores and no effects relating to the boundary are visible.

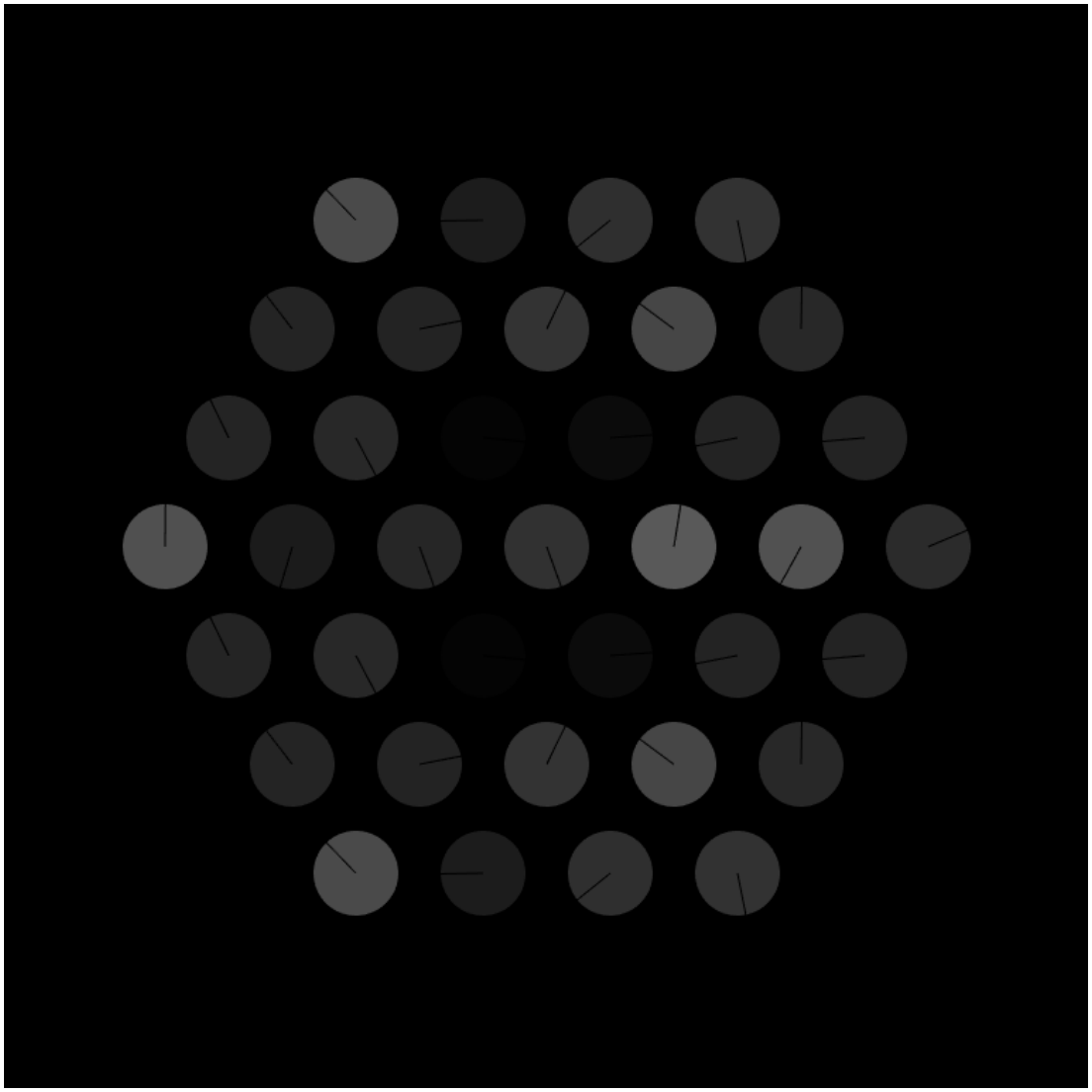

Figure 5-7: Schematic representation of the calculated output light from a 37 site triangular lattice of cores. Each core is represented as in Figure 5-6 by a circle with brightness proportional to the amplitude present in the core and phase indicated by the angular position of a radial line from the centre of each circle. Here light has been initially injected into the position immediately to the right of the centre and evolved for a larger number (7000) steps. Amplitude has reached the outer most positions and coupled inward again.

in the encircled region and is also not consistent between all cores of the outer ring. The marked jump in properties at the outermost ring represents a departure from the idealized view in which a walk on a Caley graph is approximated. In principle we are only interested in behavior prior to amplitude reaching the outermost cores. Despite this propagation barrier there are 42 nearest neighbour pairwise couplings involved in the interference pattern before any coupled light to the outermost ring is considered, still a relatively complex network, and cumbersome to reproduce in a form other than coupled waveguides (e.g. in fibre components).

While working under bright light the fibre is cleaved back to $20mm$ length, Over the reduced length the observed interference pattern (Figure 5-9) has not spread as far as the outermost ring, but has evolved significantly outside of the central core in which the input was injected. Here some of the minute non-uniformity of the stack is seen to have impacted the interference pattern. The non-uniformity is approximately symmetric about (30 deg counter clockwise from the horizontal axis of Figure 5-9) a stacking axis of the fibre, leading to the assumption that a systematic coupling rate error exists in addition to any pairwise variations.

5.6 Single Photon Interference

To explore weather the fabricated multi core fibre is sufficiently low loss for single photon experiments, and to confirm that the coupling into and out of the fibre are acceptable, an experiment using single heralded photons was constructed using the free space BBO source presented in Section 2-7. Although the correlation counts in each core are expected to be observed in the same proportions as would be found for a coherent state, by using a heralded photon source we will confirm the behaviour of a single photon at a time having taken a random walk and being detected in one specific output mode.

Figure 5-8: Interference / core power distribution with $50\mu W$ $800nm$ laser light. A length of 38mm of the multi-core fibre was used, and imaged at the distal end with 40x magnification onto an Andor Luca EMCCD camera. The interference pattern displayed is asymmetric and similar to patterns seen in the Master equation model where light is initially coupled to a core adjacent to the central core and subsequently allowed to propagate beyond reaching the outermost cores. Although the pattern is sufficiently recognizable to conclude that the gross behavior is correct, it is evident from the deviations from symmetry that non-uniformity in couplings are present.

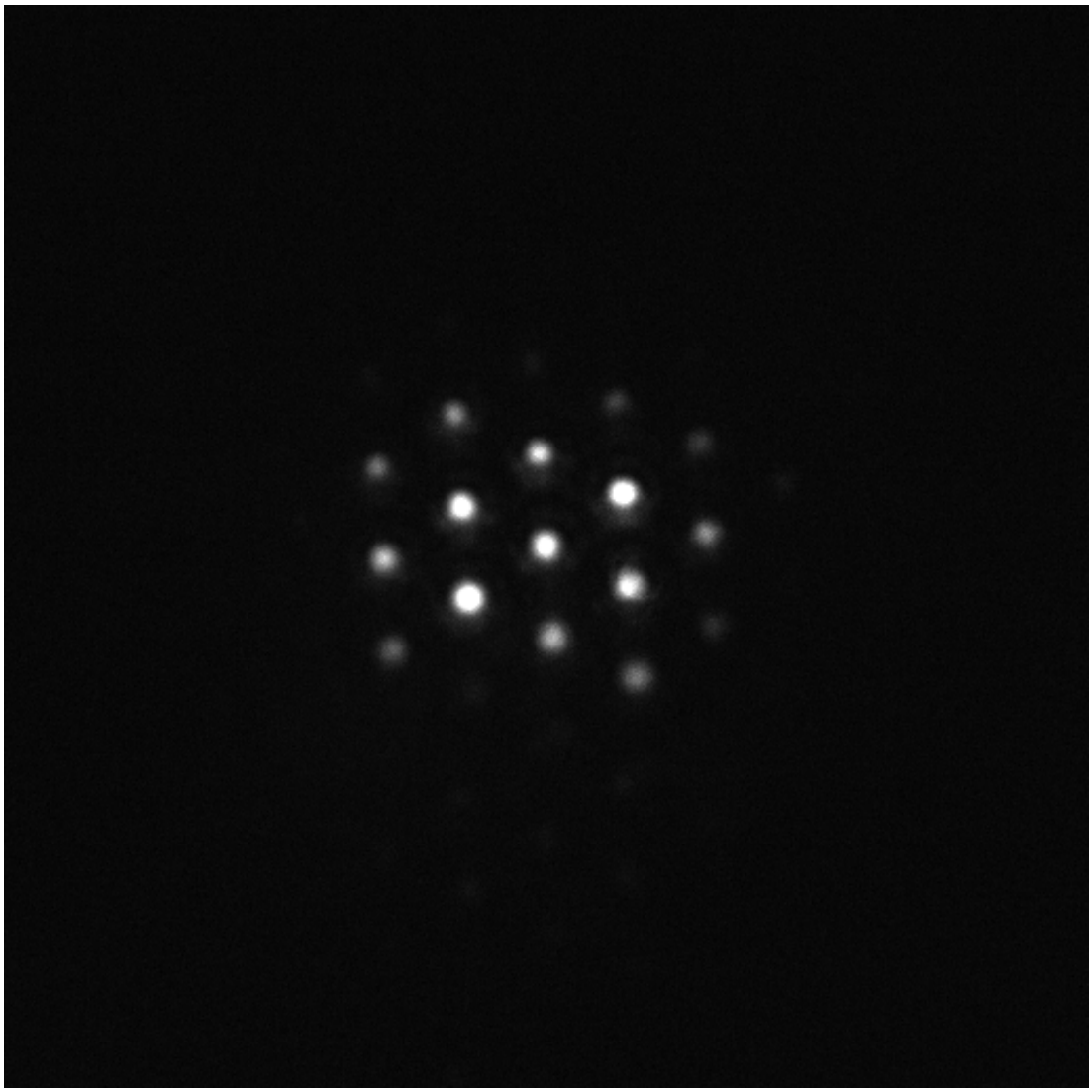

Figure 5-9: A shortened section of multi-core fibre only $20mm$ in length is illuminated from the central core under the same conditions as per Figure 5-8. The propagating light has not detectably reached the outermost cores however it is noted that the illumination pattern is symmetric only in one stacking axis. The radial non-uniformity along one stacking axis indicates a systematic coupling error in the direction seen. During fabrication this axis may have become distorted relative to the others during the jacketing phase (non-concentric annular collapse) or due to misalignment of the necked region and the furnace hot-zone.

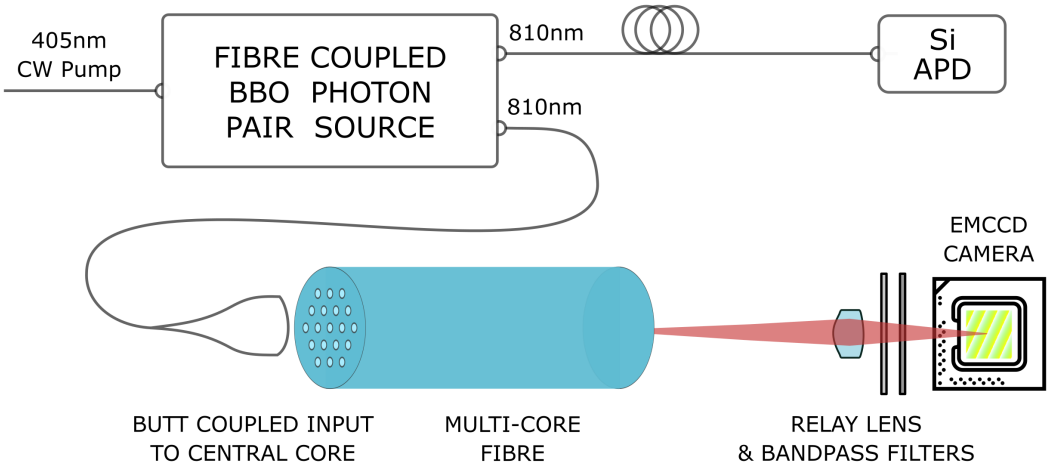

Figure 5-10: Schematic arrangement of the experiment used to image the photon interference directly onto an Electron Multiplying CCD camera. The β-BBO source presented in Figure 2-7 is butt coupled into the central core of a multi-core fibre. The output face of the fibre is imaged by an aspheric relay lens onto the EMCCD via a 10nm bandpass filter and a wide bandpass glass filter. Only a single photon of down converted light is present in the multi-core fibre at a time, requiring an integration over 12s in order to produce the image presented in Figure 5-11.

Both outputs of the photon source are coupled to optical fibre and subsequently into Si APDs. The APD counts are first delayed by a delay module as discussed in Section 3-7 and finally correlated by an FPGA counter. The raw coincidence rate is approximately $350s^{-1}$ with the alignment used at the time, hence only one photon at a time was expected to be present in a quantum walk experiment within the fibre.

The fibre is first imaged (as before with bright $800nm$ light) with the EMCCD camera as shown in Figure 5-10 using a long integration time of 12 seconds. Displayed in Figure 5-11 is the integrated image with level adjustments to make the interference pattern visible. The focus for imaging is not perfect, however despite the poor focus the interference pattern is clearly visible.

After imaging the fibre directly with the camera, photon counting measurements were performed as shown in Figure 5-12 by coupling photons into the central core of the multi-core fibre and collecting photons from a number of cores in sequence. Heralded

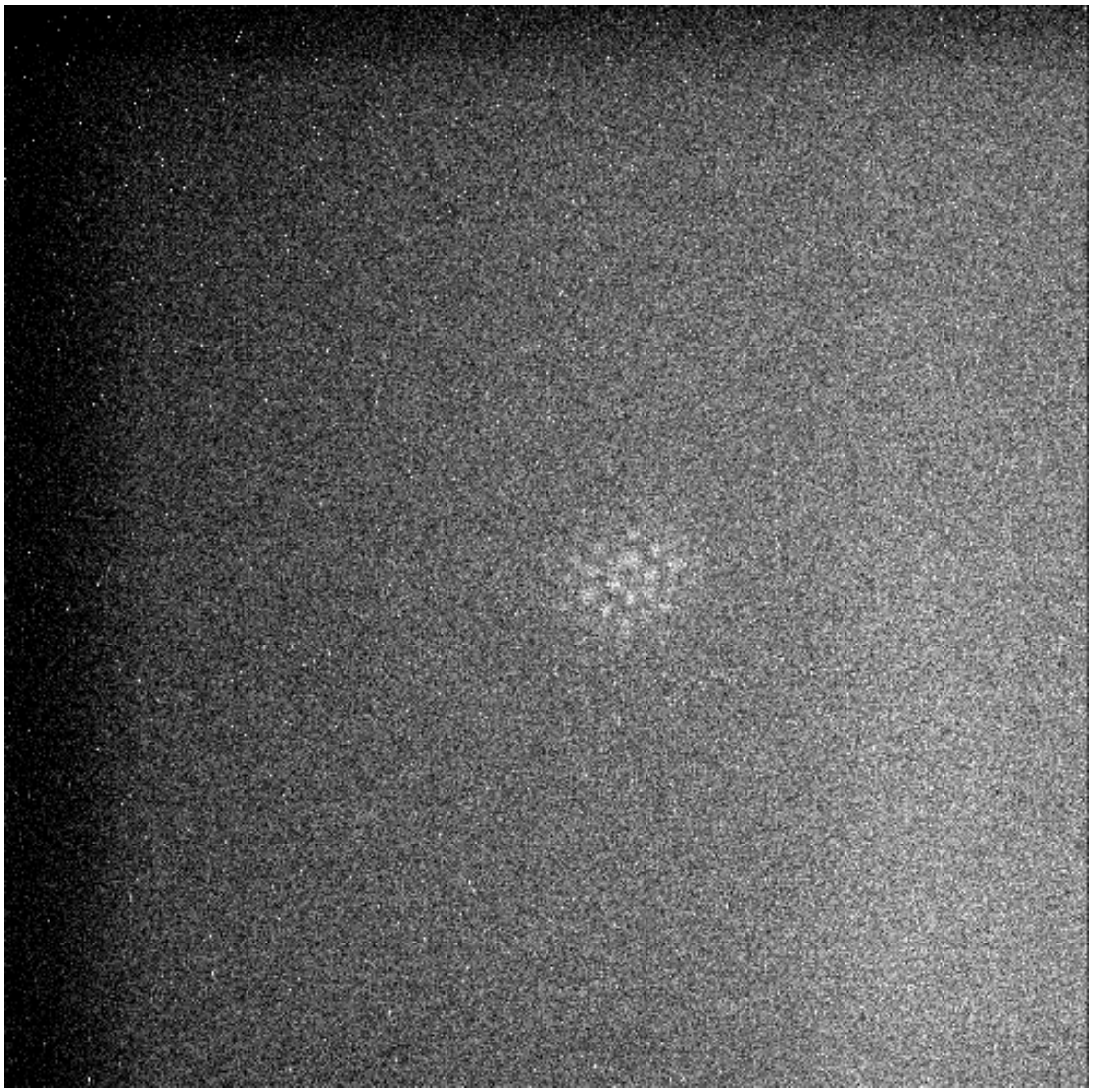

Figure 5-11: Light at $810nm$ from the collinear BBO photon pair source, imaged by the Ando Luca EMCCD camera. The image was taken with a 12 second exposure and maximum gain settings for the camera. Due to stray light from an undiscovered source additional back cloth baffles were added to the camera. Due to the long exposure period it was challenging to focus the image better than to the degree shown.

Core	Coincidence Rate
1	$70.3s^{-1}$
2	$35.0s^{-1}$
3	$41.9s^{-1}$
4	$21.4s^{-1}$
5	$54.7s^{-1}$
6	$49.2s^{-1}$
7	$22.6s^{-1}$
8	$12.2s^{-1}$

Table 5.2: Measured coincidence rate between detected herald photons and signal photons coupled into the central core of the multi-core fibre and out from various cores at the distal end. Cores beyond the eight central cores were not measured due to breakage of the sample.

single photons were butt coupled in and out of the fibre for this experiment as the $4\mu m$ core of SM800 patch cord closely matches that of the multi-core fibre under test.

Initially the central core both in and out of the $20mm$ multi-core fibre was coupled to SM800 fibre through witch one arm of the photon pair source was passed en route to a Si APD detector. The timing delay was optimized to give a maximum coincidence counts; it is assumed that the delay will not noticeably change from this point onwards. A coincidence rate of $70s^{-1}$ was observed for the central core. Other cores were sought by moving the output fibre on a three axis flexure stage positioned along one of the fibre axes until coincidence counts were found. The position of the collecting fibre was then optimized to achieve the highest coincidence rate.

Eight of the cores of the multi-core fibre were successfully reached by this process before a stage collision occurred and broke the sample preventing further exploration. Table 5.2 and Figure 5-13 display the results in tabular and graphical form for the observed single photon coincidence rate at each core position (graphical positions are schematic and not measured).

Below saturation the pixel value recorded by the EMCCD camera is assumed to be proportional to intensity. By thresholding the image to produce a binary mask of

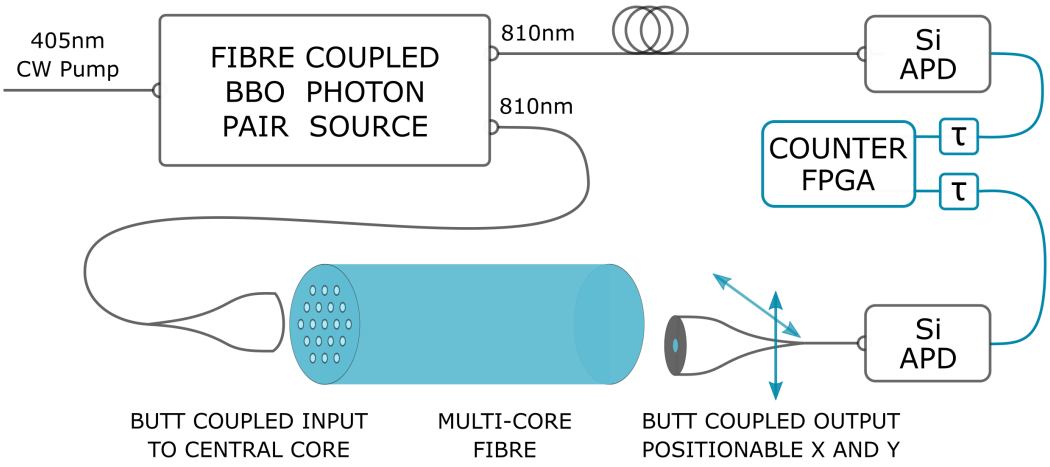

Figure 5-12: Schematic arrangement of the experiment used to implement the two dimensional quantum walk in multi-core fibre. The β-BBO source presented in Figure 2-7 is butt coupled into the central core of a multi-core fibre from a single mode fibre output of the photon pair source. The output from a selected core is coupled out into a second single mode fibre and detected with an avalanche photo diode. Both input and output couplings are positioned with three axis flexure micro-positioners (not shown) in order to maintain correct alignment. Coincidence events between the herald detection and the output detection avalanche photo diodes are counted by the FPGA counter electronics previously described. The data in Table 5.2 was collected by integrating the coincidence counts over a 300s interval while the output fibre is positioned at the relevant core.

Core	Normalized Mean Value	Normalized Integrated Value
1	Clipped	Clipped
2	3.491	1.510
3	3.832	1.658
4	2.138	1.163
5	Clipped	Clipped
6	Clipped	Clipped
7	2.135	1.658
8	1	1

Table 5.3: Image analysis of $800nm$ bright light interference pattern. Values are obtained by thresholding the image shown in Figure 5-9 to approximate the core boundaries and processing the pixel values within each core. The raw values have been normalized against core eight. Due to saturation of the camera no reliable value can be found for cores 1, 5 and 6.

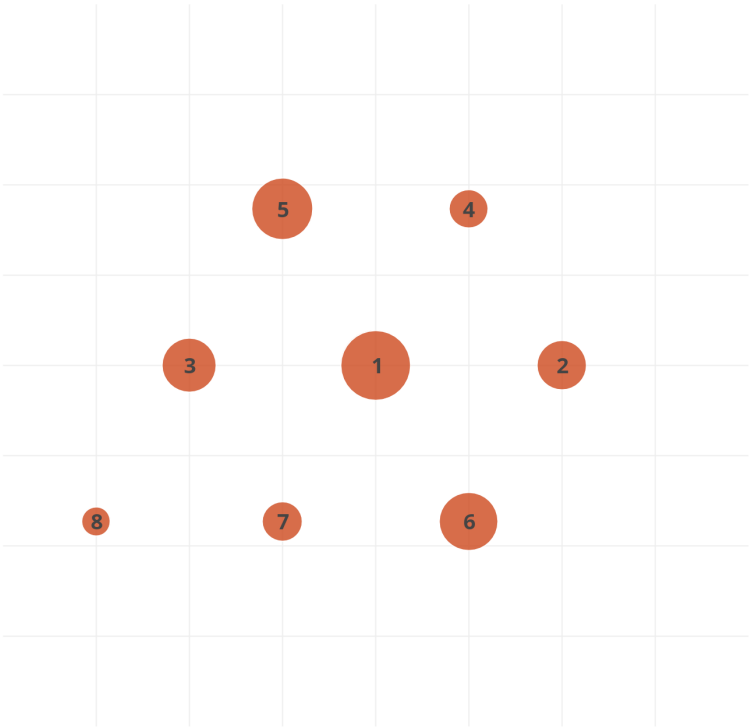

Figure 5-13: Schematic Representation of the observed coincidence rate for given output core locations. Eight cores were successfully measured, all eight are broadly in line with expected intensity, and conclusively demonstrate the fibre is suitable to be used for investigating quantum walk behavior. Specific values for the count rates indicated are provided in Table 5.2.

Core	Normalized Intensity	Normalized Coincidences	% Difference
1	Clipped	N/A	N/A
2	3.491	2.869	-21.70%
3	3.832	3.434	-11.59%
4	2.138	1.754	-21.91%
5	Clipped	N/A	N/A
6	Clipped	N/A	N/A
7	2.135	1.852	-15.25%
8	1	1	0%

Table 5.4: Image analysis of the $800nm$ bright light interference pattern shown in Figure 5-9. Values are obtained by first thresholding the image shown to approximately locate the core boundaries and subsequently processing the pixel values within each boundary. The raw values have been normalized against core 8. Due to saturation of the camera no reliable value can be found for cores 1, 5 and 6. For comparison the single photon coincidence rates measured for the same cores and also normalized to the rate measured in core 8 are shown. The percentage difference between the pattern measured with $800nm$ bright light and $810nm$ single photons is less than 22% demonstrating similarity between the two cases.

regions representing the estimated core boundaries can be found. For each core the pixels enclosed by the approximated boundary are listed and can be analyzed for their mean and integrated values which are proportional to intensity within the core. The values found for the cores regions that did not saturate the camera are shown in Table 5.3. Although the image analyzed has been taken with a different centre wavelength ($800nm$ as opposed to $810nm$), and not with identical input coupling, a clear visual similarity to the distribution of counts from the single photon walk is seen.

By comparing the normalized count values with normalized pixel intensity we can quantify the degree of similarity between the bright light and photon counting experiments. The lowest intensity core (8) was normalized about since it appears to be the least distorted in the image, and has no pixels close to the clipping level. Shown in Table 5.4 are the normalized integrated intensity values along with a percentage difference between normalized count rate (also normalized around core 8) and intensity. Although this test does not take into account the difference in wavelength between the two experiments it is an indicator that the interference is similar for the two cases.

Repeating the imaged intensity analysis with the capture shown in Figure 5-11 where the EMCCD was used in conjunction with the photon pair source output is not possible due to the low quality of the image. In either case photons have been recorded in cores other than the starting central core and the interfering pattern directly captured as correlated single photon detections.

The inhomogeneity of the coupling rate between cores is evident from the asymmetry of the interference pattern in both the photon counting and bright light experiments. Refinement of the fibre and the fibre drawing technique may result in greater similarity in a future development. The mean variations in core to core coupling strength can be approximated by further analysis of the bright light interference as detailed in [67] using a Monte Carlo type search.

By successfully detecting both the integrated interference pattern and single heralded photons at the output cores of a multi-core optical fibre we have implemented a two dimensional photonic quantum walk on 37 sites.

5.7 Proposed Future Work

With confirmation that a fibre can be practically fabricated correctly sized and with acceptable variations for the envisaged walk experiments, and that single photon interference is successfully observed, the next step is to implement a known single photon walk experiment such as the Grover [71][72] search or a delayed choice experiment [73].

Alternatively we can place more than one indistinguishable single photon into the walk at the same time. With multiple identical photons the interference is expected to display profoundly different character to that of a single photon, due to the Hong Ou Mandel interference between photons.

Coupling two modes in and two modes out of the multi-core fibre by butt coupling is not

practical. Ideally all cores should be made addressable at input and output. This could be achieved by imaging the fibre core arrangement through a single lens onto an array of lenses each coupling the subsection containing one core onto an input or output fibre. An alternative solution is a fused coupler similar to a *photonic lantern* [74], however crosstalk issues during the waist region of such devices make this potentially difficult to fabricate. Consider that at the minimum waist interface the cores are ideally identical and coupled, any inhomogeneity in the the necking down region will impact the quantum walk by coupling between cores in a dissimilar way.

Addressing Cores by Alternative means

Adaptive addressing of multiple cores simultaneously may be achieved using holographic techniques or a spatial light modulator. A scheme of this type would apply a virtual and controllable lens(s) allowing multiple modes to be coupled out of the waveguide and into single mode fibers. A pair of SLMs, one each for input and output coupling would probably be required for the flexibility to couple arbitrarily into a multi-core fibre for quantum walk applications.

Another alternative method would employ an array of Si avalanche photo diodes on a wafer in a triangular lattice pattern. A single relay lens arrangement would then be able to map all output cores to one APD. This technique does not address the input requirements, however due to photon source limitations it is unlikely that all cores would be coupled simultaneously to a photon source.

Further Applications of the Walk Fibre

The ability to control the initial state of a quantum walk is desirable. In a generic quantum information processing scenario we first prepare the qubit in a desirable state. In the case of the multi-core fibre the initial state of a photon in a particular position

is achieved simply by selecting the core to initially couple into. More advanced state preparation such as a superposition of three locations would be achieved by additional optical elements prior to entering the fibre.

If instead it were possible to modify the coupling rates along the fibre in a defined manner, the initial state coupled into a single input site could be evolved into the correct starting state before continuing along a region of identical cores to undergo the walk. Dynamic control of a quantum walk has been demonstrated by Silberhorn et al.[75] by controlling the coin operation in order to bias evolution of the walk or in the extreme make the operation deterministic. The phase matching between cores can be inhibited by cross phase modulation to prevent coupling between a modulated core and an unmodulated core. The modulation could be provided by a bright laser source sufficiently different in wavelength to the photon source that it does not couple significantly between cores over the length of interest. By applying counter propagating pulses of bright light with appropriate timing it may be possible to control coupling of the photon(s) in the walk and prepare a desired initial state, or conversely to route the output of a particular core at the end of a walk to an arbitrary other core for output. combinations of these techniques may simplify readout of single photons by initializing and detecting arbitrary core occupation states, while permanently coupling only select locations to detectors and photon sources.

Chapter 6

Summary

In this thesis three interrelated pieces of work have been set out. Temporal multiplexing of single heralded photons by a fibre integrated delay loop was constructed and demonstrated. Four time bins derived from separate pump pulses of a pulsed photonic crystal fibre heralded photon pair source have been combined together into a single time bin with improved delivery probability. The improvement factors attainable with the implemented system indicate a successful enhancement of heralded photon statistics post generation. The system was able to produce measurable and significant improvement despite introducing insertion losses in excess of 1dB per delay time, indicating the viability of future schemes in which low loss optical switches are available.

A custom 37 core optical fibre was fabricated and used to implement a two dimensional quantum walk of single heralded photons. The implementation is a significant first step towards implementing a quantum walk based computational task which displays quantum advantage, in a fibre integrated and room temperature apparatus. A two dimensional single photon quantum walk was observed using photons from a β-BBO heralded photon pair source in the fabricated fibre.

Effective and simple electronics have been designed and demonstrated for the control

and detection of photons in the discussed systems. An FPGA based correlation counter has been designed and successfully used to detect coincidence rates for the two presented single photon sources and for the subsequent random walk and temporal multiplexing experiments. Precision time delay modules have been designed and used throughout all temporally aligned measurements and control experiments. Finally an FPGA based multiplexing control system has been designed and constructed in order to operate an optical delay loop in a real-time and feed-forward manner.

Bibliography

[1] Valerio Scarani, Helle Bechmann-Pasquinucci, Nicolas J. Cerf, Miloslav Dušek, Norbert Lütkenhaus, and Momtchil Peev. The security of practical quantum key distribution. *Rev. Mod. Phys.*, 81:1301–1350, Sep 2009.

[2] Vittorio Giovannetti, Seth Lloyd, and Lorenzo Maccone. Quantum-enhanced measurements: Beating the standard quantum limit. *Science*, 306(5700):1330, Nov 2004.

[3] Katherine L. Brown, William J. Munro, and Vivien M. Kendon. Using quantum computers for quantum simulation. *Entropy*, 12(11):2268–2307, 2010.

[4] P. Shor. Polynomial-time algorithms for prime factorization and discrete logarithms on a quantum computer. *SIAM Journal on Computing*, 26(5):1484–1509, Oct 1997.

[5] Jelena Vuckovic, David Fattal, Charles Santori, Glenn S. Solomon, and Yoshihisa Yamamoto. Enhanced single-photon emission from a quantum dot in a micropost microcavity. *Applied Physics Letters*, 82(21):3596–3598, May 2003.

[6] Charles Santori, Matthew Pelton, Glenn Solomon, Yseulte Dale, and Yoshihisa Yamamoto. Triggered single photons from a quantum dot. *Phys. Rev. Lett.*, 86:1502–1505, Feb 2001.

[7] Charles H. Bennett and David P. DiVincenzo. Quantum information and computation. *Nature*, 404:247 EP –, Mar 2000. Review Article.

[8] K. Hennessy, A. Badolato, M. Winger, D. Gerace, M. Atatüre, S. Gulde, S. Fält, E. L. Hu, and A. Imamoglu. Quantum nature of a strongly coupled single quantum dot-cavity system. *Nature*, 445:896 EP –, Jan 2007.

[9] Anonymous. Proceedings of the american physical society. *Phys. Rev.*, 69:674–674, Jun 1946.

[10] Christian Kurtsiefer, Sonja Mayer, Patrick Zarda, and Harald Weinfurter. Stable solid-state source of single photons. *Phys. Rev. Lett.*, 85:290–293, Jul 2000.

[11] D. Riedel, F. Fuchs, H. Kraus, S. Väth, A. Sperlich, V. Dyakonov, A. A. Soltamova, P. G. Baranov, V. A. Ilyin, and G. V. Astakhov. Resonant addressing and manipulation of silicon vacancy qubits in silicon carbide. *Phys. Rev. Lett.*, 109:226402, Nov 2012.

[12] P. W. Anderson and J. M. Rowell. Probable observation of the josephson superconducting tunneling effect. *Phys. Rev. Lett.*, 10:230–232, Mar 1963.

[13] E. Knill, R. Laflamme, and G. J. Milburn. A scheme for efficient quantum computation with linear optics. *Nature*, 409:46 EP –, Jan 2001. Article.

[14] C. Klempt, O. Topic, G. Gebreyesus, M. Scherer, T. Henninger, P. Hyllus, W. Ertmer, L. Santos, and J. J. Arlt. Parametric amplification of vacuum fluctuations in a spinor condensate. *Phys. Rev. Lett.*, 104:195303, May 2010.

[15] R. P. Wang and H. R. Zhang. Theory for quantum state of photon pairs generated from spontaneous parametric down-conversion nonlinear process. *Optics and Spectroscopy*, 103(1):148–152, 2007.

[16] The quantum theory of the emission and absorption of radiation. *Proceedings of the Royal Society of London. Series A*, 114(767):243, Mar 1927.

[17] Noah Linden, Sandu Popescu, Anthony J. Short, and Andreas Winter. Quantum mechanical evolution towards thermal equilibrium. *Phys. Rev. E*, 79:061103, Jun 2009.

[18] J. H. Eberly. Schmidt analysis of pure-state entanglement. *Laser Physics*, 16(6):921–926, 2006.

[19] C. K. Hong, Z. Y. Ou, and L. Mandel. Measurement of subpicosecond time intervals between two photons by interference. *Phys. Rev. Lett.*, 59:2044–2046, Nov 1987.

[20] T. B. Pittman, D. V. Strekalov, A. Migdall, M. H. Rubin, A. V. Sergienko, and Y. H. Shih. Can two-photon interference be considered the interference of two photons? *Phys. Rev. Lett.*, 77:1917–1920, Sep 1996.

[21] Mark Fox. *Quantum Optics - An Intrduction.* Oxford University Press, Great Clarendon Street, Oxford OX2 6DP, first (with corrections) edition, 2006.

[22] Edo Waks Yamamoto, Eleni Diamanti, and Yoshihisa. Generation of photon number states. *New Journal of Physics*, 8(1):4, 2006.

[23] Interferometry of the intensity fluctuations in light - i. basic theory: the correlation between photons in coherent beams of radiation. *Proceedings of the Royal Society of London. Series A. Mathematical and Physical Sciences*, 242(1230):300, Nov 1957.

[24] T. A. Birks, J. C. Knight, and P. St J. Russell. Endlessly single-mode photonic crystal fiber. *Optics Letters*, 22(13):961–963, 1997.

[25] Govind P. Agrawal. *Nonlinear Fibre Optics.* Academic Press, 30 Corporate Drive, Suite 400, Burlington, MA 01803, USA, fourth edition, 2007.

[26] COMSOL Inc. Multiphysics.

[27] G.J. Pearce. *Plane-wave methods for modelling photonic crystal fibre*. PhD thesis, Bath, UK, 2015.

[28] Kunimasa Saitoh and Masanori Koshiba. Empirical relations for simple design of photonic crystal fibers. *Optics Express*, 13(1):267–274, 2005.

[29] P. A. M. Dirac. *The Principles of Quantum Mechanics*. Oxford University Press, Great Clarendon Street, Oxford OX2 6DP, fourth edition edition, 1981.

[30] Rodney Loudon. *The Quantum Theory of Light*. Oxford University Press, Great Clarendon Street, Oxford OX2 6DP, third edition edition, 2000.

[31] A. Yu Bogdanov, Yu I. Bogdanov, and K. A. Valiev. Schmidt modes and entanglement in continuous-variable quantum systems. *Russian Microelectronics*, 35(1):7–20, 2006.

[32] K. Garay-Palmett, H. J. McGuinness, Offir Cohen, J. S. Lundeen, R. Rangel-Rojo, A. B. U'Ren, M. G. Raymer, C. J. McKinstrie, S. Radic, and I. A. Walmsley. Photon pair-state preparation with tailored spectral properties by spontaneous four-wave mixing in photonic-crystal fiber. *Optics Express*, 15(22):14870–14886, 2007.

[33] Paul Campagnola. Second harmonic generation imaging microscopy: Applications to diseases diagnostics. *Anal Chem*, 83(9):3224–3231, May 2011. 21446646[pmid].

[34] Paul G. Kwiat, Klaus Mattle, Harald Weinfurter, Anton Zeilinger, Alexander V. Sergienko, and Yanhua Shih. New high-intensity source of polarization-entangled photon pairs. *Phys. Rev. Lett.*, 75:4337–4341, Dec 1995.

[35] D. H. Andrews, W. F. Brucksch, W. T. Ziegler, and E. R. Blanchard. Attenuated superconductors i. for measuring infra-red radiation. *Review of Scientific Instruments*, 13(7):281–292, Jul 1942.

[36] Roger A. Smith, Dileep V. Reddy, Dashiell L. P. Vitullo, and M. G. Raymer.

Double-heralded generation of two-photon-states by spontaneous four-wave-mixing in the presence of noise. *Optics Express*, 24(6):5809–5821, 2016.

[37] A. P. Worsley, H. B. Coldenstrodt-Ronge, J. S. Lundeen, P. J. Mosley, B. J. Smith, G. Puentes, N. Thomas-Peter, and I. A. Walmsley. Absolute efficiency estimation of photon-number-resolving detectors using twin beams. *Optics Express*, 17(6):4397–4412, 2009.

[38] Robert J. A. Francis-Jones, Rowan A. Hoggarth, and Peter J. Mosley. All-fiber multiplexed source of high-purity single photons. *Optica*, 3(11):1270–1273, 2016.

[39] Robert J.A. Francis-Jones. *Active Multiplexing of Spectrally Engineered Heralded Single Photons in an Integrated Fibre Architecture*. PhD thesis, Bath, UK, 2015.

[40] Robert J. A. Francis-Jones Mosley and Peter J. Fibre-integrated noise gating of high-purity heralded single photons. *Journal of Optics*, 19(10):104005, 2017.

[41] *IEEE Std 1364-2005 (Revision of IEEE Std 1364-2001)*, chapter IEEE Standard for Verilog Hardware Description Language. 2006.

[42] *IEEE Std 1076-1987*, chapter IEEE Standard VHDL Language Reference Manual. 1988.

[43] Lightweight usb framework for avrs. http://www.fourwalledcubicle.com/LUFA.php.

[44] R. A. Hoggarth Mosley, R. J. A. Francis-Jones, and P. J. Resource-efficient fibre-integrated temporal multiplexing of heralded single photons. *Journal of Optics*, 19(12):125503, 2017.

[45] J. Sperling, W. Vogel, and G. S. Agarwal. True photocounting statistics of multiple on-off detectors. *Phys. Rev. A*, 85:023820, Feb 2012.

[46] Oliver J. Morris, Robert J. A. Francis-Jones, Keith G. Wilcox, Anne C. Tropper,

and Peter J. Mosley. Photon-pair generation in photonic crystal fibre with a 1.5ghz modelocked vecsel. *Optics Communications*, 327(Supplement C):39–44, 2014.

[47] Robert J. A. Francis-Jones and Peter J. Mosley. Temporal loop multiplexing: A resource efficient scheme for multiplexed photon-pair sources. *arXiv:1503.06178v1*, 2015.

[48] Mercedes Gimeno-Segovia, Hugo Cable, Gabriel J. Mendoza, Pete Shadbolt, Joshua W. Silverstone, Jacques Carolan, Mark G. Thompson, Jeremy L. O'Brien, and Terry G. Rudolph. Relative multiplexing for minimizing switching in linear-optical quantum computing. *arXiv:1701.03306v2*, 2017.

[49] C. Xiong, X. Zhang, Z. Liu, M. J. Collins, A. Mahendra, L. G. Helt, M. J. Steel, D.-Y. Choi, C. J. Chae, P. H. W. Leong, and B. J. Eggleton. Active temporal multiplexing of indistinguishable heralded single photons. *Nature Communications*, 7:10853 EP –, Mar 2016. Article.

[50] Gabriel J. Mendoza, Raffaele Santagati, Jack Munns, Elizabeth Hemsley, Mateusz Piekarek, Enrique Martín-López, Graham D. Marshall, Damien Bonneau, Mark G. Thompson, and Jeremy L. O'Brien. Active temporal and spatial multiplexing of photons. *Optica*, 3(2):127–132, 2016.

[51] Fumihiro Kaneda, Bradley G. Christensen, Jia Jun Wong, Hee Su Park, Kevin T. McCusker, and Paul G. Kwiat. Time-multiplexed heralded single-photon source. *Optica*, 2(12):1010–1013, 2015.

[52] Andrew M. Childs, Richard Cleve, Enrico Deotto, Edward Farhi, Sam Gutmann, and Daniel A. Spielman. Exponential algorithmic speedup by quantum walk. *arXiv:quant-ph/0209131v2*, 2002.

[53] Markus Gräfe Szameit, René Heilmann, Maxime Lebugle, Diego Guzman-Silva,

Armando Perez-Leija, and Alexander. Integrated photonic quantum walks. *Journal of Optics*, 18(10):103002, 2016.

[54] A. Schreiber, K. N. Cassemiro, V. Potoček, A. Gábris, P. J. Mosley, E. Andersson, I. Jex, and Ch. Silberhorn. Photons walking the line: A quantum walk with adjustable coin operations. *Phys. Rev. Lett.*, 104:050502, Feb 2010.

[55] A. Schreiber, K. N. Cassemiro, V. Potoček, A. Gábris, I. Jex, and Ch. Silberhorn. Decoherence and disorder in quantum walks: From ballistic spread to localization. *Phys. Rev. Lett.*, 106:180403, May 2011.

[56] Thomas Nitsche Silberhorn, Fabian Elster, Jaroslav Novotný, Aurél Gábris, Igor Jex, Sonja Barkhofen, and Christine. Quantum walks with dynamical control: graph engineering, initial state preparation and state transfer. *New Journal of Physics*, 18(6):063017, 2016.

[57] Andreas Schreiber, Aurél Gábris, Peter P. Rohde, Kaisa Laiho, Martin Stefanák, Václav Potocek, Craig Hamilton, Igor Jex, and Christine Silberhorn. A 2d quantum walk simulation of two-particle dynamics. *Science*, Mar 2012.

[58] Andrea Crespi, Roberto Osellame, Roberta Ramponi, Vittorio Giovannetti, Rosario Fazio, Linda Sansoni, Francesco De Nicola, Fabio Sciarrino, and Paolo Mataloni. Anderson localization of entangled photons in an integrated quantum walk. *Nature Photonics*, 7:322 EP –, Mar 2013. Article.

[59] Filippo Caruso, Andrea Crespi, Anna Gabriella Ciriolo, Fabio Sciarrino, and Roberto Osellame. Fast escape of a quantum walker from an integrated photonic maze. *Nature Communications*, 7:11682 EP –, Jun 2016. Article.

[60] Nicolò Spagnolo, Chiara Vitelli, Marco Bentivegna, Daniel J. Brod, Andrea Crespi, Fulvio Flamini, Sandro Giacomini, Giorgio Milani, Roberta Ramponi, Paolo Mat-

aloni, Roberto Osellame, Ernesto F. Galvão, and Fabio Sciarrino. Experimental validation of photonic boson sampling. *Nature Photonics*, 8:615 EP –, Jun 2014.

[61] Alexander Szameit Nolte and Stefan. Discrete optics in femtosecond-laser-written photonic structures. *Journal of Physics B: Atomic, Molecular and Optical Physics*, 43(16):163001, 2010.

[62] J. O. Owens White, M. A. Broome, D. N. Biggerstaff, M. E. Goggin, A. Fedrizzi, T. Linjordet, M. Ams, G. D. Marshall, J. Twamley, M. J. Withford, and A. G. Two-photon quantum walks in an elliptical direct-write waveguide array. *New Journal of Physics*, 13(7):075003, 2011.

[63] Konstantinos Poulios, Robert Keil, Daniel Fry, Jasmin D. A. Meinecke, Jonathan C. F. Matthews, Alberto Politi, Mirko Lobino, Markus Gräfe, Matthias Heinrich, Stefan Nolte, Alexander Szameit, and Jeremy L. O'Brien. Quantum walks of correlated photon pairs in two-dimensional waveguide arrays. *Phys. Rev. Lett.*, 112:143604, Apr 2014.

[64] Alberto Politi, Martin J. Cryan, John G. Rarity, Siyuan Yu, and Jeremy L. O'Brien. Silica-on-silicon waveguide quantum circuits. *Science*, 320(5876):646, May 2008.

[65] Alberto Peruzzo, Mirko Lobino, Jonathan C. F. Matthews, Nobuyuki Matsuda, Alberto Politi, Konstantinos Poulios, Xiao-Qi Zhou, Yoav Lahini, Nur Ismail, Kerstin Wörhoff, Yaron Bromberg, Yaron Silberberg, Mark G. Thompson, and Jeremy L. OBrien. Quantum walks of correlated photons. *Science*, 329(5998):1500, Sep 2010.

[66] Hugo Defienne, Marco Barbieri, Ian A. Walmsley, Brian J. Smith, and Sylvain Gigan. Two-photon quantum walk in a multimode fiber. *Science Advances*, 2(1), Jan 2016.

[67] Peter J. Mosley, Itandehui Gris-Sanchez, James Stone, Robert Francis-Jones, Rowan A. Hoggarth, Douglas J. Ashton, and Tim A. Birks. Reconstructing core-to-core variations of propagation constant in coupled multicore fiber for quantum walks. In *CLEO: 2015*, OSA Technical Digest (online), page SM2L.4, San Jose, California, 2015. Optical Society of America.

[68] A.W. Snyder and J. Love. *Optical Waveguide Theory*. Springer US, first edition edition, 1983.

[69] L. Jacomme. Modal dispersion in multimode graded-index fibers. *Applied Optics*, 14(11):2578–2584, 1975.

[70] G. Yabre. Comprehensive theory of dispersion in graded-index optical fibers. *Journal of Lightwave Technology*, 18(2):166, 2000.

[71] Lov K. Grover. From schrödinger's equation to the quantum search algorithm. *American Journal of Physics*, 69(7):769–777, Jun 2001.

[72] Lov K. Grover. A fast quantum mechanical algorithm for database search. In *Proceedings of the Twenty-eighth Annual ACM Symposium on Theory of Computing*, STOC '96, pages 212–219, New York, NY, USA, 1996. ACM.

[73] Youn-Chang Jeong, Carlo Di Franco, Hyang-Tag Lim, M. S. Kim, and Yoon-Ho Kim. Experimental realization of a delayed-choice quantum walk. *Nature Communications*, 4:2471 EP –, Sep 2013. Article.

[74] T. A. Birks, I. Gris-Sánchez, S. Yerolatsitis, S. G. Leon-Saval, and R. R. Thomson. The photonic lantern. *Advances in Optics and Photonics*, 7(2):107–167, 2015.

[75] Thomas Nitsche Silberhorn, Fabian Elster, Jaroslav Novotný, Aurél Gábris, Igor Jex, Sonja Barkhofen, and Christine. Quantum walks with dynamical control: graph engineering, initial state preparation and state transfer. *New Journal of Physics*, 18(6):063017, 2016.